A CHEMICAL AND THERMAL MODELLING STUDY OF THE ACTIVE LAYER ON HERSCHEL ISLAND, YUKON TERRITORY

Leigh-Ann Williams-Jones

Department of Geography McGill University Montreal, Quebec, Canada

December, 2012

A thesis submitted to McGill University in fulfillment of the requirements of the degree of Master of Science

ABSTRACT

An essential requirement in evaluating the potential impacts of climate warming in Polar Regions, is a greater understanding of the nature and behavior of the active layer and the permafrost system. Numerous studies have documented the inherent capacity of permafrost to limit significant degradation from seasonal thawing because of the ability of overlying soil layers to dissipate influxes of heat. However, information on the degree to which these layers are able to act as buffers to permafrost degradation is limited, and thus further research on this system is needed.

The research presented in this thesis is based on a field and laboratory study of the permafrost environment of Herschel Island, in the Southern Beaufort Sea. This research involved field description, sampling and chemical analyses of a series of soil profiles exposed in the headwall of a retrogressive thaw slump. Exposures contained a cross-section of the current active layer, a paleo-active layer and the upper part of permafrost. The second part of this research modelled the effect of global warming on the active layer thickness that incorporated measurements of active layer thickness from an adjacent monitoring grid. The active layer monitoring (ALM) site includes measurements made from June 24th, 2011 to August 24th, 2011 at 10 m spacing on a 100 m by 100 m grid, located several meters upslope from the receding headwall of the retrogressive thaw slump.

Results are presented in the form of two manuscripts. The first manuscript (Chapter 3) discusses the role of chemical processes in the soil weathering regime on Herschel Island. Three distinct

cryostratigraphic layers were observed in the soil profiles, including; (1) the modern active-layer located immediately below the ground surface (0 - 39 cm); (2) a paleo-active (transition layer), extending from the bottom of the modern active layer to the top of an undisturbed permafrost layer (39 – 192 cm); and (3) the underlying permafrost. These layers are marked by two thaw unconformities that separate the modern active layer from the transition layer and the transition layer from the permafrost layer, respectively. The two thaw unconformities were distinguished by abrupt breaks in the cryogenic texture and peaks in the concentrations of several chemical components. The upper thaw unconformity, located at the base of the modern active layer, coincided with a doubling in the concentration of major soluble cations and a tripling in the organic matter content compared to those of the overlying soil horizons. The lower thaw unconformity is marked by the highest concentration of Al₂O₃ and K₂O in the entire profile and the second highest concentration of Na₂O. Between these two unconformities, (i.e. in the transition zone), soluble cation concentrations varied considerably, the bulk soil SiO₂ concentration increased significantly and there was a noticeable decrease in the concentrations of Al₂O₃, Fe₂O₃, CaO, MgO and K₂O in the depth interval of 82-107 cm. Chemical weathering indices recorded an overall decrease in the intensity of chemical weathering with depth; the soil layers immediately above the first thaw unconformity were the most weathered and the deeper permafrost layer was the least weathered.

The second manuscript (Chapter 4) employs a heat conduction algorithm (Stefan equation) based on the composition and thermal properties of the soils discussed in Chapter 3, and measured active layer depth values, to evaluate heat transfer from the ground surface to the underlying permafrost. Thermal constants (the square root of the ratio of twice the thermal conductivity of

the unfrozen soil to the latent heat of fusion of ice) were calculated using the De Vries method and were compared to empirical thermal constants derived from measurements of active layer depths and the corresponding thawing degree days using the Stefan equation. The theoretical constants are approximately 38% lower than those derived empirically, a difference that is likely due to the fact that the Stefan equation does not consider advective heat transfer and that the active layer depths were probably overestimated because of the method of measurement (resistance to penetration of a metal probe). Third generation Canadian Global Coupled Models (CGCM 3.1/T63) from the Canadian Centre for Climate Modelling and Analysis (CCCma), based on the IPCC SRES A2 and B1 scenarios, were used in conjunction with the theoretically and empirically derived thermal constants to predict active layer depths for 2050 and 2100. These calculations suggest that the active layer will thicken by up to 41.76 % before the end of this century.

This thesis provides new insights into the important role that the active and transition layers play in controlling the response of permafrost systems to climate change. It demonstrates the need to consider chemical processes in evaluating weathering of ice-rich terrains and, through a quantitative evaluation of the response of frozen soils to changes in the thermal regime, provides a better understanding of how ongoing climate warming will affect future active layer development and might change landscape morphology.

RÉSUMÉ

Une condition essentielle pour évaluer les impacts potentiels du réchauffement climatique dans les régions polaires est l'acquisition d'une meilleure compréhension de la nature et du comportement de la couche active du pergélisol. De nombreuses études ont documenté la capacité inhérente du pergélisol de limiter une dégradation significative par le dégel saisonnier en raison de la capacité des couches de sol superficielles de dissiper l'afflux de chaleur. Cependant, les connaissances sur la mesure dans laquelle ces couches sont capables d'agir comme des tampons efficaces contre la dégradation du pergélisol sont encore assez limitées, et donc de nouvelles recherches sur ce système sont nécessaires.

La recherche présentée dans cette thèse est basée sur une étude de terrain et de laboratoire sur l'environnement périglaciaire de l'île Herschel, dans le sud de la mer de Beaufort. Cette recherche a impliqué principalement la description, l'échantillonnage et des analyses chimiques d'une série de profils de sol exposés le long de l'escarpement d'un versant de dégel régressif. Les parties exposées contenaient une section transversale des couches active et paléo-active et de la couche superficielle du permafrost. La seconde partie de cette étude visait à modéliser l'effet du réchauffement climatique sur l'épaisseur de la couche active en faisant usage de mesures d'épaisseur de couche active provenant d'un réseau de surveillance adjacent. Ce réseau de surveillance (ALM) de la couche active comprend des mesures relevées du 24 juin 2011 au 24 août 2011 à intervalles de 10 m sur une grille de 100 m par 100 m, située plusieurs mètres en amont de l'escarpement du versant de dégel régressif.

Les résultats sont présentés sous la forme de deux manuscrits. Le premier manuscrit (chapitre 3) examine le rôle des processus chimiques dans le régime d'altération du sol sur l'île Herschel. Trois couches distinctes cryostratigraphiques ont été observées dans les profils de sol: (1) la couche active moderne située immédiatement sous la surface du sol (0 - 39 cm), (2) la couche paléo-active (couche de transition) s'étendant de la base de la couche moderne active à la partie supérieure de la couche de pergélisol non perturbée (39 - 192 cm) et (3) le pergélisol sous-jacent. Ces couches sont marquées par deux discordances de dégel séparant la couche active moderne de la couche de transition et la couche de transition de la couche de pergélisol, respectivement. Ces deux discordances de dégel ont été identifiées grâce à la présence de ruptures brutales dans la texture cryogénique et par des pics dans la concentration de plusieurs composants chimiques. La discordance de dégel supérieure, située à la base de la couche moderne active, coïncide avec un doublement de la concentration des principaux cations solubles et un triplement de la teneur en matière organique par rapport aux horizons sus-jacents. La discordance de dégel inférieure est marquée par la plus forte concentration en Al₂O₃ et en K₂O de l'ensemble du profil et par la deuxième plus forte concentration en Na₂O. Entre ces deux discordances (c'est à dire dans la zone de transition), les concentrations en cations solubles varient considérablement, la concentration en SiO₂ du sol brut s'accroit de façon significative et on observe une diminution notable des concentrations en Al₂O₃, Fe₂O₃, CaO, MgO et K₂O dans l'intervalle de profondeur de 82-107 cm. Les indices d'altération chimique ont enregistré une diminution globale de l'intensité de l'altération chimique avec la profondeur ; les couches de sol immédiatement au-dessus de la première discordance de dégel sont les plus altérées et la couche profonde du pergélisol est la moins altérée.

Le second manuscrit (chapitre 4) utilise un algorithme de conduction de la chaleur (équation Stefan) basé sur la composition et les propriétés thermiques des sols examinés au chapitre 3 et sur les mesures des valeurs de profondeur de la couche active afin d'évaluer le transfert de chaleur de la surface du sol au pergélisol sous-jacent. Des constantes thermiques (la racine carrée du rapport entre deux fois la conductivité thermique du sol non gelé et la chaleur latente de fusion de la glace) ont été calculées en utilisant la méthode de De Vries et comparées aux constantes thermiques empiriques issues des mesures de profondeur de la couche active et des degrés-jours de dégel correspondant en utilisant l'équation de Stefan. Les constantes théoriques sont environ 38% inférieures à celles obtenues empiriquement, une différence qui s'explique probablement par le fait que l'équation de Stefan ne considère pas le transfert de chaleur par advection et que les profondeurs de la couche active ont probablement été surestimées en raison de la méthode de mesure (résistance à la pénétration d'une sonde métallique). La troisième génération du modèle couplé climatique global canadien (CGCM 3.1/T63) du Centre canadien de la modélisation et de l'analyse climatique (CCmaC), basée sur les scénarios A2 et B1 du IPCC SRES, a été utilisée en conjonction avec les constantes thermiques théoriques et empiriques pour prédire les profondeurs de la couche active pour 2050 et 2100. Ces calculs suggèrent que la couche active s'épaissira de jusqu'à 41,76% avant la fin du siècle.

Ce mémoire apporte un nouvel éclairage sur le rôle important que les couches actives et de transition jouent dans le contrôle de la réponse des systèmes de pergélisol au changement climatique. Il démontre également la nécessité de considérer les processus chimiques dans l'évaluation de l'altération des terrains riches en glace et, à travers une évaluation quantitative de la réponse des sols gelés aux changements dans le régime thermique, permet une meilleure

compréhension de la façon dont le réchauffement climatique en cours aura une incidence sur le développement futur de la couche active et pourrait changer la morphologie du paysage.

CONTRIBUTION OF AUTHORS

This thesis is divided into seven chapters of which two are manuscripts that will be submitted to international refereed journals. Their titles are *Soil Weathering Processes on Herschel Island, Yukon* and *Active Layer Thickening on Herschel Island, Yukon*, and they will be co-authored by Leigh-Ann Williams-Jones, Dr. Wayne Pollard and Dr. William Hendershot.

I conducted the field work with the guidance of Dr. W.H. Pollard during the summer of 2011. I also conducted the various chemical analyses, interpreted the data with the assistance of Dr. W.H. Pollard and Dr. W.H. Hendershot, and carried out the numerical modelling reported in the second manuscript. Drs. Pollard and Hendershot helped in the development of the hypotheses that were tested and the overall evaluation of the results of the research. I prepared initial drafts of the manuscripts, which were revised based on their comments. Funding for the research was provided by NSERC Discovery, NSTP, PCSP and ArcticNet grants to Dr. W.H. Pollard, and an NSERC discovery grant to Dr. W.H. Hendershot. Licensing pertaining to the fieldwork portion of this research was granted by the Yukon Government.

ACKNOWLEDGEMENTS

I would like to thank my supervisor, Dr. Wayne Pollard, for giving me the opportunity to travel to the Western Arctic and experience the captivating Herschel Island landscape for almost two months. Most importantly, his knowledge and insights of everything pertaining to periglacial environments were vital for my fieldwork and understanding the significance of my observations. Secondly, I would like to thank my co-supervisor, Dr. William Hendershot, whose guidance in interpreting the soil geochemistry of the active layers on Herschel Island was essential in helping me understand the impact of global warming on soil processes. His constant support and encouragement were a huge help in enabling me to complete my thesis in timely fashion. To Helene Lalande, whose extensive expertise in the laboratory, helped me obtain excellent analytical data for my thesis, and whose enthusiasm and eagerness made the long hours in the laboratory pleasurable, I would like to convey my enormous gratitude. To Dina Schwertfeger for all your help with my chemical analyses and to my volunteer field assistants, Michael Angelopolous, Heather Sloan, Dave Fox, Jared Simpson and Beatrice Beaubien, my heartfelt thanks. Thank you, Tim Moore, for your valuable comments and encouragement. My many thanks to the Herschel Island park rangers, Richard Gordon, Leejon Meeyook, Samuel McLeod, Ricky Joe and Paden Lennie for their generosity and helpfulness in the field. To my friends at home and at McGill University, thank you for breaking up the monotony of sitting at a computer or processing soil all day. Finally, an extra special thanks to my family, especially my Mum and Dad, for their support, input, patience and willingness to put up with me throughout the course of my project: I couldn't have done it without you.

TABLE OF CONTENTS

ABSTRACT		ii
RÉSUMÉ		V
CONTRIBUTIO	ON OF AUTHORS	ix
ACKNOWLED	GEMENTS	X
LIST OF FIGU	RES	xiv
LIST OF TABI	LES	xvi
CHAPTER 1:	INTRODUCTION	1
1.1.	INTRODUCTION	2
1.2.	OBJECTIVES OF THE STUDY	4
1.3.	THESIS ORGANIZATION	5
CHAPTER 2:	BACKGROUND	7
	ROST	
	TIVE LAYER	
	ERING IN POLAR SOILS	
	ECT OF GLACIAL HISTORY ON POLAR SOIL PROFILES	
	ERING INDICES	
2.6. GROUN	D THERMAL MODELLING	16
PREFACE TO C	CHAPTER 3	19
CHAPTER 3:	Soil Weathering Processes on Herschel Island, Yukon	20
ABSTRACT		21
3.1 INTROL	DUCTION	22
3.2 POLAR	SOILS	24
3.2 STUDY	SITE	26
3.3 CLIMAT	ΓΕ AND VEGETATION	31
3.4 MATER	IALS AND METHODS	34

3.5 RESULTS AND DISCUSSION	36
3.5.1. THE SOIL PROFILES	37
3.5.2. PARTICLE SIZE AND EXCHANGEABLE CATIONS	44
3.5.3. PROFILE DISTRIBUTION OF EXTRACTABLE IRON, ALUMINUM, AND IR	ON,
ALUMINUM OXIDES	49
3.5.4. BULK SOIL CHEMISTRY	
3.5.5. WEATHERING INDICES	56
3.5.6. SOIL WEATHERING AND THE PALEO-ACTIVE LAYER	62
3.6 CONCLUSION	64
PREFACE TO CHAPTER 4	67
CHAPTER 4 Active Layer Thickening on Herschel Island, Yukon	68
ABSTRACT	69
4.1. INTRODUCTION	70
4.2. BACKGROUND AND STUDY SITE	72
4.3.1. THERMOKARST AND RETROGRESSIVE THAW SLUMPS	74
4.4. METHODOLOGY	79
4.3.1. ALM GRID	80
4.3.2. STEFAN EQUATION	81
4.3.3. SURFACE TEMPERATURE MEASUREMENT AND ESTIMATION	83
4.3.4. THE DE VRIES EQUATION	83
4.4. RESULTS AND DISCUSSION	87
4.5.1. THAWING DEGREE DAYS	87
4.5.2. ACTIVE LAYER DEPTHS	91
4.5.3. THERMAL CONSTANTS	93
4.6. GLOBAL WARMING AND THE STATE OF THE ACTIVE LAYER	97
4.6.1. THERMOKARST AND GROUND SUBSIDENCE	105
4.6.2. IMPACT OF GLOBAL WARMING ON THE PALEO-ACTIVE LAYER	108
4.7. CONCLUSIONS	

CHAPTER 5	CONCLUSIONS	112
5.1. CONCLU	JSIONS	
CHAPTER 6	REFERENCES	116
6.1. REFERE	NCES	117
CHAPTER 7	APPENDICES	138
7.1. APPEND	OIX	139

LIST OF FIGURES

Fig. 3. 1.: Study area map of Herschel Island showing the location of study site indicated by the	•
red star2	
Fig. 3. 2.: Aerial view of the polycyclic nature of retrogressive thaw slumps on Herschel Island	
(August 2004) Three active slumps $(A1 - A3)$ are evident within an older, stabilized	
slump (S)	8
Fig. 3. 3.: Aerial photo of Retrogressive Thaw Slump A with red stars indicating sampled soil	
profile sites2	9
Fig. 3. 4.: Headwall view within the undisturbed section of Slump A, with lines demarcating	
the thaw unconformity	
Fig. 3. 5.: Mean Active Layer Depths for ALM site from June 14th to August 8th, 2011 3	
Fig. 3. 6.: Annotated photographs of soil profiles at sites 5 (202cm) and 3 (282cm)	
Fig. 3. 7.: Macroscopic examples of soil material with varying ice and sediment content 3	9
Fig. 3. 8.: A photograph of the soil profile at site 3, showing a change in colour from greyish	
brown to bluish grey (arrow)	0
Fig. 3. 9.: Depiction of a normal fault within the massive ice section at site 5. Vertical drop	_
from A to A1 is approximately 26.5 cm	1
Fig. 3. 10. :A normal fault within the massive ice and the boundary between disturbed and	
undisturbed soils, near site 4. The vertical drop from A to B is approximately 48cm.	
Ti 2.11 A.1	2
Fig. 3. 11. : A photograph of the soil profile at site 2 showing evidence of cryoturbation	_
disruption. Mineral tongues are outlined in green and organic tongues in red	
Fig. 3. 12. :Relationship between the soil organic matter content (SOM) and the cation exchange	
capacity (CEC)	O
Fig. 3. 13. :Relationship between Fe and Al extracted with pyrophosphate (Fep and Alp) and	
organic carbon content in the soil profile for Site 3. The solid yellow triangles	
correspond to the Fep concentrations, and the solid red circles the Alp concentrations	
Fig. 3. 14. : Soil profile at site 3 showing the two ice enriched peaks . Peak 1 (82-107 cm) is	ı.
indicated by the red lines and peak 2 (157-192 cm) by the yellow lines	1
Fig. 3. 15.: Weathering indices WR and CIW for site 3	
Fig. 3. 16.: Isolating mobile Ca, Mg, Na and K oxides in weathering indices WR for site 3 6	
Fig. 3. 17.: Weathering indices WIP for site 3	
rig. 3. 17 Weathering indices will for site 3.	_
Fig. 4. 1.: Study Area map of Herschel Island showing the location of study site indicated by th	
red star	3
Fig. 4. 2.: Aerial photograph depicting a retrogressive thaw slump (Slump D) on Herschel	_
Island, Yukon	
Fig. 4. 3.: Aerial photograph of study site depicting dimensions of retrogressive thaw slump A	
and location of a tundra pond	
Fig. 4. 4.: Thaw unconformities present in undisturbed soil profile at Slump A	ð

_	Schematic diagram of retrogressive thaw slump A, showing location of ALM site and sampled soil profile
Fig. 4. 6. :	Difference in mean daily air temperatures measured between June 27th, 2011 to July 21st, 2011
Fig. 4. 7. :	Correlation between mean daily temperatures measured by Environment Canada and from the HOBO between June 27 th , 2011 to July 21st, 201190
Fig. 4. 8. :	Variations in mean daily air temperatures measured between June 27th, 2011 to July 21st, 2011 at the ground surface and at 1.2m using data from HOBO data loggers
Fig. 4. 9. :	Active layer depth change between sites on June 24th, 2011 and August 24th, 2011.
Fig. 4. 10.	: Statistical relation between thaw depth and accumulated degree days95
Fig. 4. 11.	Cumulative mean temperatures for measured (2011) and modelled (2050) data from June 24 th to August 24 th
Fig. 4. 12.	Cumulative mean temperatures for measured (2011) and modelled (2100) data from June 24 th to August 24 th
Fig. 4. 13.	Relationship between the cumulative mean temperatures generated from the IPCC SRES A2 scenario and those measured at Herschel Island, YK in 2011
Fig. 4. 14.	Relationship between the cumulative mean temperatures generated from the IPCC SRES B1 scenario and those measured at Herschel Island, YK in 2011
Fig. 4. 15.	: Measured daily temperature for 2011 and projected daily temperatures for 2050 and 2100 for the A2 scenario from May 1st to October 31 st
Fig. 4. 16.	: Measured daily temperature for 2011 and projected daily temperatures for 2050 and 2100 for the B1 scenario from May 1st to October 31st
Fig. 4. 17.	Projected percent increase/decrease in maximum thaw depths for 2011, 2050 and 2100

LIST OF TABLES

Table 2. 1. : List of weathering indices, in molecular proportions, and their descriptions 15
Table 3. 1.: Climatic Data for Herschel Island from January to December, 2010 and 2011 32 Table 3. 2.: pH and electrical conductivity (EC) values of soil profiles sampled at Slump A
Table 4. 1. : Changes in soil characteristics with depth for a soil profile located within the undisturbed section of Slump A.79 Table 4. 2. : Changes in mean thaw depth, cumulative temperature, thawing days, thawing degree days and themal constants for 2011 thaw season and end of 2010 thaw season.96 Table 4. 3. : Thermal Constants using the De Vries method.97 Table 4. 4. : Thawing season changes based on IPCC SRES A2 and B1 scenarios using CGCM3.1/T63103
Table 4. 5. : Excess ice contents with depth. 108
Table 7. 1.: Active layer depth measurements within the ALM grid from June 24th, 2011 to August 24th, 2011
Table 7. 4.: Bulk soil chemical composition with depth for site 3 using XRF analysis. 146 Table 7. 5.: Bulk soil chemical composition with depth for site 3 using XRF analysis (cont) 147

CHAPTER 1

INTRODUCTION

1.1. INTRODUCTION

In polar environments, the surface layer that seasonally freezes and thaws is called the active layer, and in most Polar Regions is underlain by permafrost, i.e., ground material that remains below 0°C for at least two consecutive years (French, 2007). Recent studies on periglacial ground systems in North America have prompted the inclusion of a third layer, known as the "transition zone", into the traditional two-layer conceptual model. The "transition zone", first identified by Yanovsky in 1933, is an ice-enriched layer that exists between the current active layer and the permafrost layer, and reflects freezing and thawing over sub-decadal to centennial time-scales (Shur et al., 2005). Periodically becoming a part of the active-layer under warming conditions, the transition zone acts as an interface between the active layer and permafrost, controlling the exchange of heat and material between these two environments. Moreover, this zone not only influences the formation of cryogenic and soil structures, but serves to impart permafrost preservation against spasmodic thawing (Shur et al., 2005; Kaverin, 2008).

Previous studies of periglacial environments have focused primarily on the notion of "cold" as the main limiting and driving factor of weathering. According to this notion, mechanical processes such as frost action are the prime agents of cryosol (permafrost-affected soils) weathering (Tedrow, 1977), and chemical processes are temperature-inhibited, often to the point that they cease to occur (Hall et al., 2002). Although mechanically driven freeze-thaw-associated weathering is a dominant process within Cryosols, often overwhelming other pedogenic processes (Rieger, 1974), the presence of significant amounts of soil water suggests that chemical reactions may also play a role in the weathering (Tedrow, 1977). Moreover, since freezing of the active layer occurs through downward extension of the freezing front and by a

slow moving upward extension from the permafrost table (Rains, 2002), any changes in the soil thermal regime from surface heating or permafrost degradation will undoubtedly affect any pedogenic processes occurring within this dynamic zone. It is thus reasonable to propose that with a warming soil thermal regime due to climate change, chemical weathering in Cryosols will become a more important pedogenic process, thereby changing the balance of chemical versus physical weathering in polar environments. However, the extent to which this pedogenic process will be affected is largely unknown. In light of this, there is a strong need for a re-examination of the nature of weathering in polar environments, particularly the role of chemical weathering.

The effects of climate change in polar regions have received much attention during the past few decades (Lachenbruch, 1959; Are and Demchenko, 1972; Outcalt et al., 1975; Goodrich, 1982; Smith 1988; Kane et al., 1991; Sturm and Johnson, 1991; Benson and Sturm, 1993; Oechel et al., 1993; Liston and Hall, 1995; Zhang et al., 1997; Brown et al., 2000; Boer and Yu, 2003; Chapin et al., 2005; Lawrence and Slater, 2005; Shur et al., 2005; Davidson and Janssens, 2006; Shur and Jorgenson, 2007; Schuur et al., 2008; Jorgenson et al., 2010), due largely to the dramatic rise in global temperature and the uncertainty surrounding the ability of polar ecosystems to adapt to a rapidly changing climatic environment. Reports from the Intergovernmental Panel on Climate Change (IPCC) have projected increase in global mean temperatures over the next century of approximately 0.3°C per decade (Houghton et al., 1990). More startling are the general circulation model (GCM) predictions, which based on the assumption of atmospheric CO₂ doubling, indicating increases of up to 8-12°C in the months of December to February and mean surface temperature rises of 1.5-4.5°C by the middle of this century (Houghton et al., 1992; Anisimov et al., 2001).

As the Arctic is one of the regions most subject to changes by global warming on our planet (IPCC, 2007), there is considerable pressure to determine more precisely the nature of these changes and evaluate their potential impact on this environment. The purpose of this thesis is to investigate some of these changes through a detailed study of the active layer in a retrogressive thaw slump and an adjacent area on Herschel Island in the South Beaufort Sea.

1.2. OBJECTIVES OF THE STUDY

The overarching objectives of this thesis are to:

- Assess the intensity of weathering in the modern active-layer. This objective will be met by assessing rates of change of parameters related to specific weathering indices, through descriptive and chemical analyses.
- Assess the degree of weathering in the paleo-active layer compared to the modern active-layer, at these sites. This objective will be satisfied by a comparison of the rates of change of parameters related to the weathering indices employed in objective 1, between the paleo-active layer and the modern active-layer at each of the four sites and will be achieved through descriptive and chemical analyses.
- 3) Identify and assess the effectiveness of the indices chosen to measure the degree of weathering within a periglacial environment. This objective will be met using correlation statistics, to test the accuracy of the tools used in objectives 1 and 2.

- Evaluate the effect of rising global temperature on active layer deepening within a periglacial environment. This objective will be achieved by using a modified Stefan's function to calculate the changes in active depth with increasing surface temperatures of between 1.1 to 6.4°C (this temperature range has been predicted by the IPCC, 2007).
- Test the effectiveness of the Stefan model to predict the extent of active layer thickening within a periglacial environment. This objective will be satisfied by comparing in-field measured active layer data with that calculated using the Stefan model.

1.3. THESIS ORGANIZATION

This thesis is divided into five chapters: a general introduction, a literature review, two manuscripts describing the results of the research, and a general conclusion plus appendices. The general introduction introduces the topic of the research, summarizes the objectives, and describes the methods used to meet these objectives. The second chapter reviews the literature on periglacial processes, specifically those related to active layer development. Both manuscripts have been prepared for publication in peer-reviewed journals. The first manuscript (Chapter 3) describes and interprets observations of soil weathering within a retrogressive thaw slump (Slump A) on Herschel Island. Particular emphasis is placed on chemical weathering and valuating the intensity of this weathering using various chemical indices. The second manuscript (Chapter 4) makes use of the Stefan equation and De Vries equations (to estimate thermal conductivity) to quantitatively predict increases in the thickness of the active layer on Herschel Island due to rising temperature. Scenarios from the Intergovernmental Panel on Climate Change's Fourth Assessment Report, showing a 1.1°C to 6.4°C temperature rise, are considered.

Furthermore, past climate temperatures, specifically those occurring during the Hypsithermal period (i.e., Holocene Climatic Optimum), are examined. Appendices follow the conclusions (Chapter 5).

CHAPTER 2

BACKGROUND

2.1. PERMAFROST

Permafrost, perennially frozen ground, is an important feature of polar and mountainous regions, and plays a central role in the geomorphic processes that shape these environments (Jorgenson et al., 2010). In many ways, permafrost can be considered a climate time keeper, as it is a product of both present and past climates spanning hundreds of thousands of years (Péwé, 1975). Moreover, approximately 33% of surficial global carbon is stored within the top 100 cm of permafrost-affected soils, making this environment a ticking time bomb since huge amounts of frozen soil carbon is predicted to be thawed by climate warming, made accessible to microbial decomposition and released to the atmosphere as CO₂ and CH₄ (Bockheim et al., 2003; Tarnocai et al., 2009). However, it is important to point out, that although persistent low surface temperature is the main reason for permafrost, it does not follow that permafrost will be present wherever temperature is low. Indeed, permafrost may be either present or absent in areas with similar climates, e.g., similar temperature and precipitation (Kudriavtsev, 1954; Shur and Jorgenson, 2007). Whether or not permafrost occurs is also dependent on the nature and extent of the vegetation, soil composition and topography (Shur and Jorgenson, 2007). Thus, any meaningful evaluation of the relationship between climate and permafrost must, of necessity, involve an assessment of a large number of other factors that may impact upon permafrost development.

2.2. THE ACTIVE LAYER

Research into the relationship between climate and permafrost has generally separated permafrost systems into two distinct layers based on thermal state. The two types of frozen ground comprise a seasonally thawed active layer, and an underlying perennially frozen

permafrost layer (van Everdingen, 1998). According to French (2007), the active layer is a direct expression of summer temperature and solar radiation, and its depth is controlled primarily by local factors such as insulating cover (i.e., snow, ice, etc.), the nature of the substrate, the vegetation and the relief. All of these, to varying degrees, affect the soil thermal regime and soil moisture content. Most of the biological and chemical activity in the Arctic takes place within the active layer. However, the extent to which these processes occur depends strongly on the thickness of the active layer, a factor controlled by the soil's thermal regime.

Vegetation plays an important role in determining the ground thermal regime, and also serves to regulate the biochemical properties and weathering processes of soil. It also provides soils with insulation, which, in turn, affects the ability of the soil to retain heat. In addition, vegetation helps mitigate mechanical surface erosion by acting as a protective barrier against rain and wind. Plant roots, penetrating into the soil from the ground surface, not only provide vectors for soil oxygenation, but also play a valuable role in soil stabilization. The type of vegetation, in turn, determines the quality of organic matter entering the soil. For example, lower C:N ratios are produced by grasses and sedges, whereas shrub vegetation is characterized by a wide range of C:N ratios (Ping et al., 1998).

It is important to point out that biological and chemical activity within the active layer proceed slowly due to the low temperature, thereby facilitating the accumulation of organic matter within the soil because of a corresponding decrease in the rate of decomposition. Similarly, slow rates of other pedogenic processes such as podzolization, decalcification, and clay translocation also help determine the nature of Arctic soil profiles (Tedrow, 1977). These processes control the

chemical, textural and structural nature of the soil profile.

2.3. WEATHERING IN POLAR SOILS

Although physical weathering processes are generally dominant in Arctic soils, there is strong evidence that at least some chemical weathering occurs (Lipson, 2010). Even though most Arctic soils form in areas with low precipitation, they "commonly display redoximorphic features and horizons with reduced colours (Munsell hues 2.5 Y and 5Y, chromas of 2 or less and values of 4 or more)" (Ping et al. (1998), pp. 28917). This can be attributed to a low evapotranspiration rate (Lipson, 2010) and a seasonally perched water-table in the soil horizons located immediately above the permafrost table (Everett et al. 1982), as well as the general micro-topography. Evidence of similar redoximorphic features is provided by the results obtained in a study by Day and Rice (1964), which showed highly reduced subsurface horizons in saturated arctic tundra soils located in the Mackenzie Valley, with reducible iron remaining constant with depth (Tedrow, 1977). Thus biochemical weathering, at least in arctic tundra soils, is controlled predominantly by redox processes (Ping et al., 1998).

Chemical weathering refers to the biochemical breakdown of rocks and minerals into more basic compounds. Some of the by-products from chemical weathering are clay minerals, soluble acidic compounds and various ionic species (Schaetzl and Anderson, 2005). In general, chemical weathering can be thought of as involving two distinct processes. The first process is congruent dissolution, which involves the complete dissolution of a mineral without the formation of an intermediate solid (e.g., gypsum and calcite). Karsts are an excellent example of congruent dissolution, in which the calcite crystals in limestone dissolve completely, creating voids which eventually result in landscape surface collapse. Conversely, minerals undergoing incongruent

dissolution will preferentially release certain ions and retain others in a reconstituted residue, e.g., the breakdown of feldspars to release Na and K to solution leaving behind a residue of phyllosilicates minerals (Schaetzl and Anderson, 2005).

According to Bland and Rolls (1998), chemical weathering in soils occurs in three distinct stages namely, 1) dissolution of ions and molecules, 2) the production of new minerals from the precipitation of ions in solution, and 3) the residual accumulation of insoluble materials. The fate of the ions liberated through chemical weathering is highly variable, with some cations and anions being leached out of the solum entirely (i.e., eluviation) or into another horizon (i.e. illuviation), and others being bio-cycled (Schaetzl and Anderson, 2005). In theory, the degree to which a soil is weathered is dependent on the amount of time it has been exposed to weathering processes (Johnson et al., 1987). In other words, the older the soil, the more it should be weathered.

2.4. THE EFFECT OF GLACIAL HISTORY ON POLAR SOIL PROFILES

In the Arctic, sediments and soils have had a long and complex history of glacial and periglacial activity, including cyclic deposition by glaciers and glacial meltwater, solifluction and cryogenic processes. In fact, most of the soils in the Canadian Arctic are derived from late Pleistocene glacial deposits (Tedrow, 1977). Thus, in many ways the pedogenic features and processes observed in Canadian Arctic Cryosols are closely linked to their complex glacial history. In fact, the earliest study of the properties of soils in the Canadian Arctic by Feustel, Dutilly and Anderson (1939), in the northern Hudson Bay area and northward to Ellesmere Island, showed a striking lag in soil development and an almost complete lack of substrate and soil horizon

differentiation.

In arctic environments, glacial abrasion and frost action are considered the primary processes driving the distribution of particle size throughout the soil profile. Indeed, data from the study of Feustel et al. (1939) indicated an 18 to 23% clay content in many of the soils sampled. Furthermore, 6 of the 25 samples contained a hydrous-mica as the dominant clay mineral (75 – 95%), with the remainder (5 – 25%) being kaolinite (Tedrow, 1977). A more extensive study by Day and Rice (1964) along the lower Mackenzie River, with sites at Reindeer Depot and Inuvik, reported significantly high contents of clay (> 60%). These consisted largely of mixed layer montmorillonite-illite, illite and kaolinite (Tedrow, 1977).

2.5. WEATHERING INDICES

A major part of the soil chemical weathering process involves the dissolution of iron and aluminum from either parent material or the products of previous weathering cycles (Skjemstad et al., 1989). Once mobilized, these cations can either become re-precipitated as oxides or bound to organic compounds present in the soil. Generally, three main extraction procedures are used for distinguishing among the various fractions of 'free' iron and aluminium oxides in soil (Skjemstad et al., 1989). These involve using dithionite/citrate to remove all forms of amorphous, crystalline and organically bound iron and aluminium (Mahaney et al., 2010 and Coffin, 1963), ammonium oxalate to differentiate between organically bound and crystalline forms of iron, and finally, pyrophosphate to extract organically bound iron and aluminum (Skjemstad et al., 1989).

Particle-size studies on soil profiles, particularly the analysis of sand, silt and clay variations with depth, often provide important information on soil weathering regimes, e.g., the smaller the particle the more weathering it has undergone. Similarly, determining the cation exchange capacity (CEC) in terms of clay abundance is often used as a tool to evaluate the degree of soil weathering. Cation exchange capacity is a measure of the soil's ability to attract and retain cations, such as calcium, magnesium, and potassium. This ability is dependent on the degree to which the clay minerals are weathered. Thus, since each type of clay mineral has a different CEC range (Birkland, 1999), inferences can be made about the extent of weathered soil material based on the type of clay found and the CEC measured. For instance, a less weathered clay, such as montmorillonite (phyllosilicate), will tend to have large negatively charged surfaces, resulting in a higher capacity (i.e., higher CEC) to attract and retain cations. By contrast, highly weathered clay, such as kaolinite will result in a low CEC, in turn permitting increased leaching of base cations from the soil (Sposito, 2008). As a general rule of thumb, cations that have ionic potentials less than 3 tend to be the first released from their host minerals during weathering (Sparks, 2003).

The availability and solubility of cations and anions within a soil profile are also largely dependent on the pH of the soil. Thus, soil pH distribution with depth is an important factor to take into account when trying to determine a soil's weathering regime. At low pH, aluminum and hydronium aka proton become mobilized and will commonly replace the base cations on the exchange sites of the clay minerals. As a consequence, more base cations will be leached from the soil. Conversely, clay surfaces in alkaline soils will have exchange sites dominated by sodium ions and a high pH, causing the aluminium ions to precipitate as Al(OH)₃, thus rendering

them immobile (Sparks, 2003).

Weathering indices are widely used for representing the nature and impact of chemical processes on weathering in pedological studies (Birkeland, 1999). The main objective of this approach is to "identify elements at the Earth's surface considered to be mobile and express them as a ratio of the immobile components" (Darmody et al., 2005, p. 161). The basic idea underlying this approach is that as weathering progresses and mobile elements become increasingly modified or removed, this will change the mobile/immobile ratios.

The element ratios used for weathering indices tend to be based exclusively on an array of geochemical proxies from mineral alteration, which rely on the selective removal of soluble and mobile elements from a weathering profile (Buggle et al., 2010). These indices are often derived from bulk major and trace element analyses, which although very effective as indicators of the extent of weathering in homogeneous profiles, have proven to lose their utility when applied to heterogeneous soils, which have undergone processes such as eluviations (Price et al., 2003). The effectiveness of this method is further compromised when applied to paleosols because of diagenetic modifications or compaction (Usai, 1996).

Table 2.1. lists a number of element indices that have been used as proxies of mineral weathering for various kinds of soils.

Table 2. 1: List of weathering indices, in molecular proportions, and their descriptions

Weathering Indices	Molecular Equation	Description	Reference
Silica/Alumina Ratio	SiO ₂ /Al ₂ O ₃	Assuming the relative insolubility of Al2O3, the loss of SiO2 with weathering could be determined through molar ratios of SiO2/Al2O3.	Ruxton, 1968
Chemical Index of Weathering (CIW)	Al ₂ O ₃ /(Al ₂ O ₃ +CaO+ Na ₂ O)×100	Measures the extent of feldspar conversion to clays.	Harnois, 1988
Weathering Ratio (WR)	(CaO+MgO+Na ₂ O)/Ti O ₂	Index is based on resistant heavy minerals, whereby changes in the elements sodium, magnesium and calcium reflect changes in the amount of feldsparalso does not include Al or Si. Note that Ti can be replaced by Zr.	Chittleborough, 1991
Silica/ Resistant Ratio (SR)	SiO ₂ /(Al ₂ O ₃ +Fe ₂ O ₃ + TiO ₂)	Uses available data from analogous alpine environments (Norway and USA) against which to compare the calculated molar ratios of SiO2/Al2O3 in the study site.	Birkeland 1997
WI-1	(SiO ₂ +CaO)/(Fe ₂ O ₃ + TiO ₂)	Si and Ca are assumed to decrease on weathering and Fe and Ti increase relative to Si and Ca.	Darmody et al. 2005
WI-2	(SiO ₂ +CaO) / (Al ₂ O ₃ +Fe ₂ O ₃ +TiO ₂)	Because Al is a well-known resistant species and showed some variability in the data collected by Darmody et al. (2005), its contribution to the WI was tested by including it to the WI equation.	Darmody et al. 2005

Finally, according to Harnois (1988), for an index to be considered useful it should:

1. Include only those elements with a consistent geochemical behaviour during

weathering,

- 2. Be independent of the degree of oxidation of the weathered material.
- 3. Be simple and easy to use.
- 4. Involve elements commonly reported for soil analyses.

2.6. GROUND THERMAL MODELLING

One of the requirements for predicting future permafrost vulnerability to climate change is that the relationship that climate shares with permafrost development and degradation be properly understood. As mentioned above, coupled global climate models (GCMs) have been the main source of information for projecting future climate change scenarios across the globe. These models are based on feedback processes and climate sensitivity to these feedbacks. In essence, they simulate changes in climate state resulting from various radiative forcings, whereby "the constant of proportionality connecting radiative forcing to temperature change is a measure of the strength of the climate feedback processes operating in the system and hence of climate sensitivity" (Boer and Yu, 2003, pp. 416).

Surprisingly, permafrost has tended not be included in many of the global climate models. Recent efforts by scholars and also the Intergovernmental Panel on Climate Change (IPCC) have attempted to rectify this omission (Stendel et al., 2007). One such effort has involved developing a permafrost model that can be included in current and future GCMs. An example of this is provided by the study of Anisimov and Reneva (2006) in which a projection of the future distribution of permafrost in Russia was undertaken. The goal of this study was to evaluate the sensitivity of a permafrost model to forcing data obtained from five different GCMs, and

involved assessing the uncertainty associated with predicting permafrost parameters in several climate scenarios. The study showed that the predicted extent of permafrost varied considerably for the different climatic scenarios. This large variance in permafrost predictions using different climate warming scenarios has been noted in other studies conducted during the past decade. For example, a study by Zhang et al. (2007) projected a 16 to 20% decrease in permafrost area within Canada between 1999 and the end of the 21st century. In contrast, a study by Lawrence and Slater (2005), using similar climate warming scenarios, predicted a 60-90% global reduction in permafrost area for the same time period. Discrepancies in these predictions were explained by the large uncertainties associated with the forcing data used and the variation in the parameters employed to simulate ground thawing and freezing depths. The main sources of the variation in simulating ground thawing and freezing depths were identified by Zhang et al. (2008) as being: 1) the types of algorithms used; 2) the parameters used to represent the thermal properties of the frozen and thawed soil; 3) the treatment of the unfrozen water content of the frozen soils; 4) the parameterization of latent energy during thawing and freezing; and 5) the model configuration settings such as boundary conditions, soil layers and the resolution of the time step associated with the thawing and freezing processes.

The logistical feasibility of obtaining sufficient field data from permafrost environments in order to effectively simulate ground thawing and freezing remains a challenge (Zhang et al., 2008) and thus it is often necessary to resort to estimates of surface forcings, soil moisture contents and thermal properties, leading to additional sources of error in the permafrost models proposed by different studies (Romanovsky and Osterkamp, 1997; Luo et al., 2003; Zhang et al., 2003; Woo et al., 2004).

Generally, the above models are based on the thermal properties of permafrost-affected soils, which allows for the determination of permafrost presence and absence, active layer depth and mean annual ground temperature, through the use of empirical and statistical relations that stem from various transfer functions related to atmosphere and ground systems (Riseborough et al., 2008). One of the most widely applied analytical approaches that models heat conduction in soils is the Stefan formula (Woo et al., 2004). This formula is an algorithm that simulates onedirectional freeze and thaw penetration within a soil column, where the depth of freeze/thaw is a function of the thermal conductivity of frozen/thawed soil, the latent heat of fusion and the number of accumulated freezing/thawing degree days (Jumikis, 1977). In temperate and tropical regions, models based on the heat conduction theory have been proven to be unreliable due to the limitation imposed on them by the effects of heat transferral by mainly ground water circulation through soil pores and fractures. However, Gold and Lachenbruch (1973) concluded that, the heat conduction model can be applied with confidence in most permafrost regions as the groundwater in the soil systems is largely immobilised either by surface forces or as ice. Nonetheless, as shown in this thesis, it is possible that this confidence may be misplaced and that advective heat transfer during the relatively long and warm recent summers may be sufficient to significantly compromise the application of the Stefan formula in the lower Arctic.

PREFACE TO CHAPTER 3

Chapter 3 reports results of this thesis that are presented in the form of a scientific manuscript which will be submitted for publication in a peer-reviewed journal. Using data from analyses of the compositions of elements and their distributions within six soil profiles of a retrogressive thaw slump, a case is made that chemical processes play an important role in the weathering of polar soils. The chapter provides new insights into weathering within periglacial environments.

CHAPTER 3

Soil Weathering Processes on Herschel Island, Yukon.

Leigh-Ann Williams-Jones¹, Wayne H. Pollard¹, and William H. Hendershot²

¹ Department of Geography, McGill University, Montreal, QC.

² Department of Natural Resource Sciences, McGill University, Montreal, QC.

ABSTRACT

Previous research pertaining to soil weathering in the Arctic has focussed mainly on physical processes, related to freeze-thaw cycles, as the primary determinants of soil morphology. Very little consideration has been given to the possible role of chemical processes. Because of its relatively long and warm summer, Herschel Island, a glacier-derived ice-thrust structure located in the Southern Beaufort Sea, provides an excellent setting in which to examine the role of chemical soil weathering processes in the lower Arctic.

The island is composed of marine and coastal derived clay, sand and silt sediments, and is underlain by extensive massive ground ice bodies. Current and past climate variations on the island have led to the development of two thaw unconformities that separate; 1) the seasonally thawed modern active layer from the Hypsithermal-thawed paleo-active layer, and 2) the paleoactive layer or "transition zone" from the perennially frozen permafrost layer. Both thaw unconformities are characterised by a structural break in the cryostratigraphy as well as a marked change in the chemical composition of the soil. The thaw unconformity at the base of the current active layer contains an accumulation zone (32-39 cm), in which a doubling in the concentration of most exchangeable cations and a tripling in the soil organic matter content, relative to the overlying soil horizon, was observed. The soil material above this accumulation zone contains higher proportions of weathered material and silt sized particles than the underlying frozen layers. This is consistent with the higher ratios (weathering indices) of mobile over immobile elements in the bulk soil. Soil within the "transition zone" varies in its ice content, suggesting past periods of prolonged climate warming. Intervals of ice-enrichment are mirrored by peaks in cation accumulation and prolonged erosional activity. A strong marine chemical signature is

evident below the second thaw unconformity (157-192 cm) within the permafrost layer. This signature takes the form of high contents of sodium and sulphate ions in the pore water. An increase in clay contents was also observed within this zone, suggesting possible soil preservation.

The results of this study provide evidence for the role that chemical processes plays in the overall development of marine derived Cryosols on Herschel Island. They also demonstrate clearly that weathering in lower Arctic environments involves a complex interplay between physical and chemical processes.

Keywords: weathering; active layer; Hypsithermal; cryostratigraphy; Herschel Island

3.1 INTRODUCTION

The nature of weathering in permafrost-affected soil systems continues to be poorly understood, in large part, because studies of arctic soils have tended to focus primarily on mechanically driven processes that are associated exclusively with freeze-thaw cycles, such as frost action, and thermokarst development (Linell & Tedrow, 1981). Chemical weathering in these environments has been thought to be temperature-inhibited and thus of little significance. Models of weathering in polar environments have been based on three main concepts, namely 1) mechanical processes dominate weathering; 2) freeze-thaw is the predominant driver in these mechanical processes; and 3) low temperature renders chemical weathering processes insignificant in periglacial environments (Hall et al., 2002). However, freeze-thaw cycles also lead to changes in soil moisture, which is a major prerequisite for chemical weathering. In fact,

arctic soils are commonly associated with perched water tables and poorly developed drainage patterns. Permafrost is also invariably present in the Arctic, creating an impermeable layer that restricts the migration of water and leachable ions from the active layers into underlying frozen layers (French, 2007). Consequently, the soil becomes highly saturated, creating a gleying soil environment (Linell & Tedrow, 1981). Although the availability of water is an essential requirement for chemical weathering, the rate of chemical weathering increases with increasing temperature. In the case of polar environments, freeze-thaw cycles occur because temperature rises above 0°C during the summer, and then drops below it in the Fall. In the lower Arctic, air temperature typically averages > 10 °C for nearly two months, which may be sufficient to promote appreciable chemical weathering.

Opinion is currently divided over the extent and magnitude to which global warming will affect arctic landscapes and particularly the processes associated with soil systems. The association of global warming with increases in atmospheric CO₂ content, and the role of CO₂ in accelerating surficial weathering, provide an important impetus for re-evaluating chemical weathering in arctic environments. According to a number of researchers, the rate of surficial weathering, particularly of silicates, correlates positively with the rate of CO₂ addition to the atmosphere and is further increased by the rise in temperature, which accompanies the production of this greenhouse gas (White et al., 1999; Walker et al., 1981; Berner and Berner 1997). It is therefore reasonable to assume that with a warming soil thermal regime related to climate change, chemical weathering in Cryosols will become a more important pedogenic process and perhaps even rival that of physical weathering in the foreseeable future. This article re-examines the nature of weathering in periglacial environments in the context of a warming climate using data

collected from a site in the lower Arctic.

3.2 POLAR SOILS

In polar environments, physical constraints, such as permanently frozen/wet ground and short thaw seasons serve to significantly limit the frequency and magnitude of weathering processes within soil systems. The presence of a perennially frozen layer, i.e., permafrost, restricts soil weathering to the active layer, i.e., the surface layer that seasonally freezes and thaws (Keller et al., 2007). Between these two layers is an ice-enriched layer called the "transition zone" that undergoes freezing and thawing cycles over sub-decadal to centennial time-scales (Shur et al., 2005). Under warming conditions, this zone acts as the principal interface between the permafrost and the active layer, controlling the exchange of heat and material between these two environments (French, 2007). Most of the biological and chemical activity in arctic soils, however, takes place primarily within the active layer (Goulden et al., 1998). Consequently, changes in the composition of the atmosphere, particularly in respect to CO₂, are recorded by corresponding changes in the chemical and biological signature of the active layer.

Owing to the physical factors affecting soil genesis, such as freeze-thaw cycles, thermokarst production and cryoturbation, and the properties of the soil produced, polar soils have been classified into a separate soil taxonomic order, namely Cryosols (Agriculture Canada Expert Committee on Soil Survey, 1987). In the Canadian soil classification system, Cryosols form the highest order of soil classification and comprise organic or mineral soils, which contain a permafrost layer ≥ 1 m below the soil surface with no marked evidence of cryoturbation (Bockheim et al., 1998). These soils have been subdivided into three distinctive suborders, i.e.,

turbic, static and organic Cryosols (Agriculture Canada, 1987). Organic Cryosols are soils containing organic material and permafrost within the top 1m of the soil profile (The Canadian System of Soil Classification, 1998). By contrast, turbic and static Cryosols are composed of mineral soils with permafrost occurring within 2 m and 1 m, respectively, of the ground surface. Unlike organic and static Cryosols, for which there is no evidence of cryoturbation, turbic Cryosols contain one or more cryoturbated horizons that make up 1/3 or more of the soil profile (Bockheim et al., 1997; Ping et al., 1998; Bockheim et al., 1998).

Cryosols are the dominant soil order in the Arctic, and make up more than 8% of the ice-free land surfaces on Earth (Smith et al., 2004). They form over a relatively wide range of temperature and moisture content, vary in morphology, and all have in common the presence of permafrost (Smith et al., 2004; French, 2007). It is the combination of a downward moving freezing/thawing front from the soil surface and a slow upward moving freezing/thawing front from the permafrost table that mainly drive the processes of soil weathering (Rains, 2002). Therefore, any changes in the soil thermal regime from surface heating or permafrost degradation will affect pedogenic processes connected to weathering. Climate warming will accelerate these processes within the current active layer. However, the extent to which this will occur is still not known (Calmels et al., 2008).

In order to gain a better understanding of soil weathering processes in the Arctic, soil analyses were conducted on a natural exposure, namely a retrogressive thaw slump on Herschel Island, Yukon. These analyses were designed to assess rates of change of parameters related to particular weathering indices, and were both qualitative and chemical in nature. As a paleo-active

layer is also exposed, a secondary part of these analyses was to compare weathering in this layer to the modern active-layer.

3.2 STUDY SITE

The study was undertaken on Herschel Island or Qikiqtaruk, meaning "Island" in Inuvialuit, which is located 60 km east of the border between Alaska and the Yukon, and approximately 5 km north of the Yukon coast at 69°42′N, 139° '01 W (*Fig.3.1.*).

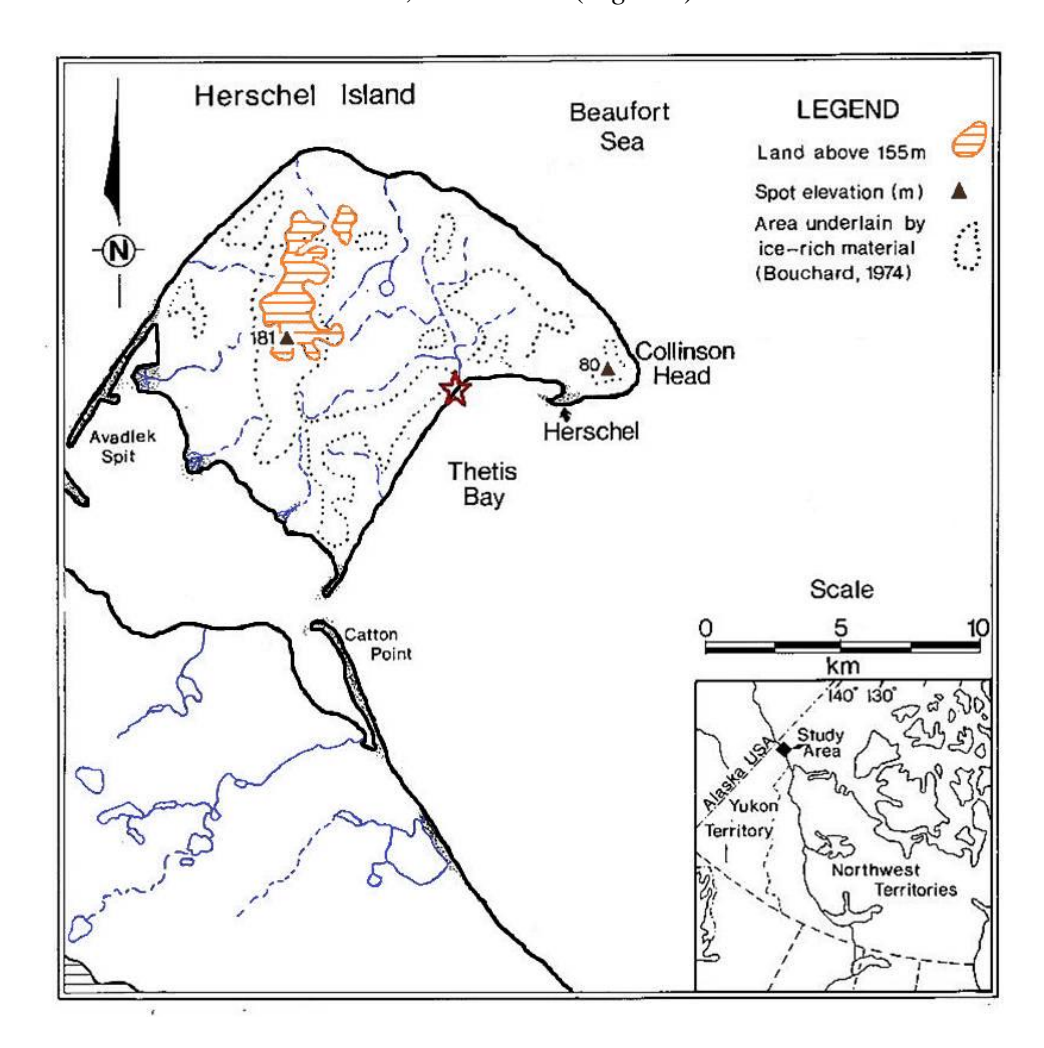


Fig. 3. 1: Map of Herschel Island showing the location of the study site indicated by the red star.

The island is an extension of the Yukon Coastal Plain physiographic region (Rampton, 1982), and is part of an ice-thrust feature formed during the Late Pleistocene (~40 ka BP), i.e., the Buckland Stage of the Wisconsinan glaciation (Mackay, 1959; Rampton 1982). Herschel Island is composed predominantly of fine-grained marine sediments and coastal deposits, and is underlain by massive ground-ice bodies that are thought to make up at least 50% of the near surface permafrost volume (Mackay, 1971; Pollard, 1990; Fritz et al., 2011). The large number of retrogressive thaw slumps along the Island's coast is an important indicator of the presence of these massive ground-ice bodies (Lantuit and Pollard, 2008).

Retrogressive thaw slumps are thermokarst features that develop when the rate of massive ice melt exceeds the rate of coastal erosion (Lewkowicz, 1987). They are therefore mainly activated by coastal erosion, and are considered a back-wasting type of thermokarst, which erodes in an inland direction, while removing extensive volumes of sediment (French, 2007). The average retreat rate of retrogressive thaw slump headwalls on Herschel Island is approximately 9.6 meters per year, outstripping the average coastal retreat rate of 0.6 meters per year (Lanuit et al., 2005). Most of these retrogressive thaw slumps are polycyclic in nature, meaning that they tend to stabilize and reactivate on a regular basis (*Fig. 3.2.*).



Fig. 3. 2: Aerial view of the polycyclic nature of retrogressive thaw slumps on Herschel Island (August 2004) Three active slumps (A1-A3) are evident within an older, stabilized slump (S).

Adapted from Lantuit and Pollard, 2005

The focus of this study is a natural exposure located at a retrogressive thaw slump (Slump A), part of which lies within an old slump floor ($Fig. 3.2. - A_3$), and the remainder of which is retreating into the undisturbed tundra land surface (Fig. 3.2. - U). Slump A is one of the few slumps on the island, which allows direct comparison of a disturbed and undisturbed headwall (Fig. 3.3.). Retrogressive thaw slumps, such as Slump A, serve to facilitate the examination of the near surface cryogenic stratigraphy, as well as a two-dimensional evaluation of a soil weathering profile.

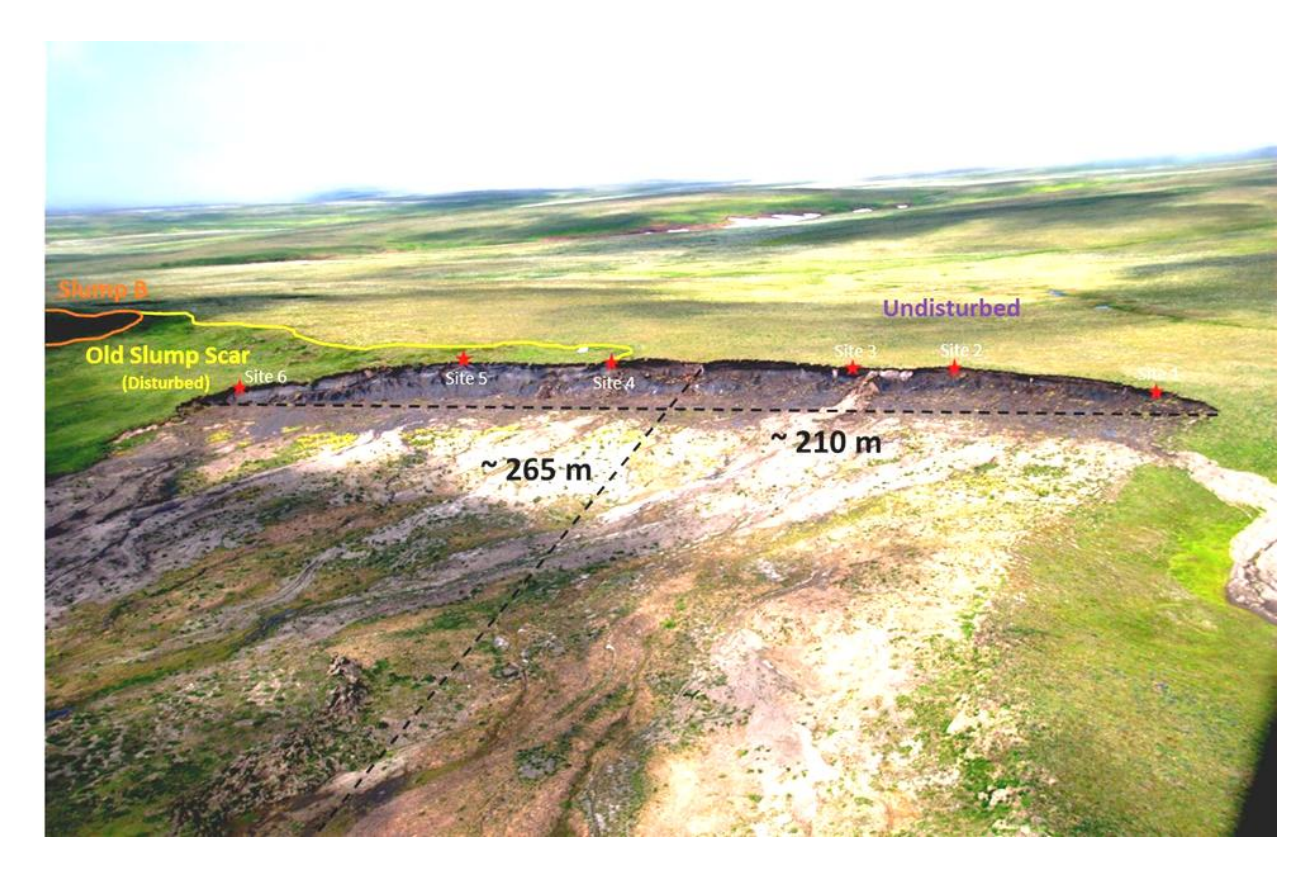


Fig. 3. 3: Aerial photo of Retrogressive Thaw Slump A with red stars indicating sampled soil profile sites.

(Photo Taken by Dr. Michael Krautblatter, 2011)

The headwall of the undisturbed part of Slump A exposes both the modern active-layer and the paleo-active layer, which is marked by a thaw unconformity (*Fig. 3.4.*) believed to have formed during the Holocene climatic optimum (i.e. the Hypsithermal warm period).



Fig. 3. 4.: Headwall view within the undisturbed section of Slump A, with lines demarcating the modern and paleo –active layer thaw unconformities.

Paleo-climatic studies undertaken in the Canadian western Arctic indicate that the early Holocene climate was approximately 2°C to 5°C warmer than it is today (Ritchie, 1984; Rampton, 1988). This warming led to the formation of a widespread thaw unconformity at the base of a paleo-active layer that was more than double the thickness of the current active layer (Mackay, 1978; Lantuit et al., 1995; Burn, 1997). The depth of the paleo-active layer on Herschel Island has been estimated to be 100 to 130 cm below the current erosional surface with a thaw-unconformity at its base (Burn, 1997; Kokelj et al., 2002). Note that these depths include excess ice and thus do not correspond to the true depth of thaw.

Six soil profiles were sampled from the headwall of retrogressive thaw slump A, on Herschel Island. As mentioned above, retrogressive thaw slumps provide natural two-dimensional exposures that help show the stratigraphic relationships between the modern-day active layer, past thaw events, thermokarst and static permafrost. Moreover, the dynamic nature of retrogressive thaw slumps ensures fresh exposure of soil/ice profiles. During the course of the present study, three soil profiles were examined within the undisturbed section of the slump (Fig. 3.3. – Sites 1-3), one at the border between the disturbed and undisturbed sections (Fig. 3.3. – Site 4) and two within the disturbed portion of Slump A (Fig. 3.3. – Sites 5 and 6). The headwall exposure in Slump A varies from 1 m to 5 m high, and reveals thick layers of supersaturated clay, clayey silt and organic matter above the permafrost and interspersed among the ice-rich permafrost (mainly clay and clayey silt) and massive ice layers. Sites 1,2 and 3 were chosen to investigate pedogenic processes and weathering profiles, and act as representative soil-landscape units, whereas sites 4, 5 and 6 were used to evaluate the extent of disturbance and distinguish between slump retreat into a primary headwall (sites 1-3) and slump retreat into a secondary headwall or old slump floor (sites 4-6). One of the main criteria for site selection within the undisturbed portion of Slump A was the presence of a paleo-active layer believed to reflect Hypsithermal thaw, a feature that is largely or completely absent within disturbed sites.

3.3 CLIMATE AND VEGETATION

Herschel Island is the site of a weather station maintained by Environment Canada, located at latitude 69°34'05.500" N and longitude 138°54'48.200" W, with an elevation of 1.20 m. The mean temperature, mean rainfall and total precipitation at this site for each month in 2010 and

2011, are reported in Table 3.1. The average daily temperature was above freezing (i.e., > 0°C) between June and September in both years, and was highest at the end of July and at the beginning of August. As active layer depth propagation is largely temperature dependent, active-layer thaw depth is likely to reach a maximum in mid to late August.

Table 3. 1.: Climatic Data for Herschel Island from January to December, 2010 and 2011.

Mean Temperatures (°C)	Jan.	Feb.	Mar.	Apr.	May	Jun.	Jul.	Aug.	Sept.	Oct.	Nov.	Dec.
2010	-24.3	-22.6	-22.5	-9.2	-4.5	3.9	10.1	9.3	2.8	-3.7	-9.8	-23.5
2011	-22.9	-20.5	-20.5	-17.7	-5.4	2.7	9.9	8.8	2.8	-4.2	-20.5	-23.3
Mean Rainfall (mm)												
2010	1.0	0.5	0.1	0.1	0.0	0.2	0.9	2.1	0.4	0.7	0.8	0.3
2011	0.3	1.2	0.2	0.4	0.4	0.6	0.5	0.5	0.5	0.3	0.1	0.2
Total Precipitation (mm)												
2010	31.4	12.7	3	2	0	6.6	28.4	65.6	12.6	21.1	23.9	8.7
2011	8.6	33.1	6.4	13.4	11	18.4	16.6	15.8	15	8.4	4.3	6.2

*Source: Environment Canada – Historical Climate Data

Data from an Active Layer Monitoring (ALM) grid located 2.5 m north of the headwall of Slump A indicate that the average active layer depth ranged from 11.4 cm to 44.8 cm between June, 24th 2011 and August 24th 2011 (*Fig. 3.5.*). The maximum depth of the active layer depth was reached near the end of July, and was above 50 cm at many locations within the ALM.

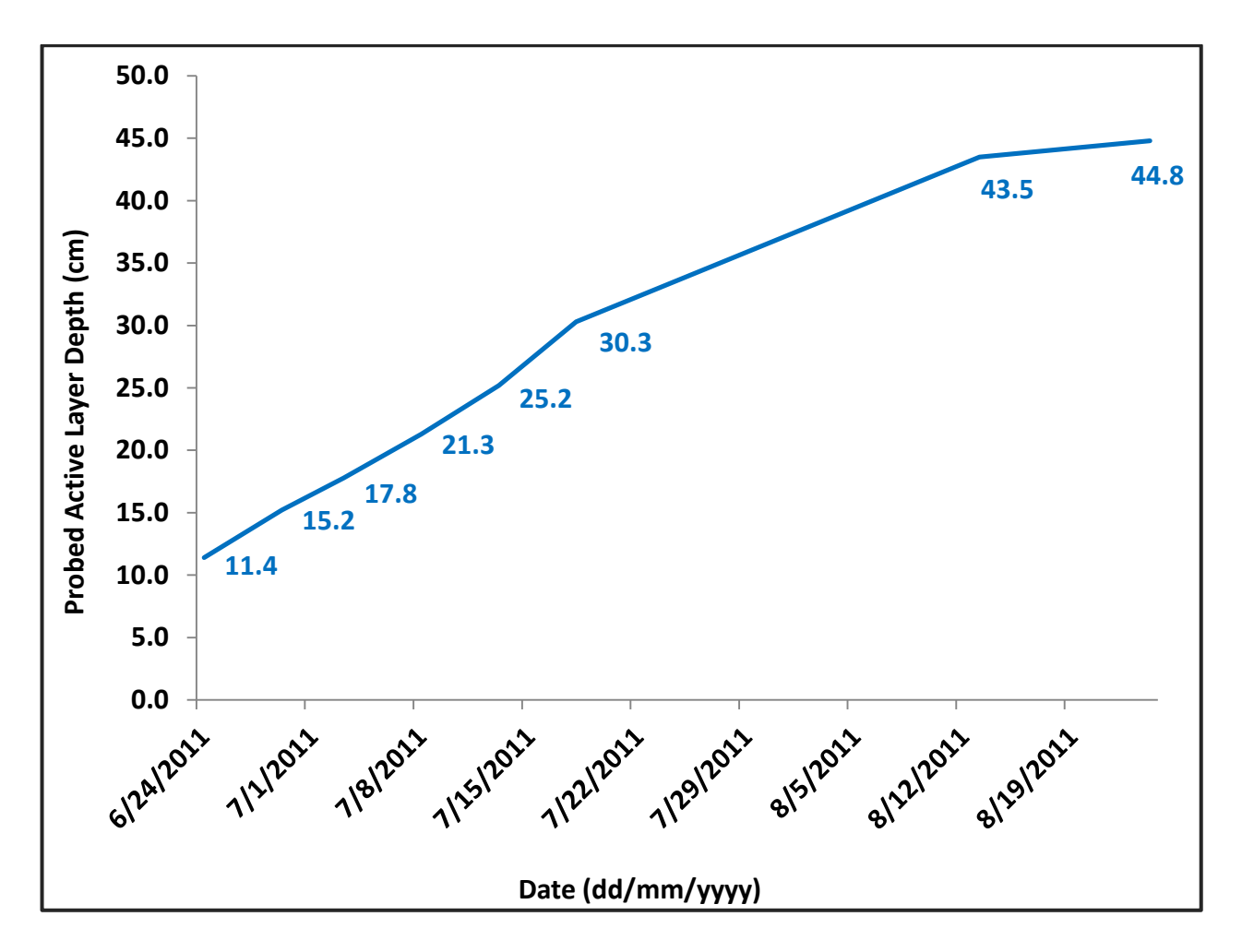


Fig. 3. 5.: Mean Active Layer Depths for the ALM site from June 24th to August 8th, 2011.

According to Statistics Canada, Herschel Island has an Arctic Tundra climate. Soil temperature data collected by Burn et al. (2009), at several sites around Collinson Head on Herschel Island, indicate a mean annual soil temperature at a depth of 1 m ranging from -7.8 to -8.3°C between 2003 and 2007. The average minimum soil temperature at the same depth for two of the ten sites studied by Burn et al. (2009) ranged from -19 to -21°C between 2004 and 2007 (Burn et al., 2009). Interestingly, the corresponding surface temperature during the same period and for the same sites was significantly lower, ranging from -36 to -41°C (Burn et al., 2009).

Herschel Island is covered predominantly by cotton grass and moss-type vegetation and its upland areas are dominated by the oldest and most stable landscape surface unit, namely tussock tundra (Smith et al., 1989). A prominent feature of the Herschel Island landscape is patterned ground, mainly in the form of non-sorted nets, circles and stripes (Washburn, 1980).

Finally, it is important point out that the glacial history of the island means that the sediments have been also heavily reworked. Nevertheless, it can be assumed that the reworked sediments were "dumped" in a somewhat uniform manner and that any changes in the soils are a reflection of modern-day or post-glacial processes. According to Rampton (1982), Herschel Island sediments can be subdivided into four basic units, namely 1) lower marine clay, 2) "mixed" preglacial sediments and peat, 3) marine clay, and 4) post-glacial lacustrine, terrestrial, colluvial and beach sediment, representing a typical Late Quaternary stratigraphy (Zazula et al., 2009). Other geomorphic and periglacial landforms on the island include: low centre polygons, unsorted nets and stripes, palsas, retrogressive thaw slumps and detachment slides (Burn and Zhang, 2009).

3.4 MATERIALS AND METHODS

Fieldwork for this study site was conducted at Herschel Island, Yukon from June 17th to July 24th, 2010, and involved collecting soil samples from six soil profiles within a retrogressive thaw slump (Slump A) and making detailed descriptions of each soil profile.

Soil profile descriptions were made using the Canadian Soil Information System (CanSIS) field manual, and included recording soil horizon boundaries, soil structure, root content, visual ice/sediment ratios, and colour. Soil samples were collected at 50 cm intervals within the frozen

layers, and at 5 to 10 cm intervals within the unfrozen layers. Subsamples were collected within these intervals wherever changes in colour or texture were evident. The soil samples were logged, double-bagged, stored in coolers in the Herschel Island ice-house and returned to a laboratory in Inuvik whenever air transport was available. All samples were maintained at a temperature below 2°C, and these temperatures were tracked using single-channel data loggers (Onset HOBO Pro Series).

Immediately on arrival in the soil science laboratory at McGill University's Macdonald campus, the soils were dried and passed through a 2-mm sieve. Dried colour descriptions were made with a Munsell Colour Chart. Measurements of pH and electrical conductivity were taken after adding a solution of distilled water to the soil so as to produce a soil-to-solution ratio of 1:2 for mineral and 1:8 for organic soil horizons (Hendershot et al., 1993). Particle size analysis was performed using the hydrometer method (Day, 1965) with a hexametaphosphate and sodium carbonate solution (Sheldrick et al., 1993). Samples containing >30 vol.% organic matter were pre-treated for particle size analysis using hydrogen peroxide to remove organic matter (Sheldrick et al., 1993). Soil organic matter content was determined using the Loss On Ignition (LOI) method (Schulte et al., 1991). This involved weighing the soil samples, drying them in an oven at a temperature of 105°C, weighing them again and further heating them in a muffle-oven to 360°C. After these steps, the sample was weighed once more and the organic carbon content was obtained from the difference between the weight after drying (at 105°C) and the final weight of the sample. Exchangeable cation concentrations (Na⁺, K⁺, Ca²⁺, Mg²⁺ and Mn²⁺) were measured by extracting the soils with a 0.1M BaCl₂ solution and analysing the leachate with an atomic absorption spectrometer. The cation exchange capacity (CEC) for each sample was taken to be

the sum of the concentrations of Na⁺, K⁺, Ca²⁺, Mg²⁺ and Mn²⁺ in the extract after correction for dilution and the mass of soil used (Hendershot et al., 1993). Base saturation was taken as the sum of the bases divided by the CEC multiplied by 100 (Hendershot, 1984). Iron, Al and Mn were extracted from soil samples ground to <0.15 mm using: 1) the sodium pyrophospate method (McKeague, 1967); and 2) the acid ammonium oxalate method (McKeague et al., 1966). The first method provided for extraction of the organically-complexed forms of these elements, and helped identify buried Ah horizons, whereas the second method enabled extraction of the sesquioxide weathering products of the soil and allowed determination of the non-crystalline or amorphous organic and inorganic forms of these elements (McKeague et al., 1966). After the extractions, the solutions were analysed for Fe, Al and Mn using an atomic absorption spectrometer. The bulk content of the major and some trace elements in the soils was determined using X-Ray Fluorescence (XRF) analysis following lithium tetraborate fusion. This analysis and the measurement of LOI (complete versus the partial LOI described above) were conducted by ACME Analytical Laboratories (Vancouver, BC).

3.5 RESULTS AND DISCUSSION

As mentioned earlier, six soil profiles were sampled in the active headwall of a retrogressive thaw slump. The slump headwall is approximately 210 m in width, varies in height from 0.4 m to 4.6 m and extends approximately 265 m from the shoreline to the centre of the slump wall (*Fig. 3.3.*). Site 4 marks the border of the disturbed and undisturbed sections of the slump. The designation of soil profiles as being previously disturbed or undisturbed reflects the extent of past retrogressive thaw slump activity, and this was based on criteria related to the

macroscopically observable presence or absence of re-incorporated organic material within the active layer (*Fig. 3.6.*).

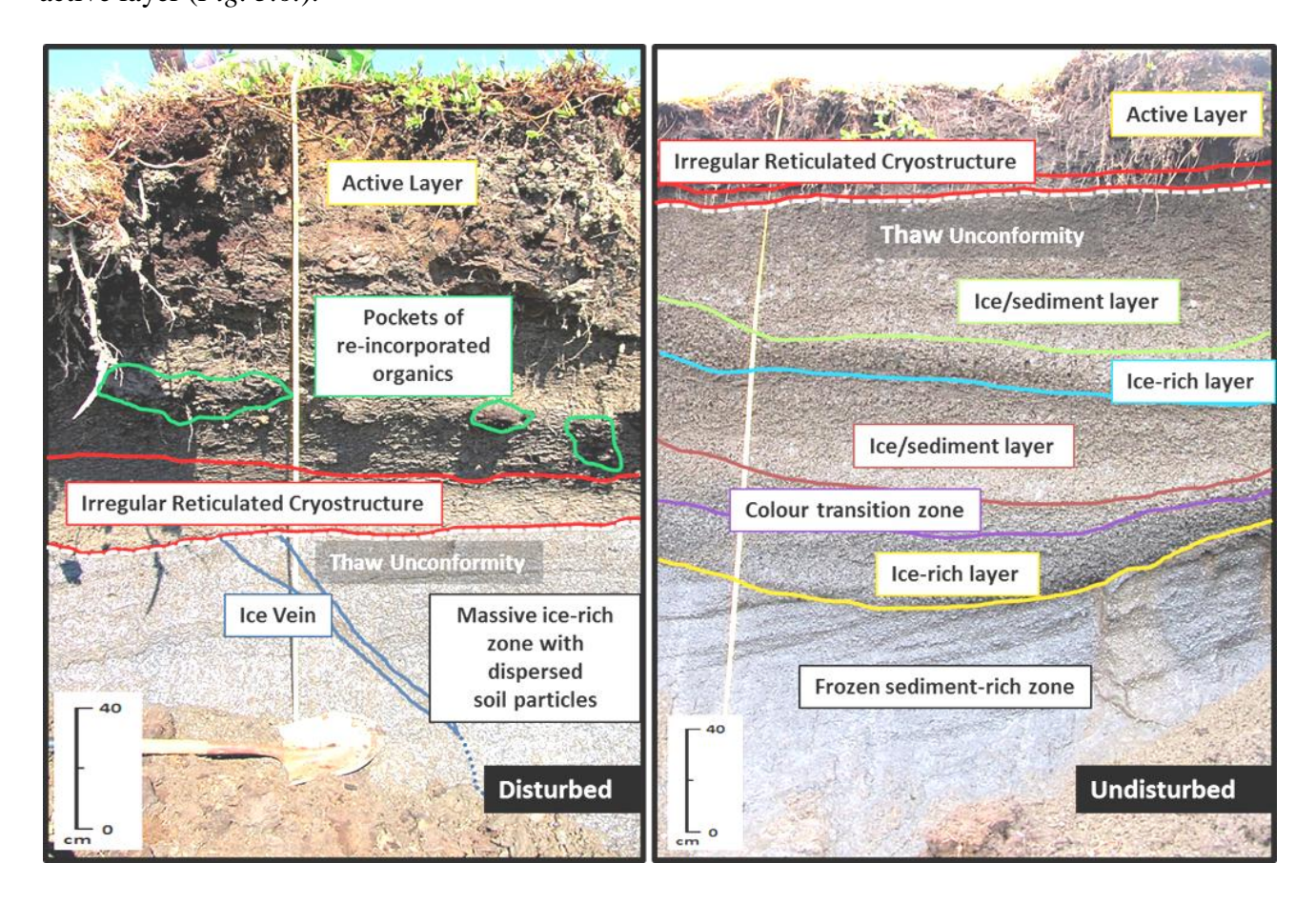


Fig. 3. 6.: Annotated photographs of soil profiles at sites 5 (202cm) and 3 (282cm).

3.5.1. THE SOIL PROFILES

Based on soil morphology, the soil profiles were divided into two groups, namely disturbed (i.e., those profiles representing the old slump floor) and undisturbed (i.e., newly exposed material). Within the disturbed profiles, the active layer extends to a depth of about 100 cm below the ground surface, whereas in the undisturbed profiles this depth is < 40 cm. Two features that are common within the modern active layer zone and present at all the sites are: 1) a thaw unconformity, i.e., a discontinuity in the nature and distribution of ice bodies, due to either thawing of frozen ground or subsequent refreezing of previously thawed material (French, 2007);

and 2) an irregular reticulated cryostructure layer. The latter is located immediately above the thaw unconformity at all sites, but varies in depth from between 100-120 cm in the disturbed sites to 35-40 cm in the undisturbed sites (*Fig. 3.6*).

According to Mackay (1974), reticulated ice layers are common in periglacial environments and are due to the shrinkage of adjacent clays. Ice veins form vertically and shrinkage cracks horizontally, drawing the bulk of their water from the adjacent clay, in turn, causing the clay to become consolidated. Consequently, thawing of these reticulated ice structures yields very little excess water and thus the retreat of the thaw face is maintained instead by either lateral erosion or by the thawing of the underlying ice-rich soils (Mackay, 1974). It is also important to note that the formation of reticulated ice layers occurs within a semi-closed hydrological system as opposed to an open hydrological system in which water migration proceeds upwards.

The thaw unconformity serves as a demarcation between permafrost and a thaw event that disrupts the primary cryostructure. In the undisturbed profiles, an unconformity occurs at a depth of ~ 40 cm, whereas in the disturbed profiles, the unconformity is at a depth of 120 cm in two of the sites and at 100 cm in the site located at the north-west end of the retrogressive thaw slump (i.e., site 6).

Soil profiles within the disturbed section of the slump are underlain by a permafrost layer, located immediately below the debris flow material that make up the present active layer, and is composed mainly of dispersed sediments embedded in an ice-rich matrix (massive ice). In contrast, the soil profiles located in the undisturbed section of the slump have a permafrost

segment that consists of multiple layers with varying ice and sediment contents. The deepest of these profiles (site 3) contains a C horizon that varies semi-continuously from ice-rich to ice-poor (*Fig. 3.7.*).

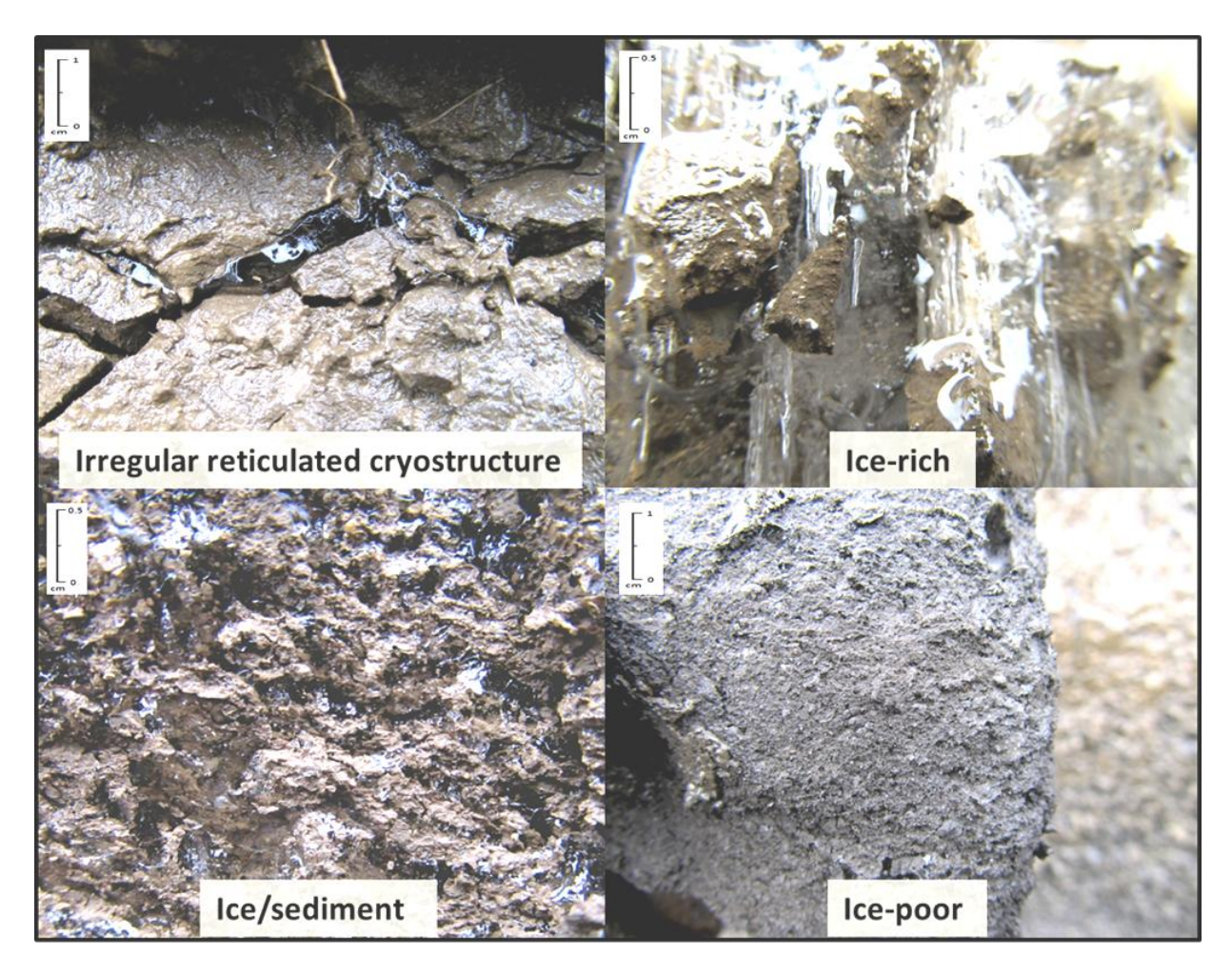


Fig. 3. 7.: Macroscopic examples of soil material with varying ice and sediment content.

At most of the undisturbed sites there is a visible colour change from light greyish-brown (10YR 7/2) to a grey to light grey (10YR 6/1) marking the transition from ice-rich to ice-poor. This transition is most pronounced at site 3 (*Fig. 3.8.*).

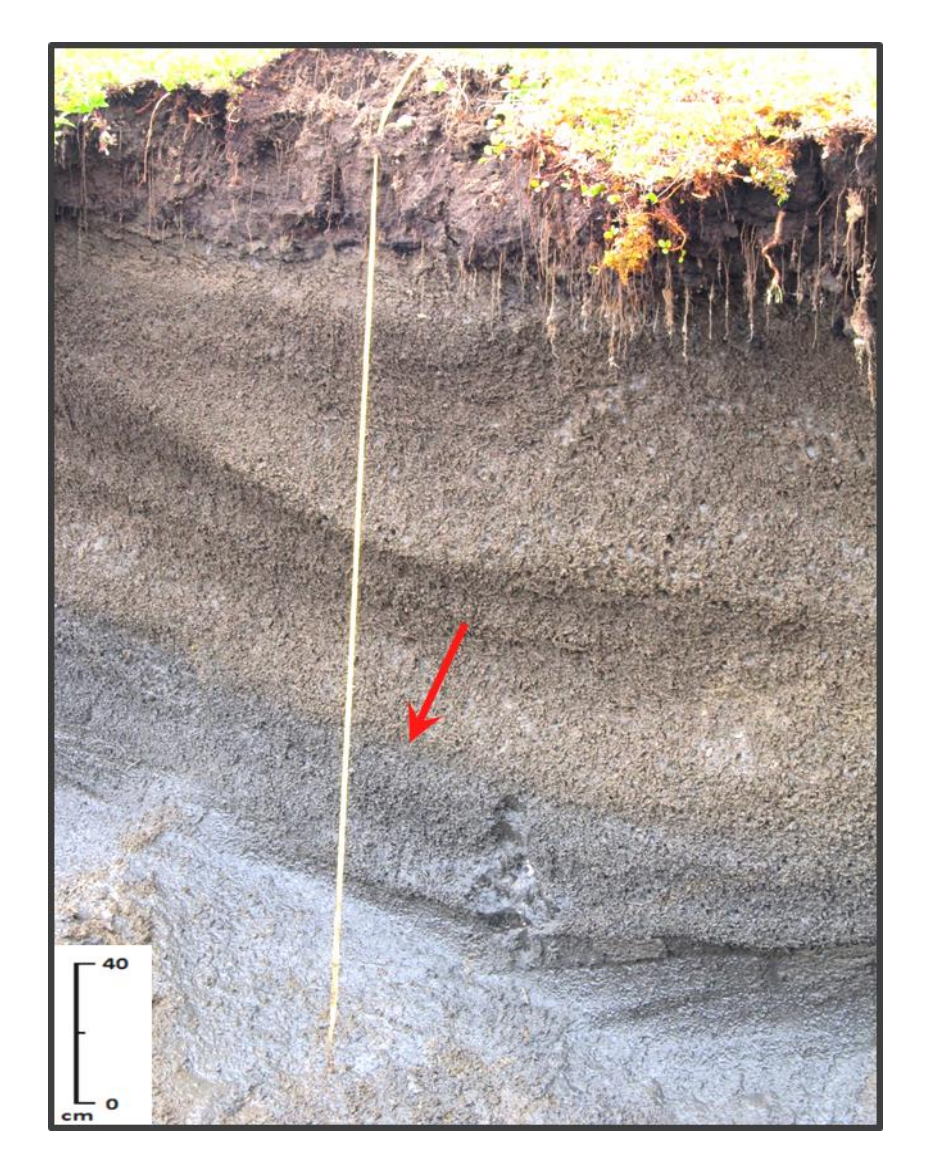


Fig. 3. 8.: A photograph of the soil profile at site 3, showing a change in colour (red arrow) from greyish brown (10YR 7/2) to light grey (10YR 6/1).

Possible explanations for the absence of a massive ice zone within the undisturbed sections could be: 1) there is no massive ice in the undisturbed section; or 2) the massive ice layer at these sites occurs at a much greater depth than in the disturbed sites. The latter seems to be the most likely explanation and is supported by two lines of evidence. The first of these is that the disturbed sites show clear signs of having undergone extensive thaw subsidence and the second is that the massive ice zones within the disturbed section of the slump have been subjected to normal

faulting. The faulting would have led to greater uplift of the disturbed section due to unloading associated with thermokarst or the overriding of ground material by an ice-sheet, resulting in the displacement of the undisturbed layer downwards. (*Fig. 3.9. and Fig. 3.10.*).

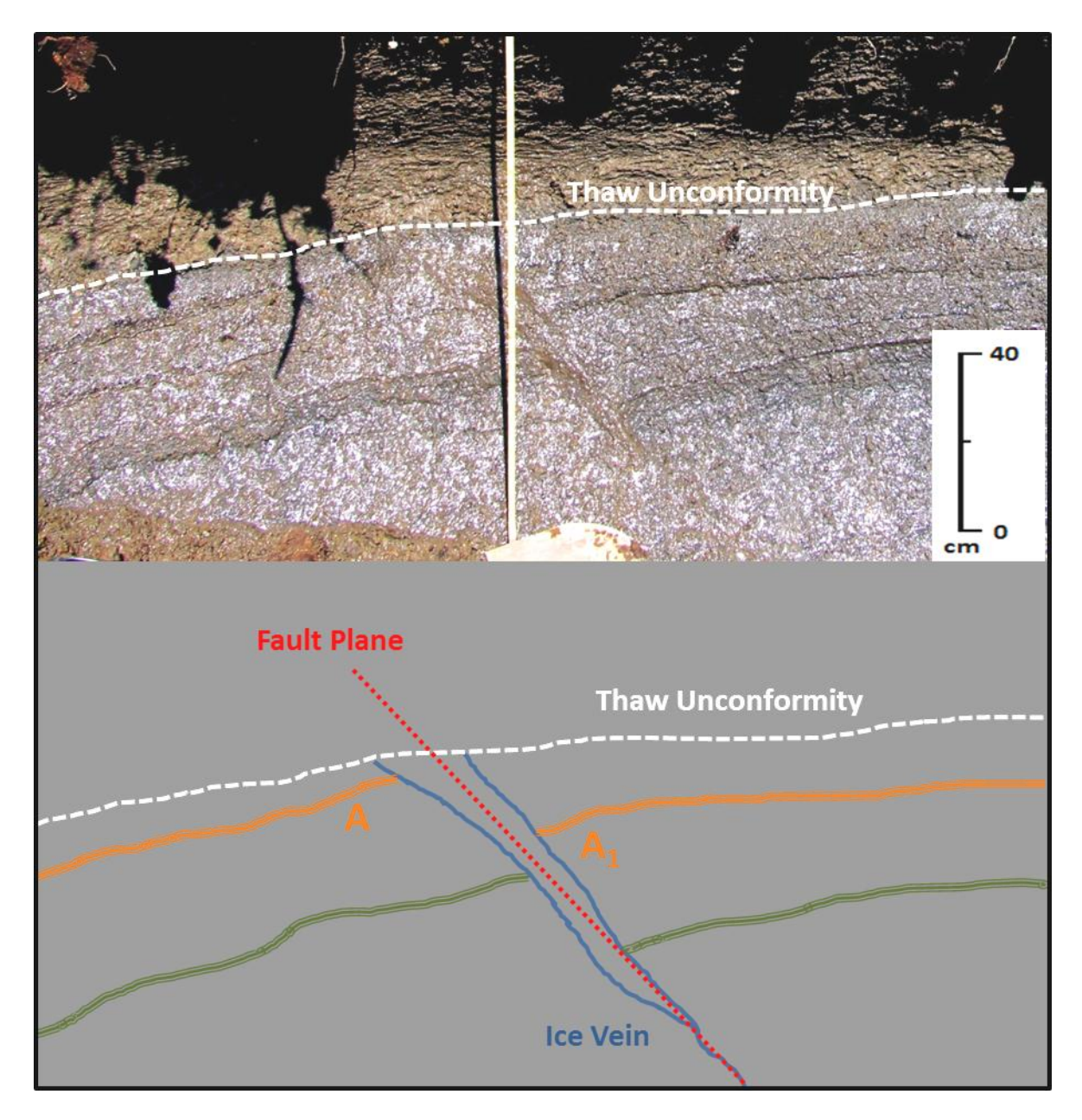


Fig. 3. 9.: Depiction of a normal fault within the massive ice section at site 5. The vertical drop from A to A1 is approximately 26.5 cm

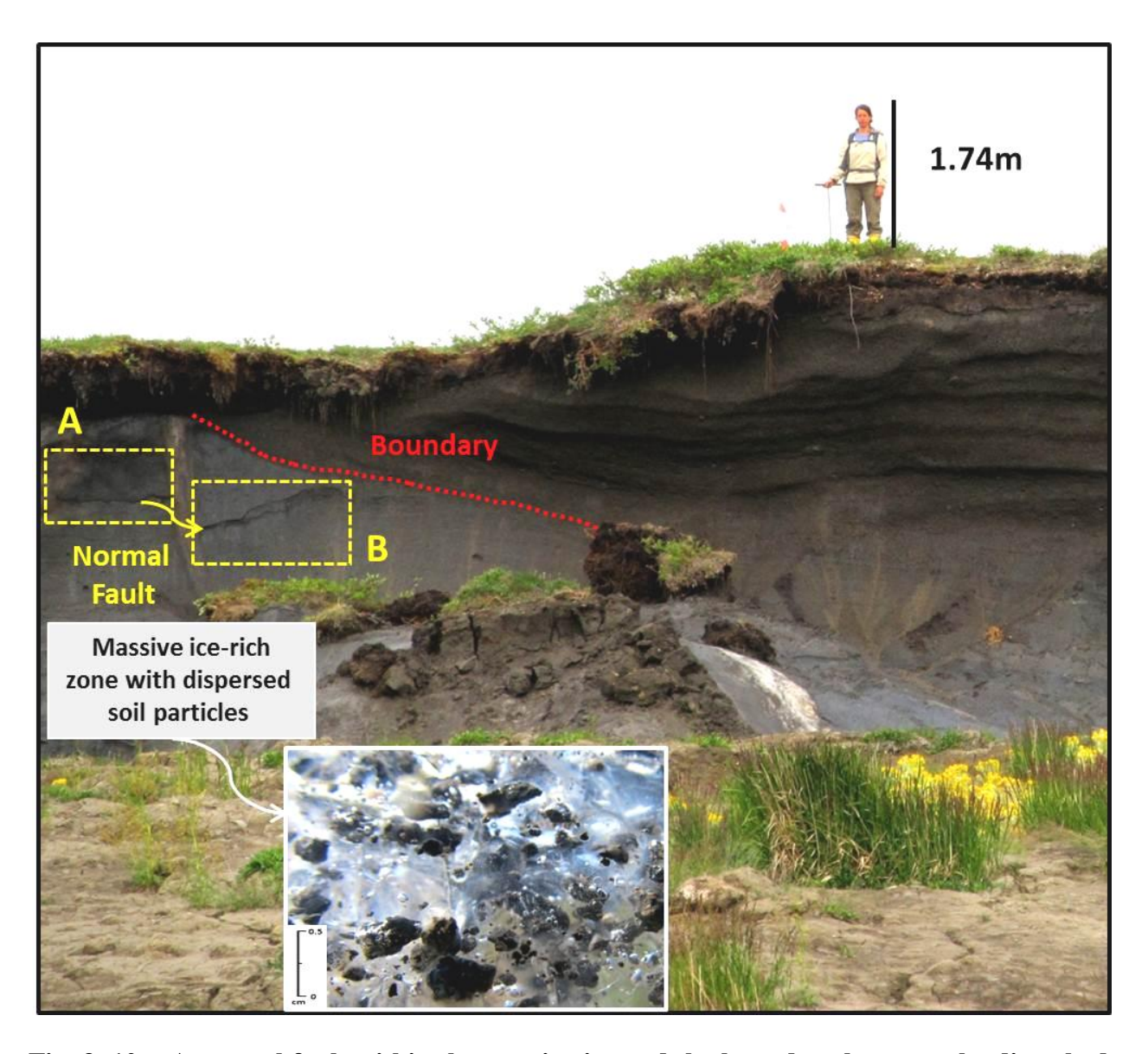


Fig. 3. 10.: A normal fault within the massive ice and the boundary between the disturbed and undisturbed soils, near site 4. The vertical drop from A to B is approximately 48cm.

In addition to massive ice deformation, all of the soil profiles within this slump show evidence of horizons that were disrupted by cryoturbation, namely tongues of mineral and organic material interspersed vertically within the present active layer (*Fig. 3.11*.). There are also oriented stones within the disturbed soil profiles. All these features are indicative of freeze-thaw cycling (Tedrow, 1977).

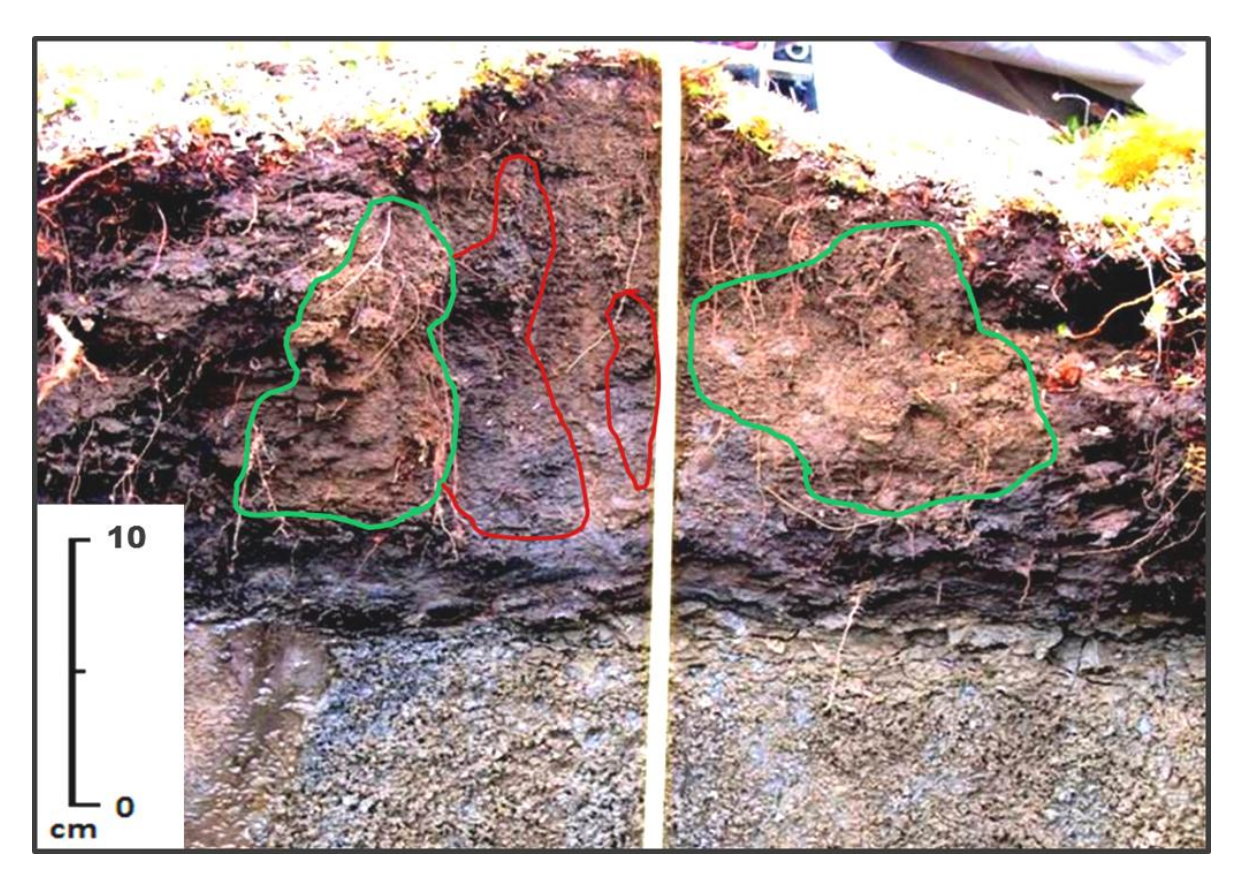


Fig. 3. 11.: A photograph of the soil profile at site 2 showing evidence of cryoturbation disruption. Mineral tongues are outlined in green and organic tongues in red.

All the soil profiles have B horizons with pH values above 5.5 and have an overall high degree of base saturation (*Table 3.2*). The horizon situated immediately above the thaw unconformity (i.e., the irregular reticulated cryostructure zone) shows evidence of gleying, a characteristic most likely associated with a perched water table above the permafrost layer (Linell and Tedrow, 1981). However, in general, distinguishable horizons are not strongly developed in any of the soil profiles. All of the above soil attributes are indicative of an orthic entric turbic Cryosol (Soil Classification Working Group. 1998).

Table 3. 2.: pH and electrical conductivity (EC) values of soil profiles sampled at Slump A.

		UNDISTURBEI)			DISTURBED	
•	Depth	рН	EC	'	Depth	рН	EC
	(cm)		(mS/cm)		(cm)		(mS/cm)
SITE 1	0-3	7.54	0.39	SITE 4	0-1	6.65	0.23
	3-13	6.83	0.11		1-21	6.06	0.25
	13-28	6.99	0.14		21-36	6.4	0.14
	28-33	7.41	0.51		36-45	7.09	0.12
	33-43	7.8	0.2		45-56	7.82	0.24
	43-53	8.06	0.34		56-71	8.2	0.39
	53-73	7.94	0.43		71-101	8.02	0.76
	73-103	7.28	0.85		106	7.57	1.85
	103-153	7.54	1.53		101-126	7.95	0.92
SITE 2	0-2	6.17	0.22		126-151	7.51	2.08
	2-7	5.87	0.14		151-191	7.68	1.55
	7-12	6.24	0.12		191-201	7.79	1.13
	12-17	6.61	0.14	SITE 5	0-2	7.42	0.15
	17-22	7.25	0.14		2-12	7.31	0.17
	22-27	7.55	0.15		12-32	7.57	0.24
	27-32	7.65	0.16		32-47	7.61	0.21
	32-37	7.73	0.17		47-67	7.95	0.27
	37-42	7.44	0.18		67-82	8.08	0.48
	42-47	7.98	0.39		82-102	7.83	1.55
	47-122	7.61	3.44		102-127	7.06	1.38
SITE 3	0-2	6.47	0.17		127-157	7.42	0.51
	2-12	6.09	0.13		157-202	7.94	1.09
	12-22	7.29	0.15	SITE 6	0-3	7.25	0.23
	22-32	7.82	0.18		3-8	7.58	0.16
	32-39	6.7	0.2		8-18	7.95	0.17
	39-47	8.1	0.4		18-28	7.94	0.18
	47-82	8.27	0.38		28-43	7.25	0.14
	82-107	8.08	0.46		43-57	7.78	0.22
	107-157	7.85	1.22		73-83	6.9	0.57
	157-192	7.89	1.87		57-108	7.69	0.32
	192-282	8.29	2.4		108-153	7.53	0.93

3.5.2. PARTICLE SIZE AND EXCHANGEABLE CATIONS

Sand, silt and clay from site 3 within the undisturbed section of the slump were analysed to determine the degree of soil modification with depth. The profile is characterised by an upward

increase in silt from 41 wt. % at the base of the profile to 50 wt. % at the surface. This trend is mirrored by an upward increase in sand content from 11 wt.% to 27 wt.%. In the case of clay, however, this distribution is reversed, and there is a downward increase from 23 wt.% at the surface to 48 wt.% at the base of the profile (*Table 3.3.*).

Table 3. 3. : Changes in soil characteristics with depth for site 3.

	Exchangeable Cations													
Depth	Sand	Silt	Clay	Ca	Mg	K	Na	Mn	CEC	B.S.	рН	EC	SOM	
cm .		% _			_ cmol	(+)	kg-1 —			- %		mS/cm	%	
0-2	27	50	23	55.7	16.2	1.2	0.5	0.1	73.8	99.8	6.5	0.2	35.6	
2-12	17	46	37	24.0	8.4	0.3	0.3	0.1	33.2	99.6	6.1	0.1	11.7	
12-22	16	50	34	30.6	7.1	0.4	0.2	0.0	38.3	99.9	7.3	0.2	11.1	
22-32	16	47	37	34.2	6.8	0.5	0.2	0.0	41.7	100.0	7.8	0.2	11.3	
32-39	17	49	35	73.5	13.2	0.6	0.5	0.2	88.1	99.7	6.7	0.2	34.4	
39-47	15	43	42	12.1	6.6	0.6	0.3	0.0	19.6	99.8	8.1	0.4	3.8	
47-82	13	42	45	8.8	5.9	0.6	0.4	0.1	15.8	99.6	8.3	0.4	2.5	
82-107	12	46	42	9.0	5.0	0.6	0.4	0.0	15.1	99.8	8.1	0.5	2.4	
107-157	12	44	44	8.9	5.5	0.6	1.5	0.0	16.5	99.8	7.9	1.2	2.2	
157-192	11	42	48	8.4	5.7	0.3	2.7	0.0	17.0	99.8	7.9	1.9	2.7	
192-282	11	41	48	5.3	5.5	0.4	6.0	0.0	17.2	99.9	8.3	2.4	2.9	

Note: $cmol(+) kg^{-1} = 1 meq / 100g$

The predominance of silt as opposed to clay in the upper parts of the profile may indicate an airfall influx of silt sized particles (Forman et al., 2002) or the physical weathering of surrounding sediments (Tedrow, 1977). The texture of these soils ranges from that of a silty loam at the surface, to a silty clay loam and silty clay at depth.

Measured cation exchange capacities (CEC) correlate strongly with organic matter content as opposed to clay content, i.e., horizons with higher clay content and lower soil organic matter content have lower cation exchange capacity. This trend is clearly evident for site 3 (*Fig. 3.12*.),

and suggests that the driving force for higher CEC cmol(+)/kg values in the upper horizons is organic matter and possibly amorphous sesquioxide-coated material. Measurements of CEC cmol(+)/kg can also be used to assess clay mineral proportions, as different clay minerals have different CEC values (Birkeland, 1999). Based on the data for site 3, it is evident that the bulk of the CEC/kg values (6 samples) cluster between 15.12 and 19.64 for organic carbon contents mainly between 2.2 and 2.9 wt.%, and that the X-axis intercept of the trend (zero organic matter) corresponds to a CEC of 11.73 (*Fig. 3.12*.). Given that the soils with CEC values between 15 and 20 have clay mineral contents of 42 to 48 vol.% (*Table 3.3*.), it seems likely that soils represented by the CEC cmol(+)/kg X-axis intercept value of 11.73 will have similar clay mineral contents.

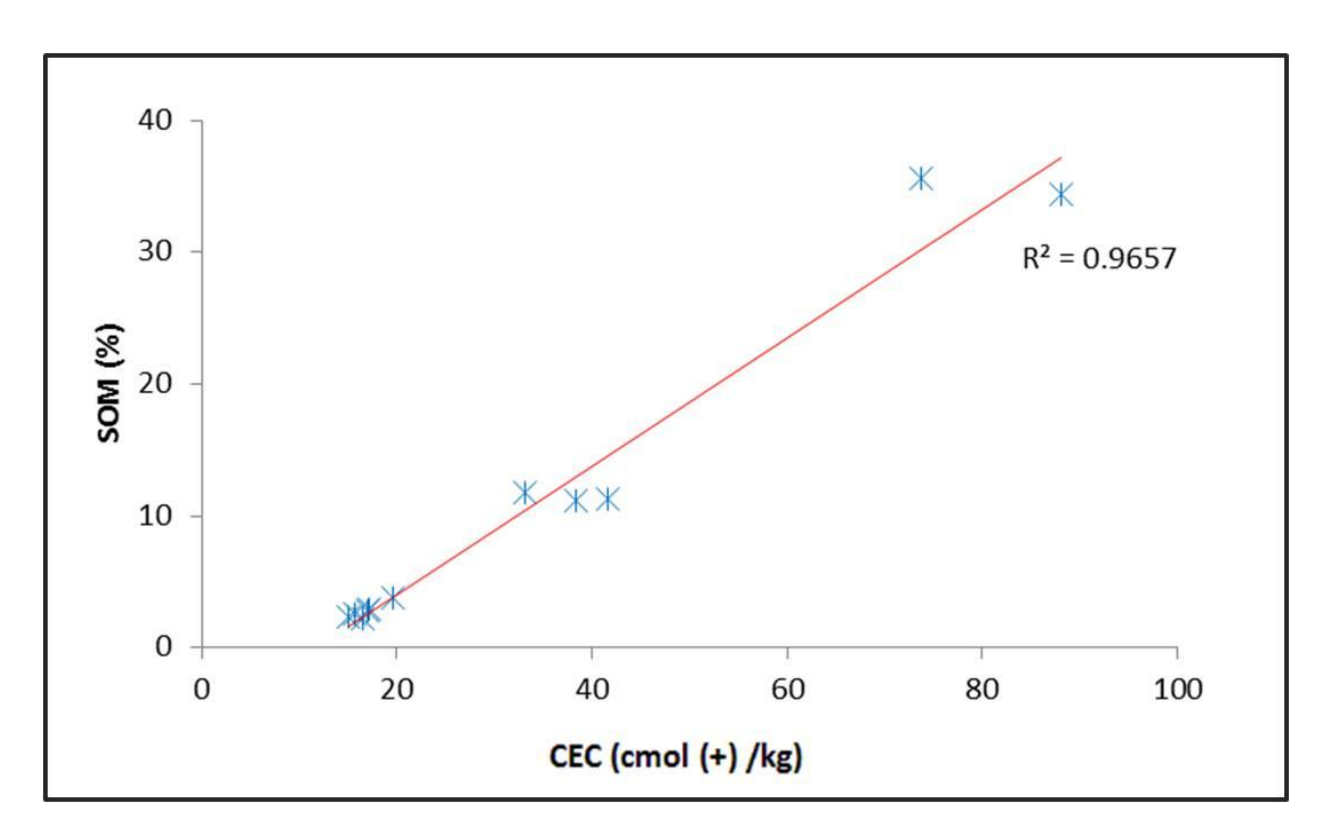
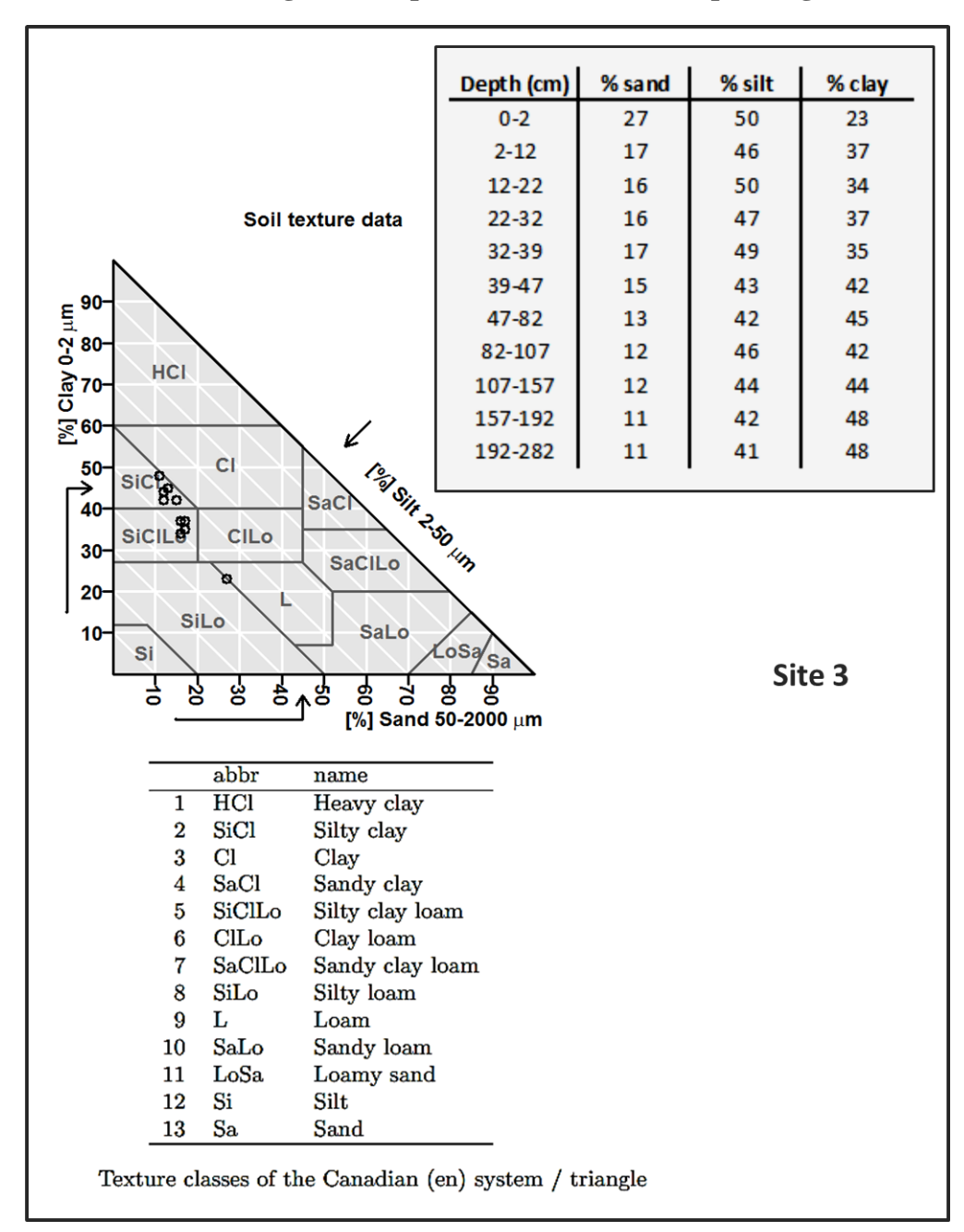


Fig. 3. 12.: Relationship between the soil organic matter content (SOM) and the cation exchange capacity (CEC).

Table 3. 4.: Particle size change with depth for site 3 and corresponding textual triangle.



(input package for R software used - Moeys, 2012)

The corresponding CEC cmol(+)/kg of the clay mineral or minerals making up this soil would be ~ 25 cmol(+)/kg, which according to the data of Meunier (2005) reported in *Table 3.5* identifies it as illite or perhaps a mixture of illite and chlorite. It should be cautioned, however, that the data of Meunier (2005) are for a pH of 7, whereas the measured pH of the organic-poor soils was

approximately 8. At this higher pH, the mineral CEC cmol(+)/kg values would be somewhat lower but would probably still identify the mineral as illite.

Table 3. 5.: Approximate values of the CEC of the main clay mineral species at pH 7.

Mineral	CEC (cmol (+) kg ⁻¹)
Kaolinite	5-15
Chlorite	5-15
Illite	25-40
Vermiculite	100-150
Montmorillonite	80-120

(Meunier, 2005)

The above interpretation is consistent with results of several previous studies in the Western Arctic, which have established illite as the dominant clay mineral in Arctic marine sediments (Ortiz, 2011); chlorite is the dominant clay mineral in the Pacific (Kalinenko, 2001). Since suspended sediment is carried by water flowing through the Bering Strait from the Pacific to the Arctic, mixing of these two clay minerals is likely (Ortiz, 2011). Moreover, clay size fractions dominated by illite and chlorite are indicative of a cold and dry environment in which the intensity of weathering is low, i.e., an environment similar to that found on Herschel Island (Bockheim, 1982; Campbell and Claridge, 1982).

The highest concentration of exchangeable cations occurs at a depth between 32 and 39 cm. At this depth, the concentrations of Ca and Mg are almost double their concentrations in the soils immediately above it (*Table 3.3.*). Moreover, the cation exchange capacity reaches a maximum of 88.1 cmol(+)/kg. The only other horizon with relatively high concentrations of exchangeable cations and cation exchange capacity (73.8 cmol(+)/kg) is the surface layer. Like the surface

layer, which has the highest soil organic matter content (35.6 wt.%), the organic matter content of the interval at 32 to 39 is very high (34.4 wt.%), over three times higher than the sample interval with the next highest organic matter content. Significantly, the 32-39 cm depth interval coincides with the transition zone between frozen and unfrozen soil. Therefore, the increase in soil organic matter and exchangeable cations could be attributed to the process of accumulation, in which the underlying frozen soil horizon acts as an impermeable layer, restricting the penetration of leachable ions from the active layers into the underlying frozen layers (French, 2007). The result is a soil horizon that is highly saturated in ions, and gleyed (Linell and Tedrow, 1981). This description accurately captures the nature of the soil in the 32-39 cm sample interval.

3.5.3. PROFILE DISTRIBUTION OF EXTRACTABLE IRON, ALUMINUM, AND IRON, ALUMINUM OXIDES

Two important weathering reactions involving Fe³⁺ and Al³⁺ are the creation of organo-metal complexes and the formation of metastable hydroxides. In order to determine the concentrations of metal ions associated with these two processes, cations were extracted using sodium pyrophosphate and ammonium oxalate (McKeague et al., 1971). As mentioned above, the sodium pyrophosphate extraction releases metals chelated by organic acids, and thus provides a direct measure of the concentration of metals bound to soil organic matter. The ammonium oxalate extraction method, in contrast, removes metals bound (adsorbed) to both organic matter and non-crystalline (amorphous) inorganic material produced during weathering. As Fe and Al species may be bound to both organic and inorganic material, the concentration of Fe and Al bound to non-crystalline inorganic material was determined by the difference in the concentration of these metals measured using the two extraction methods (Stumm, 1992; Masiello et al., 2004).

The concentrations of Fe determined by ammonium oxalate extraction, i.e., the extractable oxalate fraction of Fe (Fe_o), range from 0.05 to 0.15 g/kg, with the highest concentrations occurring near the bottom of the profile at depths between 157 and 282 cm (*Table 3.6*). The Fe_o ion contents range between 0.01 and 0.05 g/kg and, as might be expected, are highest in the 32-39 cm interval. Interestingly, the 2-12 cm interval has the next highest content of Fe_o ions rather than the overlying, organic-rich surface layer. In the permafrost, all intervals sampled have Fe_o ion contents of 0.01 g/kg Fe_o except for the interval immediately below the active layer, which contains 0.02 g/kg of Fe_o.

Inorganically bound Fe (Fe_p) concentrations vary between 0.03 and 0.14 g/kg and reach peaks at 39-47 cm, i.e., immediately below the thaw unconformity (0.08 g/kg) and between 157 and 192 cm. Concentrations of Al determined by ammonium oxalate (Al_o) extraction are much lower than those obtained for Fe_o, and vary from 0.01 to 0.02 g/kg. The Al_o ion concentration is 0.01 g/kg in all intervals sampled within the active layer, except for the 32-39 cm interval (0.02 g/kg), and is below detection in the permafrost. Only two intervals in the active layer, 12-22 and 22-32 contain detectable Al_p (0.01 g/kg).

Table 3. 6.: Changes in extractable Fe, Al and Mn with depth for site 3.

Extractable Ions												
Depth	Fe _f	Fe _o	Fe _p	Al _o	Al_p	Fe _{o-p}	Al _{o-p}	pН	SOM			
cm -				— g/kg —					%			
0-2	0.09	0.05	0.02	0.01	0.01	0.030	0.00	6.5	35.6			
2-12	0.13	0.08	0.04	0.02	0.01	0.042	0.00	6.1	11.7			
12-22	0.15	0.09	0.03	0.02	0.01	0.053	0.01	7.3	11.1			
22-32	0.13	0.07	0.02	0.02	0.01	0.049	0.01	7.8	11.3			
32-39	0.14	0.09	0.05	0.02	0.02	0.032	0.00	6.7	34.4			
39-47	0.17	0.10	0.02	0.01	< DL	0.085	0.06	8.1	3.8			
47-82	0.10	0.06	0.01	0.01	< DL	0.045	0.06	8.3	2.5			
82-107	0.09	0.05	0.01	0.01	< DL	0.040	0.06	8.1	2.4			
107-157	0.09	0.05	0.01	0.01	< DL	0.039	0.09	7.9	2.2			
157-192	0.25	0.15	0.01	0.01	< DL	0.136	0.09	7.9	2.7			
192-282	0.25	0.15	0.01	0.01	< DL	0.135	0.09	8.3	2.9			

^{*%} Ferrihydrite (% Fe_p) = % Fe_0 x 1.7 (Childs, 1985).

According to Schwertmann et al. (1982), acid-oxalate extraction also can be useful in estimating ferrihydrite (Fe_f) concentration in soils. The latter can be easily calculated by multiplying the Fe_o concentration by a factor of 1.7 (Childs, 1985). However, it is important to note that this calculation assumes that complete dissolution is achieved and that only ferrihydrite is dissolved by the acid-oxalate reagent (Parfitt et al., 1988). It should also be noted that this calculation was developed for tropical/temperate soils and therefore may not apply directly to arctic soils. The values reported in Table 3.6 for ferrihydrite concentration follow the same trend as the Fe_{0-P} data. These show that both inorganic Fe ion concentrations reach peaks in the 39-47 and 157-192 cm intervals.

Overall, the Fe_p and Al_p values within site 3 are very low and decrease with depth (*Table 3.6*), reflecting a corresponding decrease in organic matter content with depth. This suggests that

pyrophosphate extracts Fe and A1 species associated with humus in this soil that are not present in large amounts. Although the Fe $_o$, and Al $_o$ values are also low, they are significantly higher than the Fe $_p$ and Al $_p$ values, especially within the frozen layers of the soil profile.

The peaks in the concentration of amorphous iron in the 2-12 cm and 39-47 cm intervals can be explained either by high rates of iron liberation from silicates due to increases in soil acidity or the downward movement of mobile organic matter (Blume et al., 1969). In the case of the 157-192 cm and 192-282 cm intervals, a low degree of aging (i.e., crystallization) caused by increases in pH, could account for the increases in Fe_o concentration (Schwertmann, 1966).

3.5.4. BULK SOIL CHEMISTRY

The bulk concentration of silica (SiO₂) in soil samples from site 3 ranges between 55.9 and 62 wt.%, except for the organic-rich surface layer (38.2 wt.%) and the 32-39 cm interval (36.3 wt.%). The highest SiO₂ concentration, however, is in permafrost soils (the two highest values, 60.7 and 62 wt.% are at depths of 39-47 and 82-107 cm (*Table 3.7.*).

Table 3. 7.: Concentration of bulk oxides with depth for site 3.

	Total Concentration												
Depth	SiO ₂	AI_2O_3	Fe ₂ O ₃	CaO	MgO	Na ₂ O	K ₂ O	MnO	TiO ₂				
cm -					— %—								
0-2	38.2	7.6	3.55	1.96	1.06	0.42	1.41	0.06	0.41				
2-12	57.3	12.27	5.07	0.96	1.34	0.61	2.2	0.07	0.62				
12-22	57.2	12.15	5.58	1.25	1.32	0.61	2.18	0.08	0.63				
22-32	55 . 9	12.47	5.37	1.81	1.58	0.61	2.26	0.07	0.61				
32-39	36.3	9.29	3.43	2.77	1.14	0.38	1.65	0.03	0.4				
39-47	60.7	12.86	5.22	3.29	2.03	0.66	2.43	0.07	0.68				
47-82	59.8	13.57	5.75	3.65	2.29	0.64	2.55	0.07	0.7				
82-107	62	13.19	5.4	3.03	2.21	0.69	2.48	0.09	0.69				
107-157	59.8	13.32	5.82	3.52	2.34	0.72	2.52	0.07	0.67				
157-192	58.3	13.91	5.51	3.7	2.29	0.73	2.64	0.07	0.67				
192-282	58.9	13.37	5.78	3.99	2.34	0.91	2.56	0.07	0.65				

In concert with silica, other major oxides have low concentrations where the bulk silica concentration is low (Al₂O₃, Fe₂O₃, MnO, Na₂O, K₂O and TiO₂), i.e., in the surface layer and in the depth interval 32-39, just above the thaw unconformity. A notable exception is CaO, which has a high concentration in the surface layer (1.96 wt.%), and below this, increases progressively in concentration with depth from 0.96 to 3.99 wt.% at the bottom of the profile. The interval of highest SiO₂ concentration, 82-107 cm, is marked by a noticeable decrease in the concentration of Al₂O₃, Fe₂O₃, CaO, MgO and K₂O compared to their concentration in adjacent depth intervals (*Table 3.7.*). Interestingly, this interval corresponds to a peak in ice content (*Fig. 3.13.*).

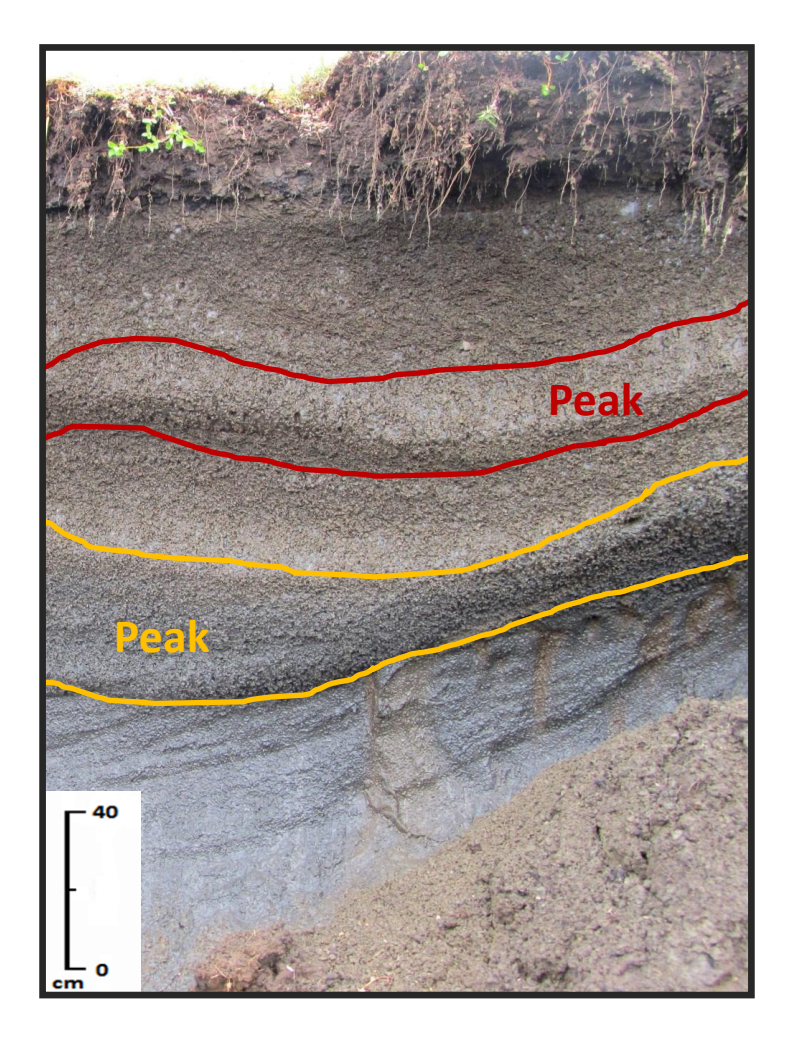


Fig. 3. 13. : Soil profile at site 3 showing the two peaks in ice content. Peak 1 (82-107 cm) is indicated by the red lines and peak 2 (157-192 cm) by the yellow lines.

Surprisingly, the second peak in ice content (157 - 192 cm) does not exhibit the same pattern in the distribution of major oxides as its shallower counterpart. On the contrary, this peak is marked by the highest concentration of Al_2O_3 and K_2O in the entire profile and the second highest concentration of Na_2O , which likely reflect the higher observed clay contents in the second peak compared to the first peak.

Among the traces elements, only Sr shows a systematic change in depth. Like Ca, which is an alkali earth and occurs immediately above it in the periodic table (it is therefore predicted to have

similar geochemical behaviour), Sr increases in concentration with depth and has its highest concentration in the permafrost (*Table 3.8.*). Two other trace elements that mimic the behaviour of some of the major element oxides are chromium and vanadium; their concentrations reach minima in the two organic-rich depth intervals, i.e., the surface layer and the 32-39 cm interval. This behaviour emphasises the control on their concentration by the primary mineralogy of the soil.

Table 3. 8.: Concentration of bulk oxides and trace elements with depth for site 3.

Total Concentration												
Depth	P_2O_5	Cr ₂ O ₃	Ni	SO3	Sr	V2.05	Zn	Zr				
cm -				<u> </u>								
0-2	0.23	0.008	0.002	0.01	0.007	0.016	0.013	0.01				
2-12	0.15	0.015	0.004	<0.002	0.007	0.029	0.01	0.014				
12-22	0.18	0.015	0.004	<0.002	0.006	0.029	0.01	0.013				
22-32	0.2	0.017	0.006	0.029	0.007	0.032	0.012	0.014				
32-39	0.17	0.013	0.005	0.008	0.011	0.022	0.01	0.009				
39-47	0.19	0.017	0.006	0.092	0.013	0.031	0.011	0.015				
47-82	0.22	0.02	0.005	0.077	0.013	0.031	0.012	0.013				
82-107	0.22	0.017	0.004	0.111	0.016	0.031	0.012	0.015				
107-157	0.22	0.027	0.015	0.115	0.013	0.032	0.013	0.013				
157-192	0.21	0.016	0.004	0.194	0.012	0.032	0.013	0.012				
192-282	0.21	0.016	0.006	0.159	0.014	0.032	0.013	0.014				

The most striking bulk chemical trend is that for SO₃ concentration, which increases by more than a factor of 10 from the base of the active layer to the permafrost, i.e., from 0.008 wt.% to 0.092 wt.%. There is a second significant increase of 0.077 to 0.111 wt.% from the depth interval, 47-82 cm, to the first ice peak (82-107 cm). The highest increase, however, 0.115 to 0.194 wt.%, is from the depth interval 107-157 to the second peak in ice content (157 to 192 cm). This latter depth interval has the highest bulk SO₃ content in the entire profile; the SO₃ content of the depth interval below it is 0.159 wt.%. The probable explanation for the high SO₃

concentration in the permafrost and particularly in the second ice wedge is that the deeper parts of the profile represent marine sediments that have not been exposed to sub-aerial chemical change. Seawater is known to have a high concentration of sulphate ions (3.5 – 9.7 mol/m³; Thomas et al., 1982). This interpretation is supported by the high concentration of Na (the principal cation in seawater) in the pore water obtained from the permafrost, which climbs steadily with depth from 40 mg/L in the depth interval 39-47 cm to 1440 mg/L at the bottom of the profile (*Table 3.9.*).

Table 3. 9.: Dissolved cation concentrations with depth in pore water at site 3.

Depth	Ca	Mg	K	Na	рН	EC
cm		mg	g/L			mS/cm
39-47	188	91	11.0	40	7.2	1.3
47-82	113	55	12.2	78	7.4	1.4
82-107	115	45	10.8	68	7.2	1.2
107-157	504	252	29.5	461	7.1	5.1
157-192	281	136	35.0	704	7.2	5.2
192-282	122	103	51.1	1440	7.3	9.9

3.5.5. WEATHERING INDICES

The use of weathering indices relies on the relationship between the selective removal of mobile and soluble elements and the enrichment of relatively immobile and non-soluble elements within a weathering profile (Yang et al., 2004). It is important to note that not all of the weathering indices mentioned above were used in the assessment of relative soil weathering within the study site. For example, weathering indices that included Fe in their formulation (i.e., SR, WI-1 and WI-2) were not used for two reasons, namely that: 1) the mobility of iron depends on its

oxidation state and these weathering indices do not account for the differences between ferric (largely immobile) and ferrous (highly mobile) iron during weathering (Price et al., 2003); and 2) the concentration of iron in a weathering environment often reflects redox reactions that occur locally in a weathering profile (Harnois, 1988). Duzgoren-Aydin et al. (2002) in a study of the applicability of weathering indices for evaluating degrees of mineral alteration, found that indices based on ratios of mobile versus immobile oxides were the best for characterizing weathering-induced changes (Price et al., 2003). Simple ratios of single oxides (SR) were found to be unsuitable due to their inability to relate to already observed trends.

The ratio of mobile to immobile (i.e., WR) and immobile to mobile (i.e., CIW) proved to be the most suitable indices for evaluating weathering of the soils within Slump A and produced trends that resemble those seen in analyses discussed earlier (*Fig. 3.14.*).

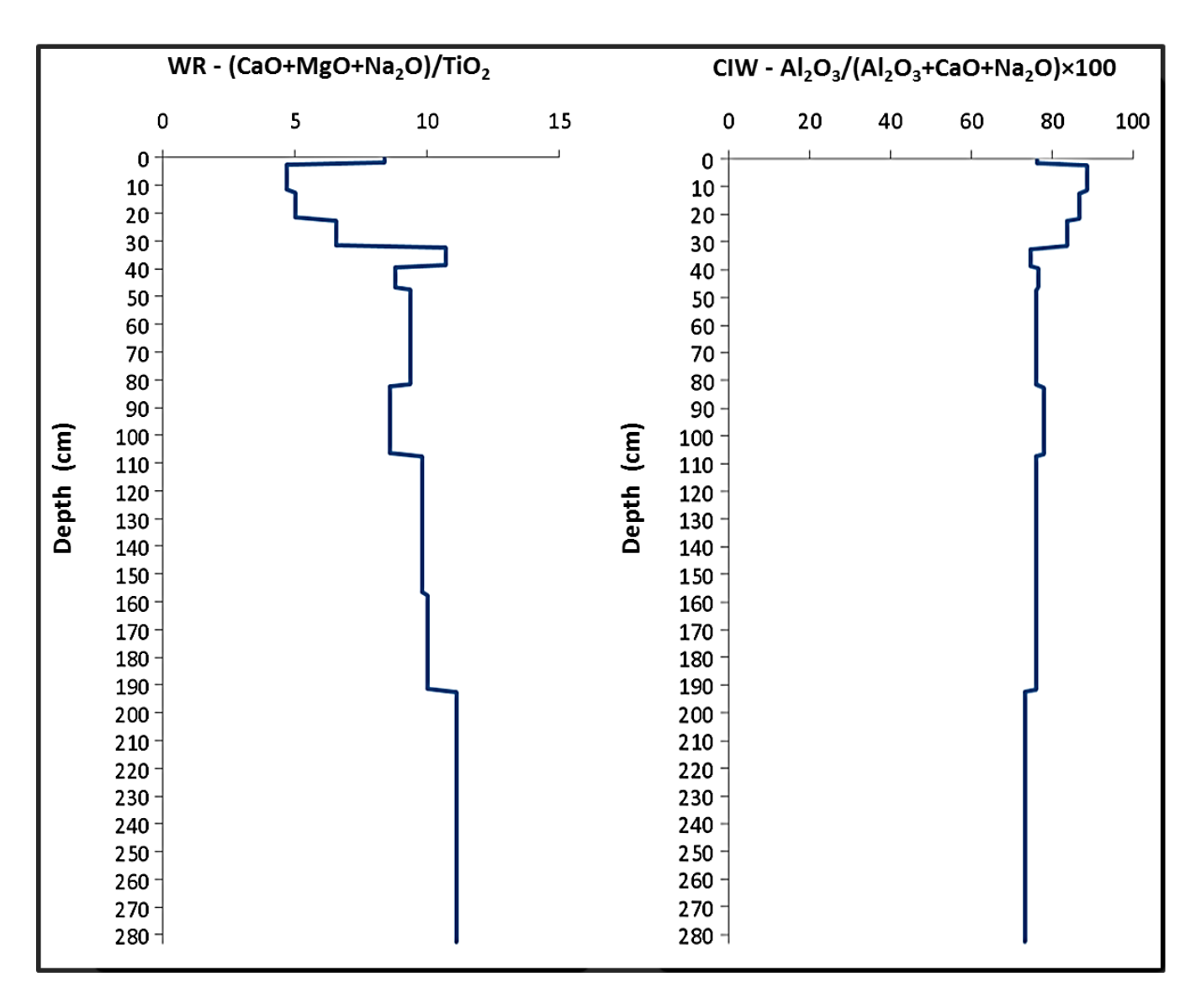


Fig. 3. 14. Weathering indices WR and CIW for site 3.

The Chittleborough (1991) weathering index (WR) uses a resistant heavy metal oxide (e.g., TiO₂) as a denominator over which to express the relative ratio of mobile to immobile oxides, such that changes in Na, Mg and Ca concentrations reflect variations in the amount of feldspar, amphibole and pyroxene. A higher ratio would therefore signify a smaller loss of the mobile Na, Mg and Ca oxides and, in turn, suggest lower intensity of weathering. The opposite would be true for horizons exhibiting lower ratios. It is thus not surprising that the lowest ratios occur

within the top 32 cm of the present active layer, where temperature and water mobility are highest. Immediately above the thaw unconformity, there is a sharp increase in the WR ratio, supporting the evidence presented earlier for an accumulation zone at the 32-39 cm depth interval, in this case of mobile Na, Mg and Ca oxides. Interestingly, an increase in weathering, i.e., loss of mobile Na, Mg and Ca oxides, is also evident within peak one (i.e. 82 –107 cm) where the WR ratio drops from a value of 9.4 in the overlying soil layer to 8.5 and then increases to 9.8 in the underlying soil layer. This increase in weathering is not mirrored in peak two (i.e. 157 – 192 cm), where instead there is a slight increase in the WR ratio to a value of 10. The deepest soil layers (192 – 282 cm) have the highest ratios, signalling a layer of little weathering.

The Harnois (1988) chemical index of weathering (CIW), like the WR index, eliminates K₂O from its formulation; K₂O was used in earlier formulations of the CIW index. The rationale behind the removal of K is that this element has been found to not show consistent behaviour during weathering, and often produces misleadingly high CIW values when the parent material is rich in K-feldspar (Buggle et al., 2010). The idea behind this weathering index is that it allows for the quantitative assessment of K-feldspar alteration by associating Al (enriched in the weathering residues) to Na, Ca and K, which are assumed to be removed from the soil profile by weathering of plagioclase (Na and Ca) and K-feldspar (Buggle et al., 2010). Therefore, increased weathering is indicated by a CIW ratio increase due to the increase in the removal of mobile Na, Ca and K. Use of this weathering index produced results that were very similar to those obtained with the WR index. Thus weathering was predicted to be much higher in the unfrozen horizons and to increase in the permafrost at peak one (82 – 107 cm).

Individual mobile elements were isolated in order to assess their relative contribution to the weathering pattern seen in the WR index (*Fig. 3.15.*).

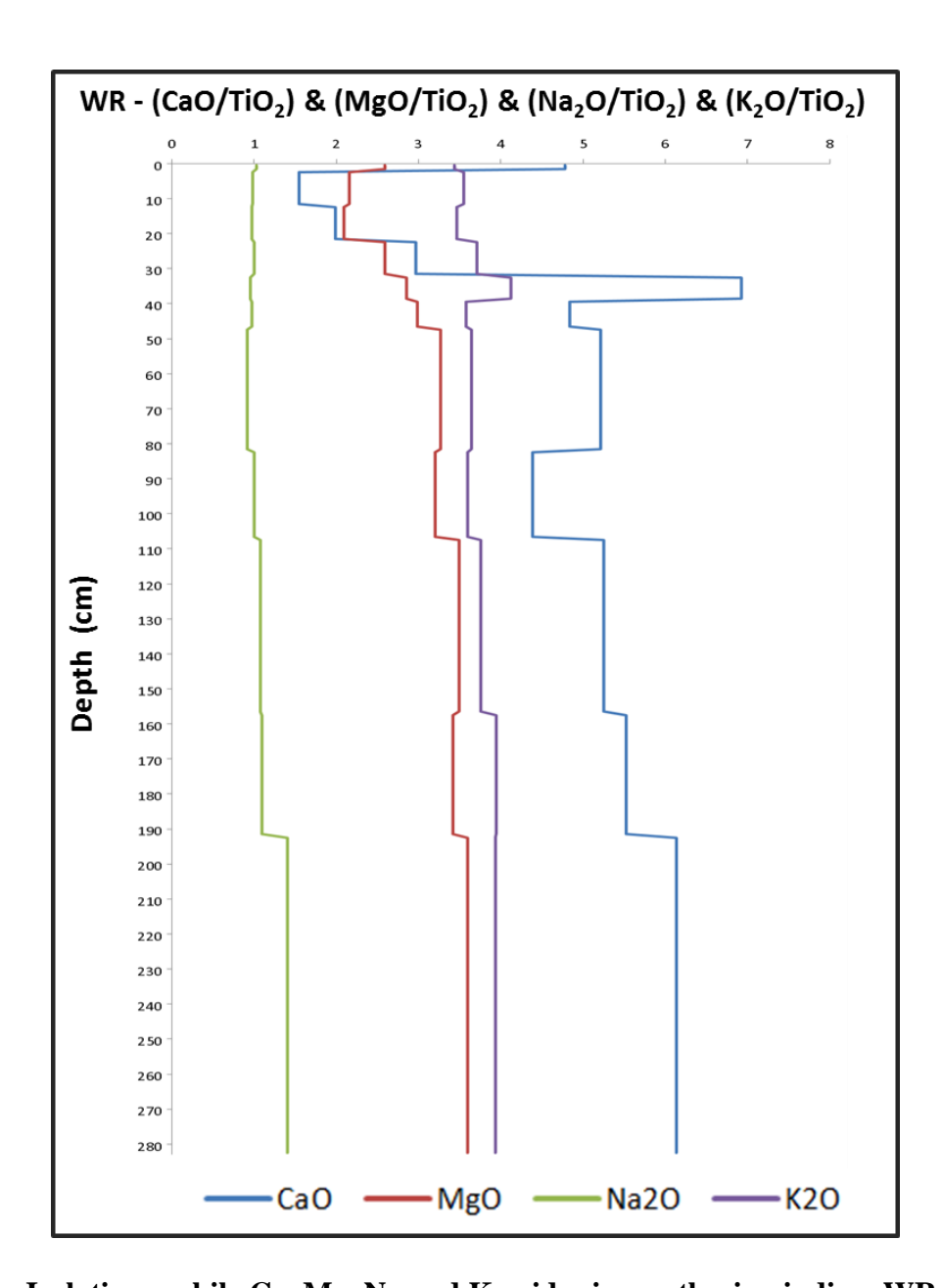


Fig. 3. 15.: Isolating mobile Ca, Mg, Na and K oxides in weathering indices WR for site 3.

Calcium oxide is clearly the main oxide driving the pattern seen in the WR curve, followed by MgO. Potassium (II) oxide was added in order to determine the importance of the breakdown of

potassic minerals through weathering processes. Interestingly, its influence is evident from the similarity of the K₂O/TiO₂ profile to those of CaO/TiO₂ and MgO/TiO₂, especially within the frozen horizons. Therefore the inclusion of K into weathering indices may be warranted in cases such as the one considered here, despite the concern of producing misleadingly high ratios.

In view of the above, a third index was employed, namely the weathering index of Parker (WIP). This index focuses exclusively on the proportions of alkali and alkali earth metals present within a given soil profile (Price et al., 2003). It not only includes K₂O in its formulation, but it also accounts for the mobility of Ca, Na, Mg, and K based on their bond strengths with oxygen (Parker, 1970). Moreover, it allows for the mobility of aluminum (Parker, 1970), an oxide deemed immobile in the other two indices. Although aluminum has often been shown to behave in an immobile fashion, studies by Cleaves (1974), Gardner et al. (1978, 1981) and Gardner (1980) have demonstrated the heterogeneous distribution of aluminum within soil profiles using isovolumetric methods. Their studies have also documented the loss of aluminum in homogeneous material. Application of Parker's weathering index to site 3 produced the same overall patterns as the previous two indices. According to this index, weathering is strongest in the current active layer, but then weakens significantly within the frozen layers where the proportions of alkali and alkali-earth metals increase, except in the first peak (82 –107 cm). There the value of the index decreased from a value of 548 in the preceding depth interval to 459 (Fig. 3.16.). The major difference in the WIP index from the WR and CIW indices is the clear incremental increase in the proportion of Ca, Mg, Na, and K oxides with depth in the active layer (except for the surface horizon; 0-2 cm).

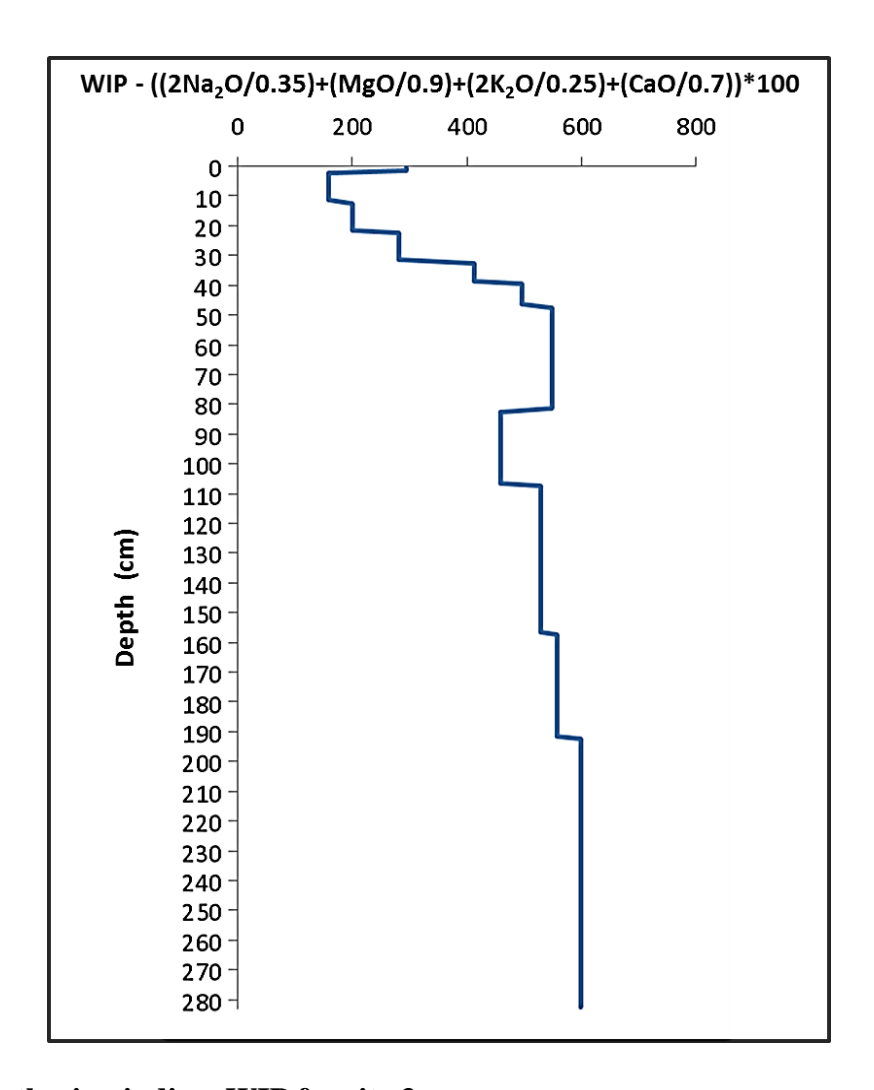


Fig. 3. 16. Weathering indices WIP for site 3.

3.5.6. SOIL WEATHERING AND THE PALEO-ACTIVE LAYER

Recognition of a paleo-active layer becomes increasingly more difficult with subsequent disturbance, particularly when it occupies the present land surface or becomes re-exposed through erosion. Fortunately, the paleo-active layer within the undisturbed section in slump A, although laterally exposed through slumping, has not been subject to any significant present day pedogenic processes. Therefore any record of soil processes within this soil layer would be associated largely with environmental factors related to an early Holocene warming (~ 9380 ±170 years, Smith et al., 1989) period (Jenkins, 1985). This layer should therefore be

distinguishable based on marked differences in chemical and physical characteristics.

Evidence of a paleo-active layer is provided by chemical differences that distinguish the two ice peaks (82 –107 cm and 157-192 cm) from the rest of the permafrost profile. The bulk chemical data and the weathering indices based on these data indicate that there was an increase in weathering at peak one. This is matched by particle size analysis data showing an increase in silt content. The chemical and particle size data for peak two indicate that weathering was not nearly as intense as in peak one, but nonetheless, peak two has a significantly higher ratio of weathered material than the layer immediately succeeding it. Furthermore, the highest concentration of SO₃ is observed at this depth interval (157-192 cm). Finally, both peaks have undergone ice enrichment (i.e., aggradational ice), and exhibit very distinct cryostructural characteristics (e.g., horizontal banding and peaks) that are laterally continuous though the undisturbed part of Slump A.

An interpretation that emerges from these observations is that a deep thawing event allowed for the development of a thaw unconformity within the depth interval 157 – 192 cm below the surface. The same conclusion has been reached in other studies on Herschel Island, which identify a Holocene thaw unconformity between 180 cm to 190 cm based on truncation of ice wedges and variations in the cryostructure of ground ice (Mackay, 1975; Burn, 1997; Kokelj et al., 2002). As at the thaw unconformity in Slump A, a zone of aggradational ice accumulated above the unconformity in other slumps, notably at Collinson Head, and is attributable to a thinning active layer (Mackay, 1972; Burn, 1988). In the case of Slump A, the thickness of the ice layer above the thaw unconformity at peak two varied from 28 to 56 cm.

A second unconformity can be seen at peak one (82-107 cm), which like peak two, contains an aggradational ice zone that varies in thickness from 17 to 28 cm. However, the degree to which the soil has been weathered in peak one is significantly higher than in peak two, indicating a more recent warming period that promoted active layer thickening and was in existence long enough to allow for in situ weathering to occur.

3.6 CONCLUSION

The fundamental challenge in studying the chemical weathering of soils in periglacial environments is to relate the chemical variations in different soil horizons to their visually distinct physical and cryotextural characteristics. In the case of Herschel Island, two thaw unconformities were observed within the undisturbed section of retrogressive thaw slump A. The first thaw unconformity occurs at the base of the current active layer and was overlain by an accumulation zone (32-39 cm), in which there was a doubling in the concentration of most cations and a tripling in soil organic matter content. Overall, the soils within the present active layer exhibit evidence of higher proportions of weathered material and silt sized particles than the underlying frozen layers.

Many are familiar with the axiom that within the present lies the key to the past. Herschel Island provides a good example of this, since it currently is the site of erosional processes, such as thermokarst development and retrogressive thaw slumping, that have allowed for the exposure of previously un-exposed soils. The occurrence of a thaw unconformity within the permafrost suggests a past period of prolonged climate warming and active layer thickening. However, the

degree of weathering and ion accumulation is not as distinct in the paleo-active layer thaw unconformity as it is in the modern active layer thaw unconformity, implying a shorter climate warming period, possibly associated with a paleo-active layer unconformity that formed during the early to mid Holocene. A greater marine influence is also evident within the paleo-active layer thaw unconformity, which continues with depth, supporting a marine derived sediment origin. The most striking evidence of this marine origin is the prominent peak in SO₃ concentration in the soil at the unconformity and in Na concentration in the pore water in the underlying ice layers. Clay contents also increase within this zone, suggesting possible soil preservation.

Most Canadian arctic soils tend to be younger than soils at more southerly latitudes, as nearly all glaciated landscapes have only been ice-free for a comparatively short period of time, i.e., within approximately the last 15 000 years (Linell and Tedrow, 1981). However, in response to a changing climate, physical and even chemical characteristics of soil will change in a periglacial setting. Though slow, this process may eventually destroy any climatic records of past periods. Now, more than ever before, it is possible to more easily study the paleo-active layer and its cryostructural expression. Moreover, the ability to use chemical weathering indices to quantify and support interpretations of different cryogenic expressions serves to highlight the important role that chemistry can play in understanding arctic soil systems. Chemical changes are especially important to document when considering the projected climate warming scenarios, since weathering profiles have been shown to adapt to changing environments. However the degree to which climate-driven changes will affect the weathering soil profiles and ultimately

modify landscape morphology in the Arctic is still unknown and will only be determined through intensive and extensive investigations of Arctic soils and sediments.

PREFACE TO CHAPTER 4

Chapter 4 reports results of this thesis that are presented in the form of a scientific manuscript which will be submitted for publication in a peer-reviewed journal. Using the Stefan's equation in conjunction with measured field data and theoretical projections, changes in active layer depth with increasing global temperature are quantified. A case is made that the morphological properties of the active layer affect, to varying degrees, the buffering capability of this important interface. The chapter provides new insights into weathering within periglacial environments and the consequences for ground heat propagation and permafrost degradation.

CHAPTER 4

Active Layer Thickening on Herschel Island, Yukon.

Leigh-Ann Williams-Jones¹, Wayne H. Pollard¹, and William H. Hendershot²

¹ Department of Geography, McGill University, Montreal, QC.

² Department of Natural Resource Sciences, McGill University, Montreal, QC.

ABSTRACT

The stability of permafrost in a projected warmer climate depends heavily on the capacity of the active layer and transition zone to dissipate the additional heat inputs entering the system. A fundamental challenge in assessing the ability of these soil media to buffer the underlying permafrost is to understand how the properties of frozen and unfrozen soils affect heat transfer from the ground surface. To gain such understanding, measurements of active layer depths were obtained from a 100 m by 100 m active layer monitoring grid, located on Herschel Island, Yukon. Stefan's equation was used in conjunction with thawing degree days to derive thermal constant values from these depths, which were compared to theoretical thermal constants calculated for a soil profile exposed in an adjacent retrogressive thaw slump. The latter constants were calculated using the De Vries method to determine the thermal conductivity of the different soils in the profile. The integrated theoretical constant is 1.39, whereas the average measured value is 2.23. This difference is likely due partly to the fact that Stefan's equation does not consider advective heat transfer and partly because the method of measurement (resistance to penetration of a metal probe) leads to overestimates of active layer depths. Third generation Canadian Global Coupled Models (CGCM 3.1/T63) from the Canadian Centre for Climate Modelling and Analysis (CCCma), employing IPCC SRES A2 and B1 scenarios, were used in conjunction with the theoretically and empirically derived thermal constants to predict active layer depths for 2050 and 2100. According to these predictions, the active layer will thicken by between 4 to 17% by the end of this century. These predicted increases are significant and will lead to important landscape changes.

Keywords: permafrost; heat transfer; active layer thickness; thermal buffer; climate

4.1. INTRODUCTION

The projected increase in global air temperature, particularly in high latitudes, is expected to dramatically affect the resilience and vulnerability of polar landscapes (Jorgenson et al., 2010). Already, changes in air temperature, vegetation, sea ice, snow accumulation, ground temperature and permafrost have been detected in Arctic environments (Pavlov, 1997; Myneni et al., 1997; Bjorgo et al., 1997; Rothrock et al., 1999; Vinnikov et al., 1999; Burn, 2000; Sturm et al., 2001; Jorgenson et al., 2001; Comiso et al., 2002; Burn and Zhang, 2009). As these changes continue due to further global warming, there is a serious threat of reaching and even surpassing the sustainability threshold of this ecosystem (Lawrence and Slater, 2005; Jorgenson et al., 2010).

An important "geoindicator" that has been widely used to assess environmental change in Arctic environments is permafrost and active layer thickness (Berger and Iams, 1996). Indeed, changing thaw depth has been shown to be an important seasonal expression of climate change (Couture et al., 2007), as its extent is directly related to the surface energy balance and exchanges between the atmosphere and the permafrost (Hinkel et al., 2001). Under most scenarios of global warming, the seasonal thawing of the soils starts earlier and ends later. There will also be greater variation in temperature (Couture et al., 2007). This is expected to result in an increase in thaw depth due to greater influx of heat from the surface and warming of the underlying permafrost. However, the nature and extent of thaw degradation continues to be a topic of debate, in large part, because of the complex nature of the relationship between the climate and permafrost (Jorgenson et al., 2010). Furthermore, the impact of climate change on permafrost is often

indirect and involves a complex set of positive and negative feedbacks related to soil properties, hydrological regimes, topography, vegetation patterns and disturbance (Shur et al., 2007; Jorgenson et al., 2010). As a result, there is considerable need to determine more precisely the character and extent of potential climate driven changes on the active layer, and to evaluate the potential impact that these changes will have on the positive and negative feedbacks controlling permafrost environments.

In this paper, the factors affecting changing active layer depth are assessed using field data, numerical models and the literature. The field study, conducted on Herschel Island, Yukon, Canada, involved determining the nature of the active layer and underlying permafrost layers exposed in the headwall of a retrogressive thaw slump, monitoring the progressive thickening of the active layer during a single thaw season and relating this change to the mean daily ground (soil) surface temperature. These data are used in conjunction with the de Vries equations (to estimate the thermal conductivity of the soils) and the Stefan equation to extract thermal constants that permit forward modelling of the effect of global warming on the active layer depth. Estimates of future temperature on Herschel Island were provided by the global coupled atmosphere-land-ocean models of the Canadian Centre for Climate Modelling and Analysis (CCCma). Based on this modelling, the active layer considered in this study is predicted to increase its current thickness by about 4 to 17% depending on the climate scenario and whether the thermal constant is empirically or theoretically determined.

4.2. BACKGROUND AND STUDY SITE

Polar soil environments have widely been described using a two-layered conceptual model that separates the seasonally thawed layer (i.e., the active-layer), from the underlying perennially frozen layer (permafrost) (Shur et al., 2005). However, this model has largely been deemed inadequate for explaining prolonged active layer/permafrost system behaviour. As a result, a third layer was introduced, based on results from studies conducted in the Russian and North American Arctic. These studies identified a soil layer which infrequently alternated between frozen and thawed states. This third layer is referred to as the transition zone. The transition zone is considered to be the primary buffer between the overlying active layer and the underlying permafrost layer, and ice-rich intervals within this layer have been taken as evidence of past climate-warming episodes spanning decades to millennia (Shur et al., 2005).

Areas of continuous permafrost, like Herschel Island, have persisted for tens of thousands of years and in some cases hundreds of thousands of years, and during this time has been responding continually to climatic changes (Froese et al., 2008; Jorgenson et al., 2010). Indeed, according to Osterkamp (2007), most permafrost is of Pleistocene age. Recent studies have documented a general warming of permafrost since the 1980s (Jorgenson et al., 2010). The response of permafrost to this warming is largely a function of the buffering capacity of the transition zone. Thus, reliable evaluation of this buffering capacity requires that soil heat propagation, and more specifically the soil thermal properties that govern this process be better understood (Arocena et al., 2012).

Herschel Island is located a few km north of the Yukon coast at 69°42′N, 139° '01 W (*Fig. 4.1.*). Covering an area of about 108 km², the island has a rolling topography with a maximum elevation of 181 m above sea-level, and is thought to have formed during an advance of the Wisconsinan Laurentide Ice Sheet (LIS) as an ice-thrust moraine (Mackay, 1959; Rampton, 1982; Pollard, 1989; Pollard, 1990). This interpretation is supported by the observation that the volume of sediment missing from Herschel Basin, a well developed basin immediately to the southeast, is strikingly similar to Herschel Island (Mackay, 1959).

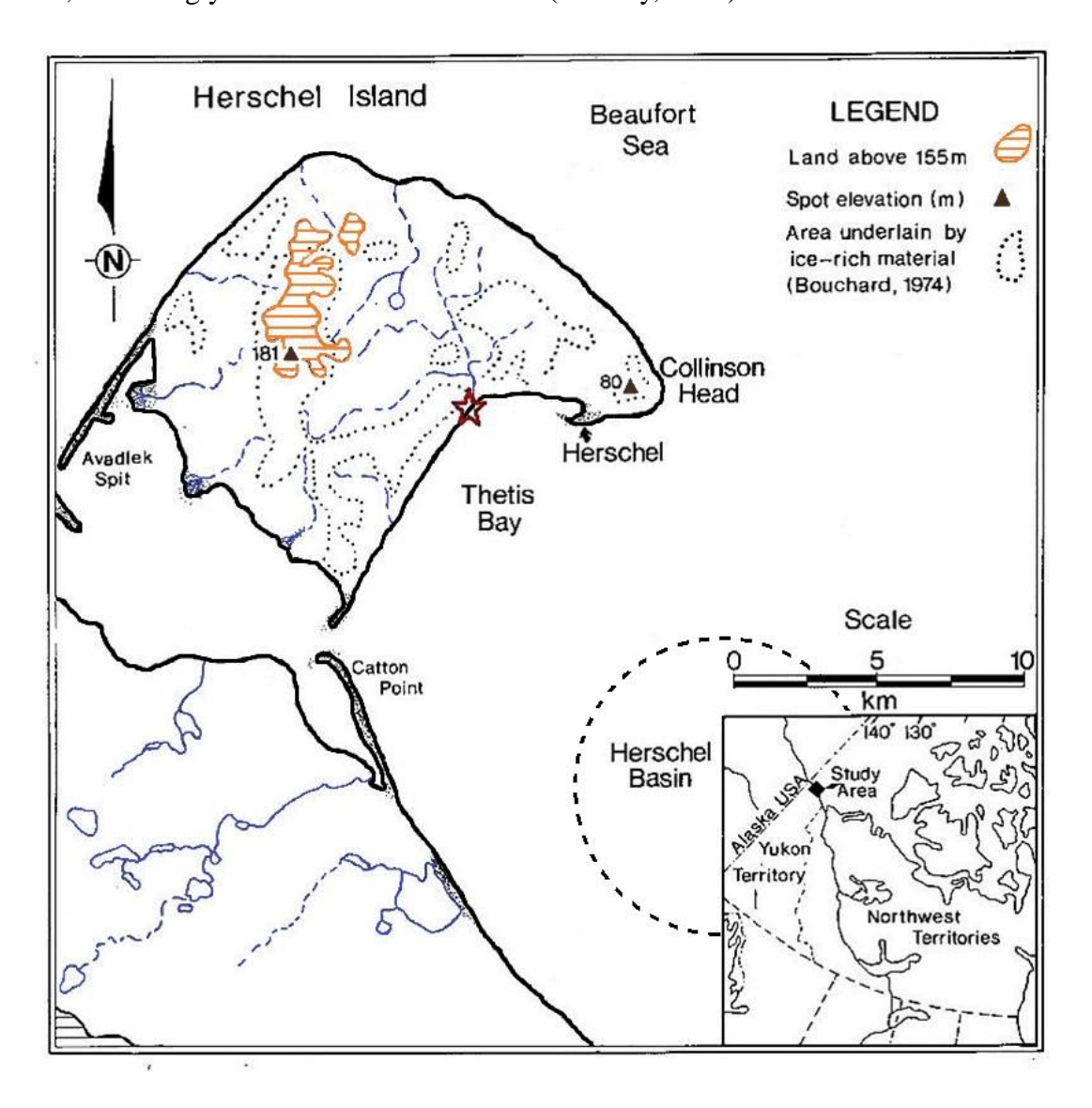


Fig. 4. 1.: A map of Herschel Island showing the location of the study site indicated by the red star.

Adapted from Pollard (1989)

The age of the island, however, remains unclear. A study by Zazula et al. (2009) attempted to determine an age for Herschel Island using radiocarbon dating of terrestrial vertebrate fossils and peat found on the island. Unfortunately, the results did not resolve the long-standing debate over the exact timing of the LIS advance responsible for the island, as the ages obtained spanned the range from 1 290 ±40 years to greater than 53 000 years. Ages >53 000 years were interpreted to indicate either that animals inhabited Herschel Island prior to the Late Wisconsinan, or alternatively that the skeletons of terrestrial mammals living on the Beaufort Plains were incorporated into sediments that were later ice-thrust by an advancing lobe of the LIS (Zazula et al., 2009).

Situated only a few kilometers offshore, Herschel Island experiences a dry polar climate with predominantly lowland tundra vegetation and a ground surface underlain by continuous permafrost and ground ice (Pollard, 1990). The island is composed of buried and deformed, icerich silt, clay and sand sediments, which are easily eroded and sensitive to geomorphic disturbances, such as wave action, ice push, mass wasting and water run-off from upland surfaces of the island (Lantuit and Pollard, 2008).

4.3.1. THERMOKARST AND RETROGRESSIVE THAW SLUMPS

The dominant type of geomorphic disturbance on Herschel Island is retrogressive thaw slumping, a phenomenon driven primarily by acute thermo-erosional and thermokarst activity. Retrogressive thaw slumps are controlled by the changes that occur in the thermal environment as a result of the thermal equilibrium maintained between the geothermal gradient and the

ground surface temperature (Lantuit et al., 2008). Permafrost stability, active layer depth and ground-ice content all play a role in governing the intensity and extent to which retrogressive thaw slumping and thermokarst development occur (Pollard, 2005).

Retrogressive thaw slumps form very distinctive bowl or C-shaped thaw structures that are characterised by a back-wasting headwall. They can be polycyclic in nature, meaning that they tend to stabilize and reactivate on a regular basis. They can extend up to hundreds of meters inland, exposing material within vertical or sub-vertical headwalls, the angles of which can vary from between 20° and 50° (Fig. 4.2.).

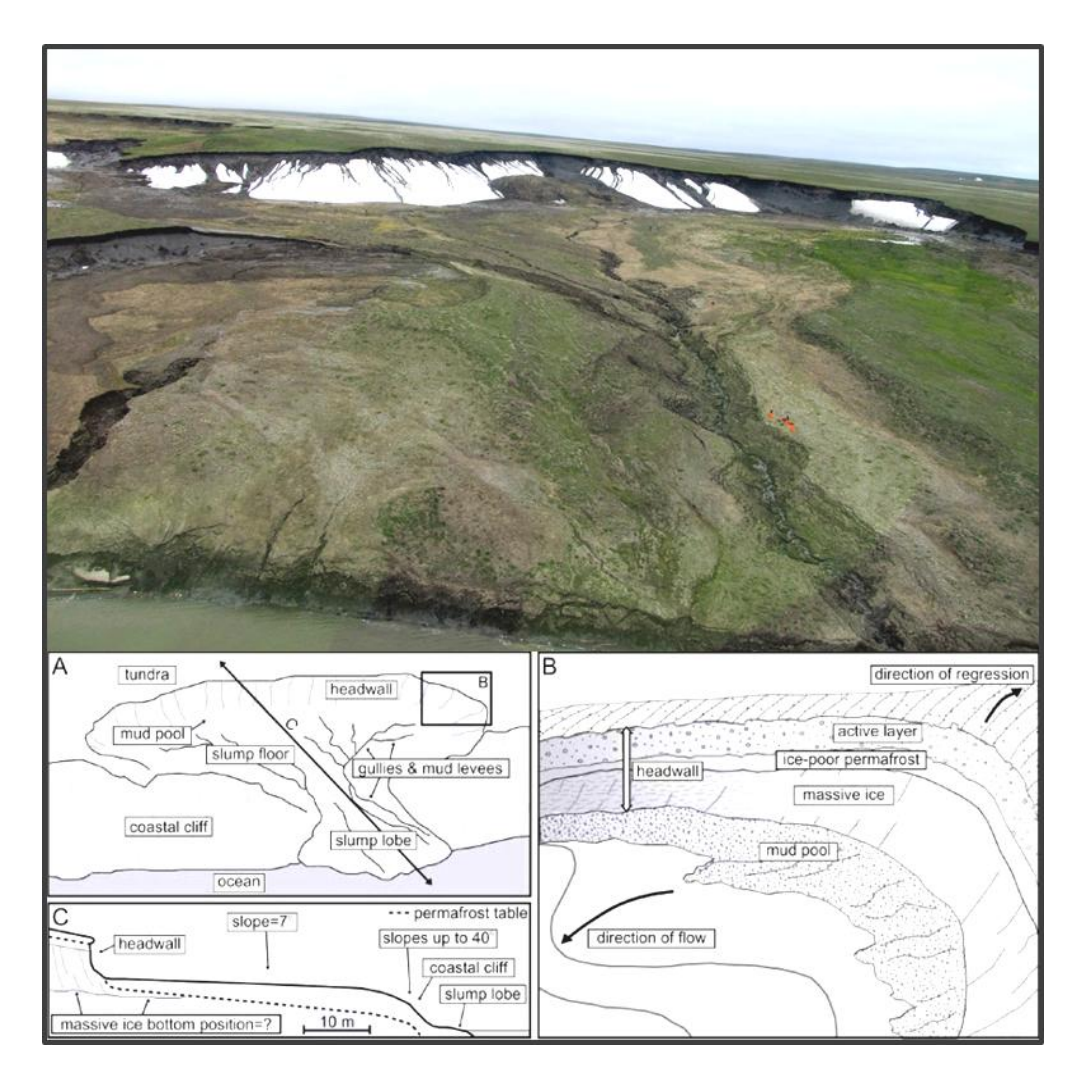


Fig. 4. 2. : Aerial photograph showing a retrogressive thaw slump (Slump D) on Herschel Island, Yukon.

Adapted from Lantuit and Pollard, 2005

This study is based on an active retrogressive thaw slump (referred to as Slump A), which includes both disturbed (i.e., a headwall receding into an old slump floor) and undisturbed (i.e., a headwall receding into undisturbed tundra land surface) sections (*Fig. 4.3.*).

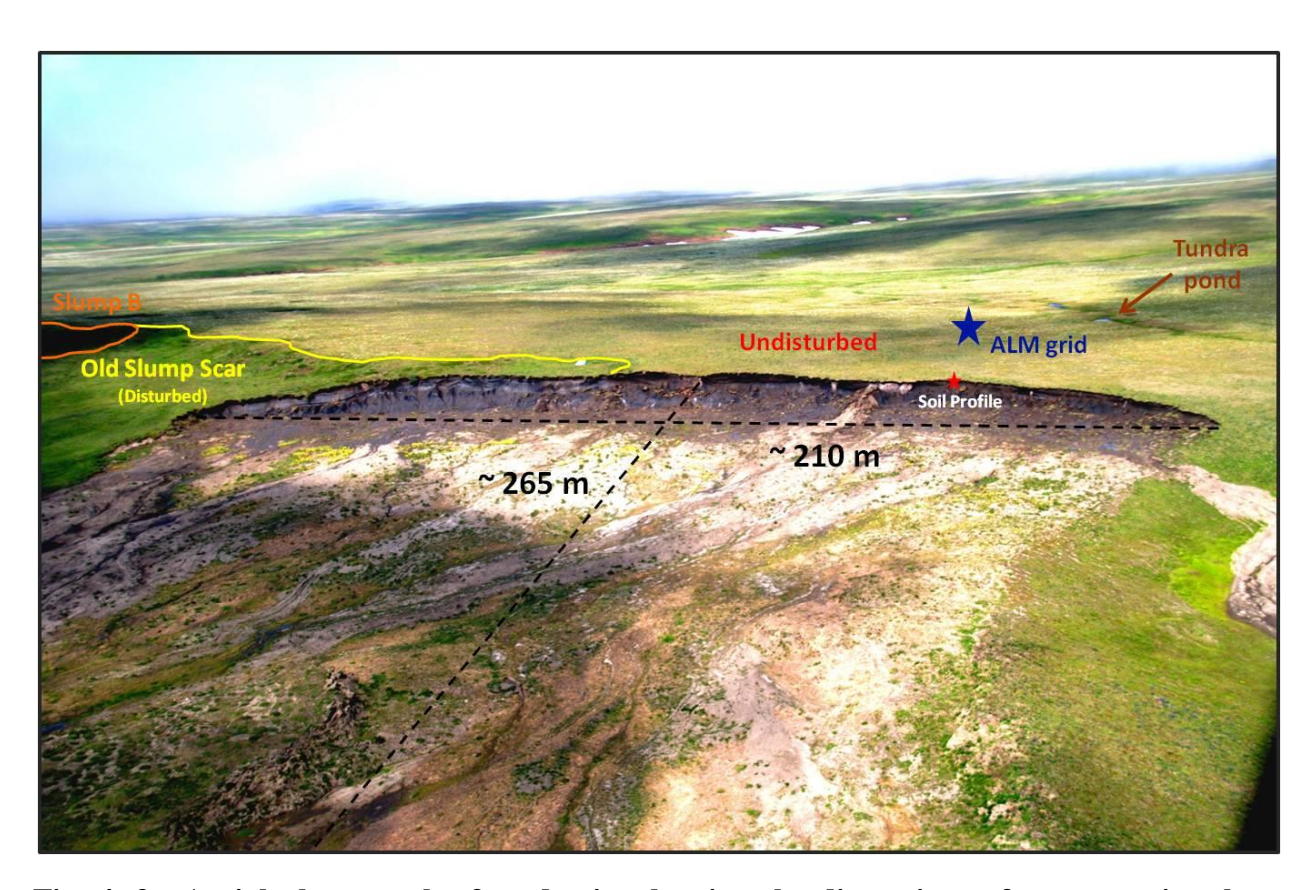


Fig. 4. 3. Aerial photograph of study site showing the dimensions of retrogressive thaw slump A and the location of a tundra pond.

(Photo Taken by Dr. Michael Krautblatter, July 2011)

The headwall of the undisturbed part of Slump A exposes both the modern active-layer and the paleo-active layer. The base of each layer is marked by a thaw unconformity overlain by aggradational ice peaks, which are interpreted to correspond to periods of warming and maximum active layer extension (Williams-Jones et al., 2012a). Based on cryogenic and chemical analyses, the paleo-active layer is believed to have formed during the early to mid Holocene (*Fig. 4.4.*).

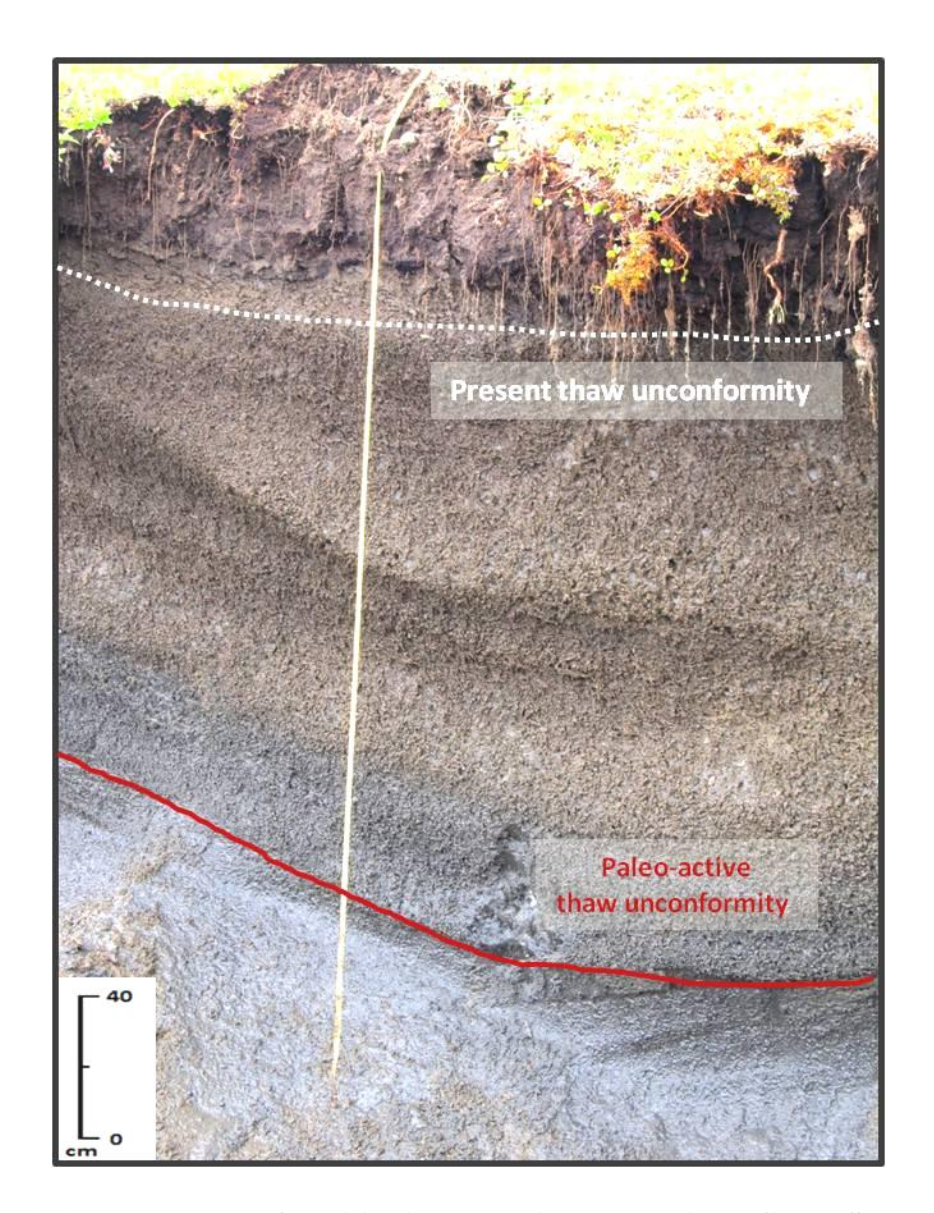


Fig. 4. 4.: Thaw unconformities in an undisturbed soil profile at Slump A.

The main vegetation above Slump A comprises cotton grass tussocks, dwarf arctic willow, bryophytes and several types of Forbes and sedges (Sloan, 2012). Soils at this site are classified as orthic eutric turbic Cryosols (CanSIS, 1998). The composition of these soils based on samples from Slump A are listed in Table 4.1.

Table 4. 1. Changes in soil characteristics with depth for a soil profile located within the undisturbed section of Slump A.

Depth	Sand	Silt	Clay	рН	EC	SOM
cm	%	%	%		mS/cm	%
2-0	27	50	23	6.47	0.17	35.60
12-2	17	46	37	6.09	0.13	11.70
22-12	16	50	34	7.29	0.15	11.10
32-22	16	47	37	7.82	0.18	11.30
39-32	17	49	35	6.7	0.20	34.40
47-39	15	43	42	8.1	0.40	3.80
82-47	13	42	45	8.27	0.38	2.50
107-82	12	46	42	8.08	0.46	2.40
157-107	12	44	44	7.86	1.22	2.20
192-157	11	42	48	7.89	1.87	2.70
282-192	11	41	48	8.29	2.40	2.90

4.4. METHODOLOGY

The field research took place over a five week period during the summer of 2011, and involved making detailed descriptions of soil profiles at the headwall of Slump A, collecting soil samples, setting up an active layer monitoring grid, installation of single-channel (Onset HOBO Pro Series) temperature loggers and conducting repeated active layer depth measurements. The active layer monitoring grid was located in an undisturbed area immediately upslope from slump A, an area of relatively flat terrain covered fairly uniformly by vegetation representative of that present on the slump's receding headwall (*Fig. 4.5.*).

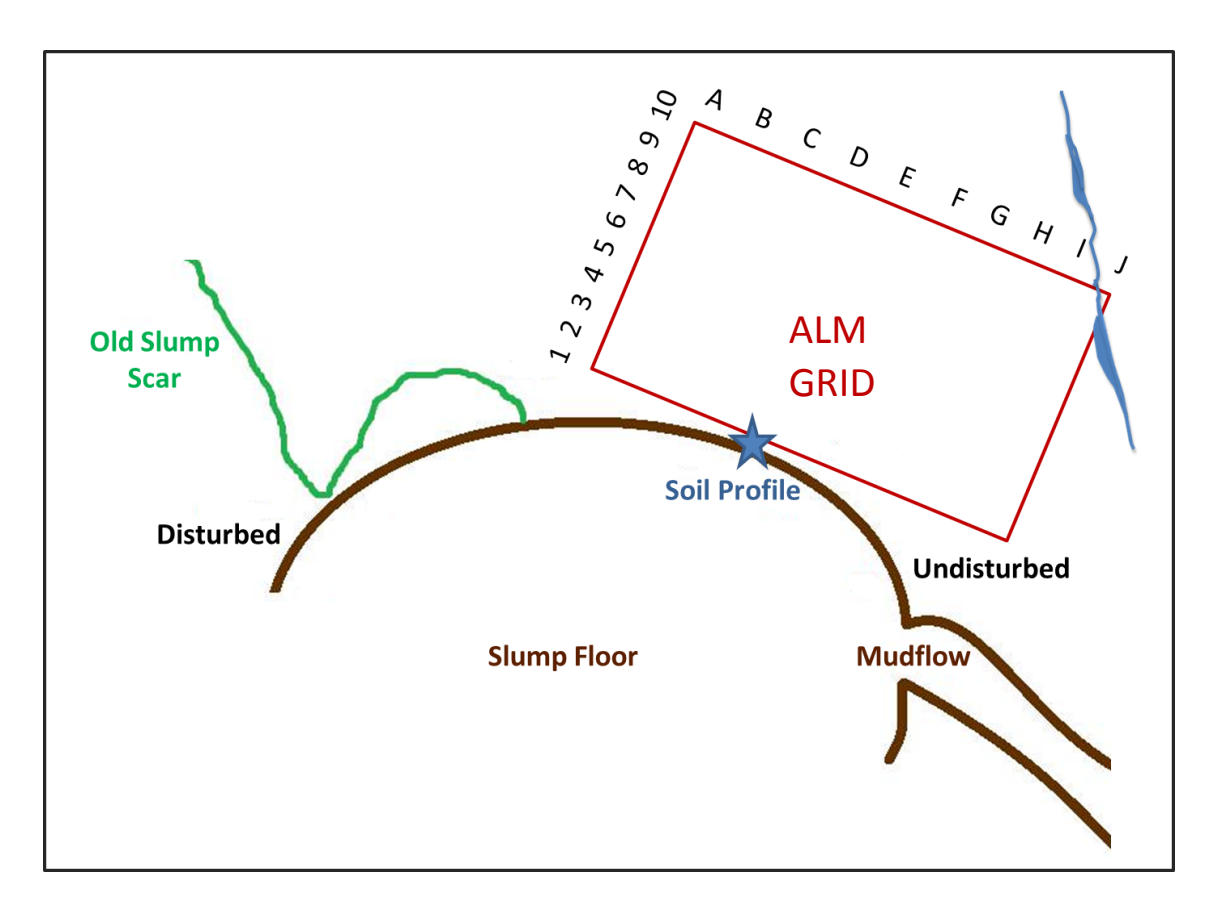


Fig. 4. 5. : Schematic diagram of retrogressive thaw slump A, showing the location of the ALM site and the sampled soil profile .

4.3.1. ALM GRID

A 100m by 100m grid starting two metres inland of the retrogressive thaw slump headwall (Slump A) was laid out north of Slump A for the purpose of monitoring increasing active layer depths at fixed time intervals. Following the Circumpolar Active Layer Monitoring (CALM) protocols, active layer depth measurements were taken at points 10 m apart. These points were marked using wooden dowels with visible flagging tape to ensure site specific repetition. An active layer probe consisting of a 1 cm demarcated graduated steel rod was used to measure the depth to the frost table (based on resistance). Depths were measured every 5 days between June 24th and July 18th, 2011, and again on August the 13th and 24th, 2011, by park staff. The ALM site reflected typical tundra conditions, i.e., slope, and vegetation.

The ALM grid was situated adjacent to Slump A so that changes in active layer depth could be correlated with soil profile characteristics. The closest points (C1 to F1) were initially 1.5 m from the headwall, whereas the furthest point within the ALM grid was located ~110 m (J10) from the receding headwall of Slump A. The distances of the grid points from the headwall decreased during the course of the sampling field season and three of the measurement points were consumed by the retreating headwall of Slump A near the end of the thaw season. A total headwall recession of approximately 1.3 – 1.8 m inland was observed. As the summer progressed, a small tundra pond formed at the intersection of two ice-wedge troughs, creating a wetland at grid points F10, H9, J8 and J9. Grid points I4 and I9 coincided with surface depressions, 6.5 cm and 5 cm deep, respectively. Cotton grass tussocks were located above grid points B2, B7, C4, E2, F9, H10, I6, J1 and J6. The height of each tussock was measured in order to make appropriate adjustments to the active layer measurements taken at these grid points.

4.3.2. STEFAN EQUATION

According to many researchers changes in the ground thermal regime in the Arctic due to thawing and redistribution of water in response to seasonal temperature can be reliably predicted using heat-conduction models (e.g., Gold and Lachenbrech, 1973). The most widely used algorithm to describe thaw penetration in frozen soils is the Stefan equation (Riseborough et al., 2008). This algorithm assumes a linear temperature distribution within the thawed soil and ignores the temperature distribution within the frozen zone (i.e., $T_{ground} = 0$). Heat advection is also ignored, and it is assumed that the available heat is employed to melt and freeze ice rather than warm or cool the soil (Woo et al., 2006).

Using the above assumptions, Nixon and Roberts (1973) developed the following simplified equation:

$$Z = (2k_u T_s t/L)^{1/2}$$

in which, Z represents the depth of thaw (m), k_u is the thermal conductivity of the unfrozen soil (W m⁻¹°C⁻¹), T_s is the step change in surface temperature (°C), L is the volumetric latent heat of fusion of the soil (J m⁻³), and t denotes time (s).

Equation 1 has been further modified to allow predictions of thaw depth by replacing the step change in the surface temperature variable (T_s) and the time variable (t) with the total number of thawing degree days (${}^{\circ}\text{C} \cdot \text{days}$) in the thaw season (Boyd, 1976):

$$Z = b(TDD)^{1/2}$$

where b represents the thermal constant, and is calculated using the relationship $(2k_u/L)^{1/2}$, and TDD is the total number of thawing degree days in the season, i.e., the number of days with a temperature above 0° C multiplied by the average temperature for these days (°C·days)

Hinkel and Nicholas (1995) showed that the thaw depth (\mathbf{Z}) at a given site increases linearly with the increase in the square root of the total number of thawing degree days (TDD) during a single thaw season, and that multiple measurements of thaw depth therefore could be used to determine the thermal constant (b) empirically using the equation:

(3)

$Z = b TDD^{1/2} + a$

in which, b represents the slope of the best fit line to a set of thaw depths and corresponding accumulated thawing degree days raised to the power of one half, TDD is the total number of thawing degree days, and a is the intercept on the thaw depth axis.

Equation 3 was applied to the data collected on active thaw depths for the ALM grid to calculate an empirical thermal constant (b) for each point on the grid.

4.3.3. SURFACE TEMPERATURE MEASUREMENT AND ESTIMATION

Single-channel temperature data loggers were installed between grid points E5 and F5, at 0 and 1.2 m above the ground to measure ambient air and ground surface temperature. Hourly temperature data were collected from June 21st to July 21st, 2011. In addition, climate data for the period January 2011 to December 2011 were obtained from Environment Canada. The Environment Canada data were from a weather station located at the Park headquarters on Herschel Island (latitude 69°34'05.500" N, longitude 138°54'48.200" W), roughly 1.5 km northeast of Slump A at an elevation of 1.2 m above sea level. These data were linearly regressed against the single-channel data logger air temperatures and the latter against the single-channel data logger ground surface temperature, thereby allowing the Environment Canada air temperature data to be used to calculate ground surface temperatures for the entire thaw season.

4.3.4. THE DE VRIES EQUATION

Active layer thermal regime is controlled primarily by the ground surface temperature and the thermal properties of the soil (French, 2007). The most important thermal properties of a soil, under thawing conditions, are its thermal conductivity, which is a measure of the ability of the

soil to transfer heat conductively along a thermal gradient, and the latent heat of fusion of the ice contained within it (Riseborough, 1990). The thermal conductivity of the soil, in turn, depends on the composition of the soil and its moisture content (Farouki, 1981). For the purpose of this study, the thermal conductivity of the soil at various depths in Slump A was estimated using information on the composition of the soil at these depths reported in Williams-Jones *at al.* (2012) (manuscript 1) and the equations of van Wiljk and de Vries (1963).

$$\lambda = (\mathbf{x}_{w}\lambda_{w} + \mathbf{k}_{a}\mathbf{x}_{a}\lambda_{a} + \mathbf{k}_{s}\mathbf{x}_{s}\lambda_{s}) / (\mathbf{x}_{w} + \mathbf{k}_{a}\mathbf{x}_{a} + \mathbf{k}_{s}\mathbf{x}_{s})$$
(4)

where $\mathbf{x_x}$ denotes the volume fraction of w –water, a – air and s – solid, λ_x is the thermal conductivity of w –water, a – air and s – solid (Wm⁻¹°C⁻¹), and $\mathbf{k_x}$ represents a weighing factor of w –water, a – air and s – solid

The matrix within the de Vries equation is subdivided into an organic and mineral fraction and is re-written as follows:

$$\lambda = (\mathbf{x}_{\mathbf{w}}\lambda_{\mathbf{w}} + \mathbf{k}_{\mathbf{a}}\mathbf{x}_{\mathbf{a}}\lambda_{\mathbf{a}} + \mathbf{k}_{\mathbf{m}}\mathbf{x}_{\mathbf{m}}\lambda_{\mathbf{m}} + \mathbf{k}_{\mathbf{o}}\mathbf{x}_{\mathbf{o}}\lambda_{\mathbf{o}}) / (\mathbf{x}_{\mathbf{w}} + \mathbf{k}_{\mathbf{a}}\mathbf{x}_{\mathbf{a}} + \mathbf{k}_{\mathbf{m}}\mathbf{x}_{\mathbf{m}} + \mathbf{k}_{\mathbf{o}}\mathbf{x}_{\mathbf{o}})$$
(5)

in which \mathbf{x}_m represents the volume fraction of the mineral soil component, xo, the volume fraction of the organic soil component, λ_m , the thermal conductivity of mineral soil (Wm^{-1o}C⁻¹), \mathbf{k}_m is a weighting factor for mineral soil, and \mathbf{k}_o , a weighting factor for organic soil

The mass of water was determined by subtracting the mass of the soil that was oven-dried at 105°C from the mass of the wet soil measured in the field. The mass of organic material was calculated by "Loss On Ignition" (LOI) (Sheldrick et al., 1993), and corresponded to the mass loss after heating oven-dried soil samples in a muffle oven at 360°C. The remaining mass was taken to correspond to the inorganic portion of the soil. The resulting masses of water, organic and mineral material were then normalized to provide mass proportions of these components in the soil.

The volumetric proportions of water, organic matter and inorganic soil were calculated assuming the density of water to be 1.0 (Oke, 1987), and the dry bulk densities of organic matter and mineral soil to be 0.21 g/cm³ and 1.37 g/cm³, respectively. The latter values were taken from a study of tundra soils along the coastal plain of Alaska by Michaelson et al. (1996). This study was chosen because of the similarity of the soils and vegetation to those on Herschel Island, i.e., at both tussock tundra is underlain mainly by orthic, turbic Cryosols with cryoturbated organic and mineral horizons.

It is important to note that the dry bulk density varies according to the mineral make-up of the soils and the degree to which they have been compacted. For example, the density of quartz is 2.65g/cm³, however, the dry bulk density of a mineral soil is normally about half that density, i.e., between 1.0 and 1.6 g/cm³ (Birkeland, 1999). A dry bulk density greater than 1.6 g/cm³ indicates that the soil has undergone compaction, whereas a dry bulk density less than 1.0 g/cm³ signals a high organic content.

Owing to the presence of excess water within all samples of soil from Slump A, the soils were assumed to be water-saturated. In a saturated soil, the water content is given by the porosity. As the porosity of these soils could not be reliably measured, it was assumed to be 40%, which corresponds to the porosity of a soil compositionally similar to that at Slump A (a mixture of silt clay and organic matter) reported in van Wiljk and de Vries (1963). The volume fraction of water (x_w) was therefore assumed to be 0.4, and the volume of solid (x_s) , the remainder; the volume proportions of the organic and inorganic parts of the solid fraction were calculated from their dry bulk densities as explained above. As the soils were water-saturated, the volume fraction of air could be ignored, simplifying equation 5 to:

$$\lambda = (x_w \lambda_w + k_m x_m \lambda_m + k_o x_o \lambda_o) / (x_w + k_m x_m + k_o x_o)$$

The weighting factor (k) for the solid part of the soil (i.e., the mineral and organic components) was calculated using the equation:

(7)

$$K_x = 1/3 \Sigma_{a,b,c} \{ 2 / (1 + [(\lambda_x/\lambda_w) - 1)] 0.125) + 1 / (1 + [(\lambda_x/\lambda_w) - 1)] 0.75)$$

Where \mathbf{x} refers to mineral (\mathbf{m}) or organic (\mathbf{o}), k_x is the weighting factor for organic or mineral soil, $\lambda_{\mathbf{x}}$ is the thermal conductivity of organic or mineral soil (Wm⁻¹°C⁻¹), and $\lambda_{\mathbf{w}}$ is the thermal conductivity of water (Wm⁻¹°C⁻¹) (Farouki, 1981).

The volumetric latent heat of fusion of the ice contained in the soil was calculated using the equation:

$$L = \rho_d L'(w/100)$$

in which, L is the volumetric latent heat of fusion of the ice component of the soil (J m⁻³), ρ_d represents dry soil density (kg m⁻³), L' is the latent heat of fusion of ice at 0 °C (J kg⁻¹), and w denotes total water content (%) (Andersland and Ladanyi, 2004).

The latent heat of fusion for ice (L) at 0°C is 333.7 x 10³ J kg⁻¹ (Farouki,1981).

4.4. RESULTS AND DISCUSSION

4.5.1. THAWING DEGREE DAYS

Values for the thawing degree days were calculated from the start of the thaw season (May 18th) to August 24th, 2011 (the last day on which the active layer depth was measured) using a combination of data collected from Environment Canada (air temperature) and the single-channel data loggers (ground and air temperature). The differences in the measured data sets were used to convert the Environment Canada data to estimates of ground temperature for the early part of the thaw season that preceded the start of fieldwork. The difference in the mean daily air temperature measured with the single-channel data loggers from that measured by Environment Canada varied from less than 3°C on some days to more than 6°C on other days (*Fig. 4.6.*).

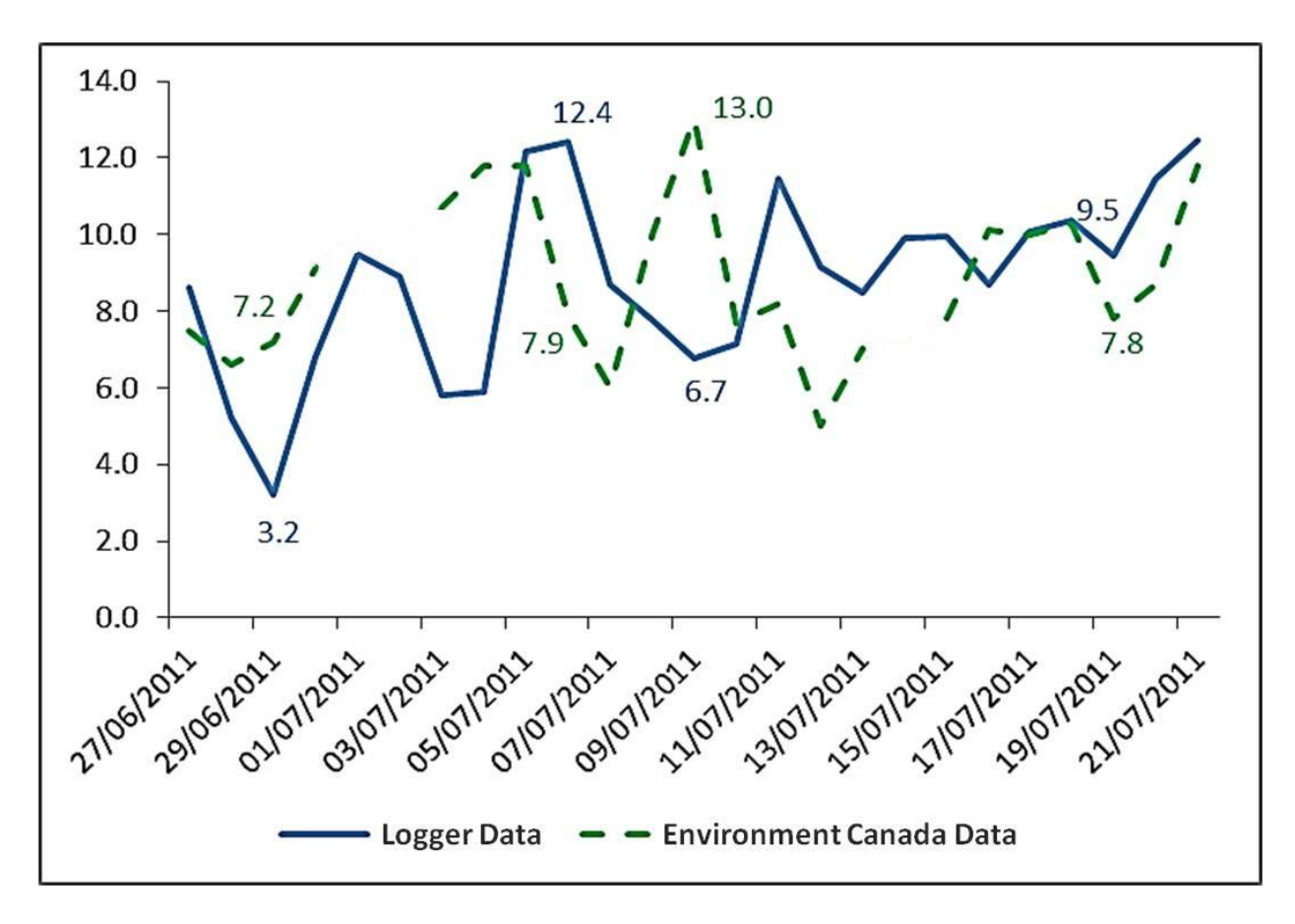


Fig. 4. 6.: Mean daily air temperatures measured between June 27th, 2011 and July 21st, 2011 from the single-channel logger data and Environment Canada.

This difference can be explained by the different setting of the two areas. As mentioned above, the Environment Canada weather station is located at an elevation of 1.2 m above sea-level, whereas the site at which the single-channel logger data was collected, was between 28-30 m above sea-level. Consequently, the two locations likely have different micro-climates (Oke, 1987). In particular, the lower elevation of the Environment Canada weather station makes it more susceptible to small differences in aspect, exposure and sea breeze from the Beaufort Sea. Nonetheless, the mean difference in temperature over the 25 days when data logger measurements were made was only 0.4 °C; the mean temperature at the study site was 8.9°C and at the Environment Canada station was 8.5°C. As "degree days" is a cumulative parameter, it is

the mean cumulative temperature rather than the mean daily temperature that is important in estimating thaw depth at any given time. Consequently, the small difference between the averaged data logger and Environment Canada air temperature data provide confidence that the latter can be used reliably to predict temperature at the study site prior to the start of the field season

The Environment Canada temperature data (T_{EC}) were corrected to the single-channel logger (T_{H}) data by linear regression, which yielded the equation $T_{EC} = 0.86T_{H} + 1.49$ with an r^{2} value of ~0.83 (Fig.~4.7.). As daily temperatures were recorded by the single-channel data loggers only from June 26^{th} , 2011 to July 21^{st} , 2011, this equation was used to adjust the Environment Canada temperature data set, so that a complete thawing season temperature data log for the ALM site could be obtained. To account for the difference between the ambient temperature and the ground surface temperature, logger data for the latter (T_{Hg}) were regressed linearly against the single-channel data logger ambient air temperature values (T_{Ha}) (Fig.~4.8.). The corresponding equation was $T_{Hg} = 0.9 T_{Ha} + 1.13$, and the r^{2} ~0.95. The ground temperatures for the full thaw season and, in turn, the thawing degree days were estimated using the Environment Canada air temperature data corrected in the manner described above.

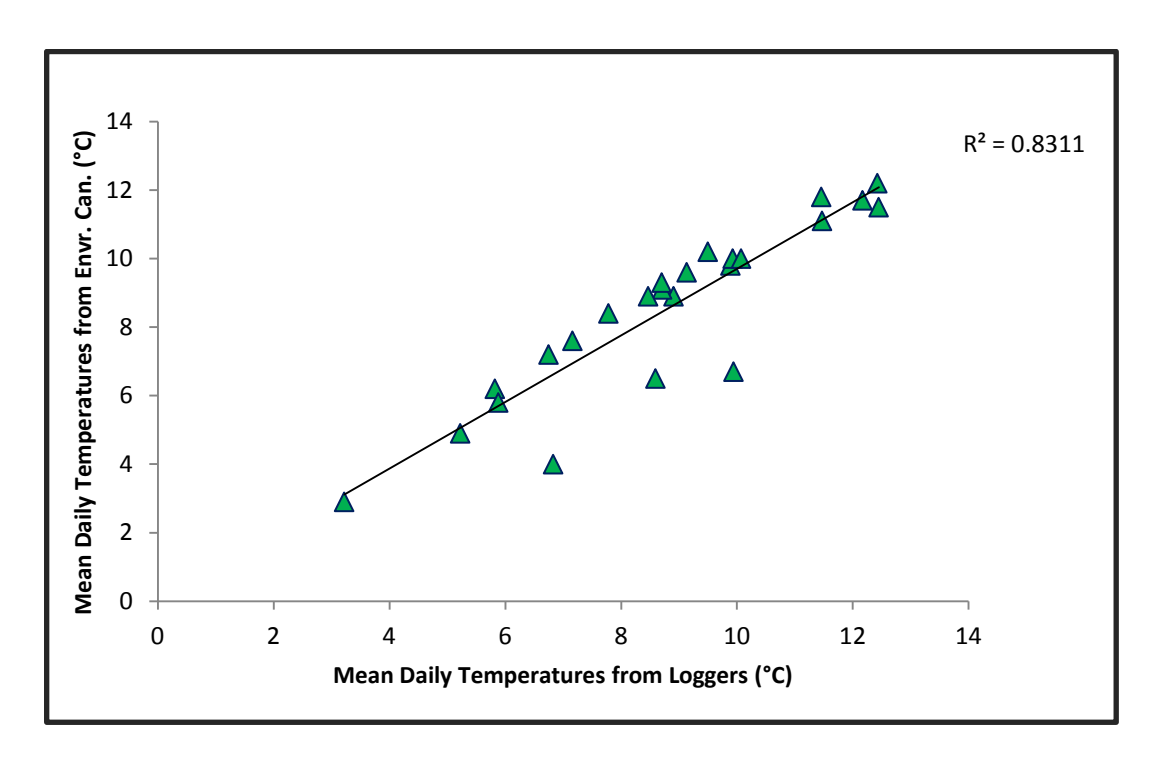


Fig. 4. 7.: Relationship between mean daily temperatures measured by Environment Canada and those by the single-channel data loggers between June 27th, 2011 and July 21st, 2011.

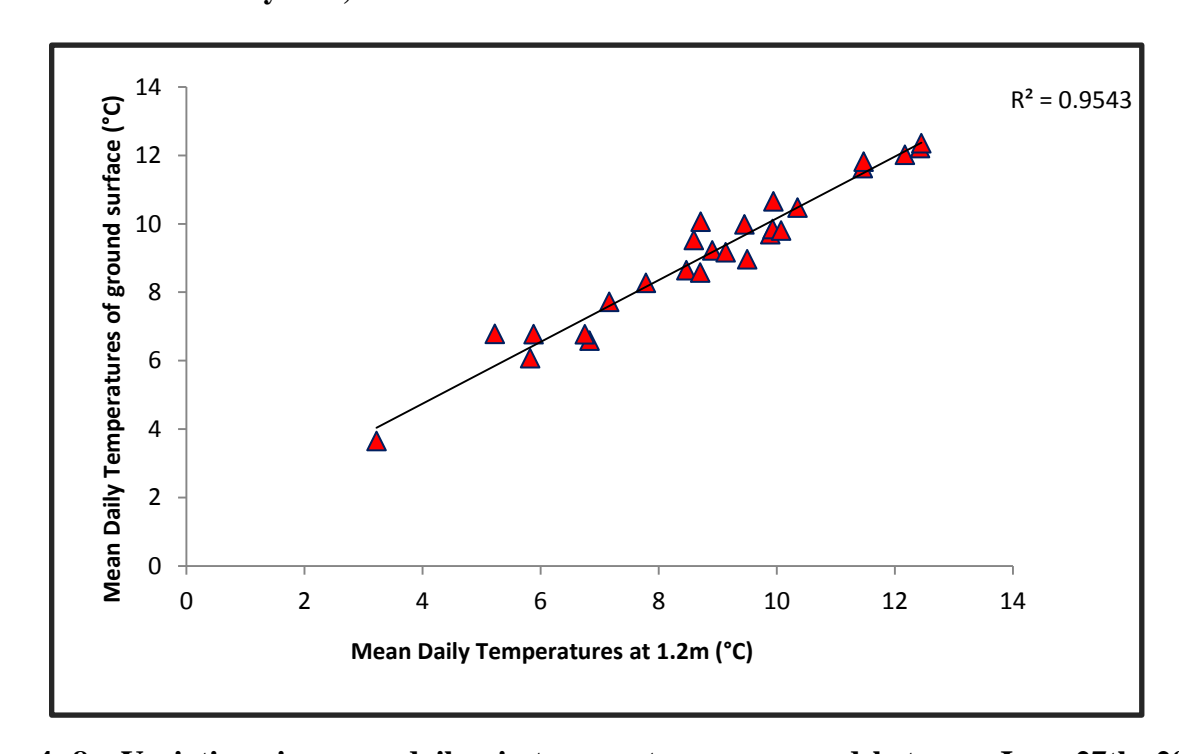


Fig. 4. 8. Variations in mean daily air temperatures measured between June 27th, 2011 and July 21st, 2011 at the ground surface and at 1.2m using data from single-channel data loggers.

Cumulative mean temperatures above 0°C ranged from 3.3°C on the 24th of June, 2011 to 7.1°C on the 24th of August, 2011. Multiplying the cumulative mean temperatures above 0°C by the number of accumulated thawing days for each of the sampling days, yielded thawing degree day (TDD) values ranging from 118 °C·days at the start of the active layer probing (24th, June, 2011), to 692 °C·days on the last day of active layer probing (24th, August, 2011). The accumulated thawing degree days calculated for the end of the 2011 thaw period (28th, September) was 767°C·days.

4.5.2. ACTIVE LAYER DEPTHS

Active layer depths across the ALM site ranged from 3.0 cm to 26.5 cm on the 24th of June, 2011, and from 29.5 cm to 56 cm on the 24th of August, 2011 (Appendix *Table 7.1.*). The variations in depths within the sites were due to the occurrence of depressions, cotton grass tussocks and the formation of a tundra pond. Thawing depths were lowest below cotton grass tussocks and greatest in the tundra pond (*Fig. 4.9.*).

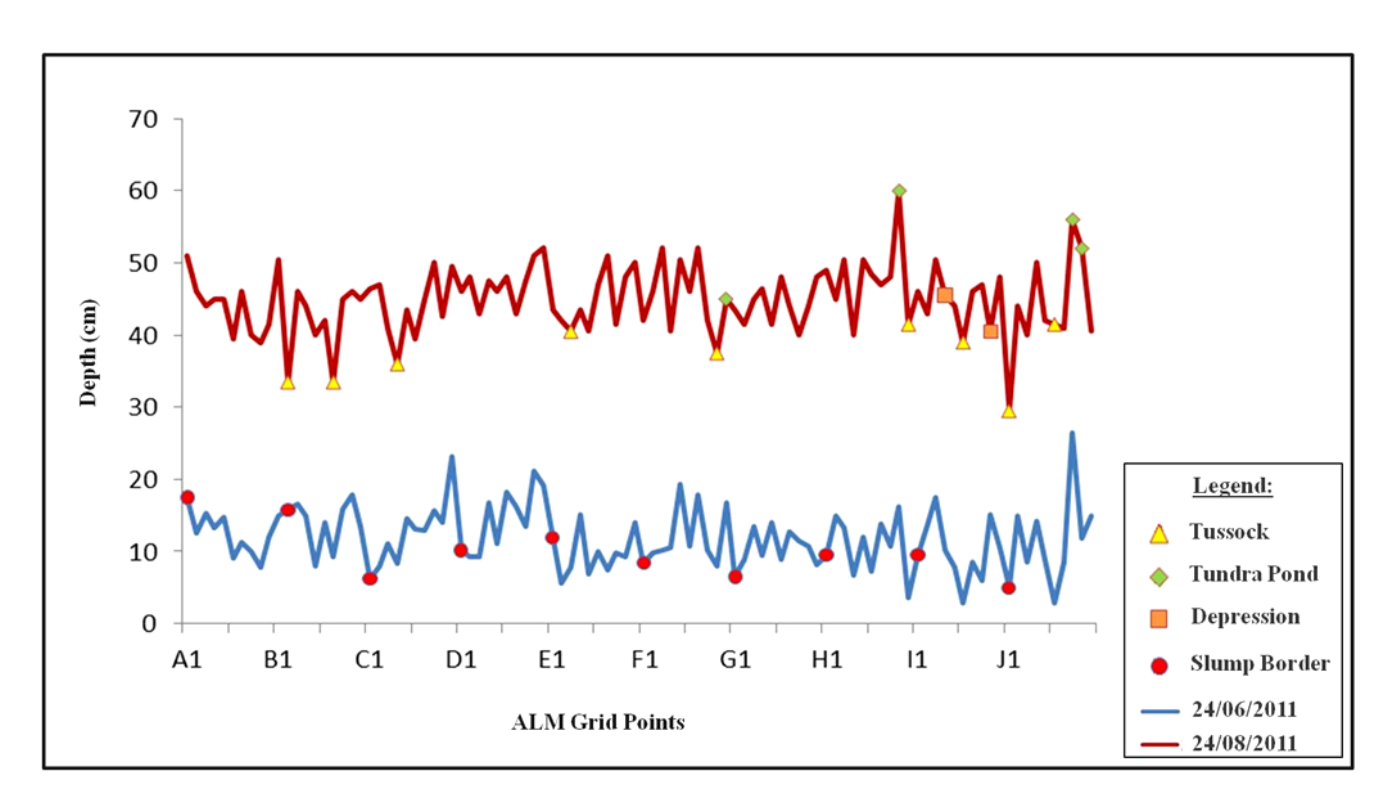
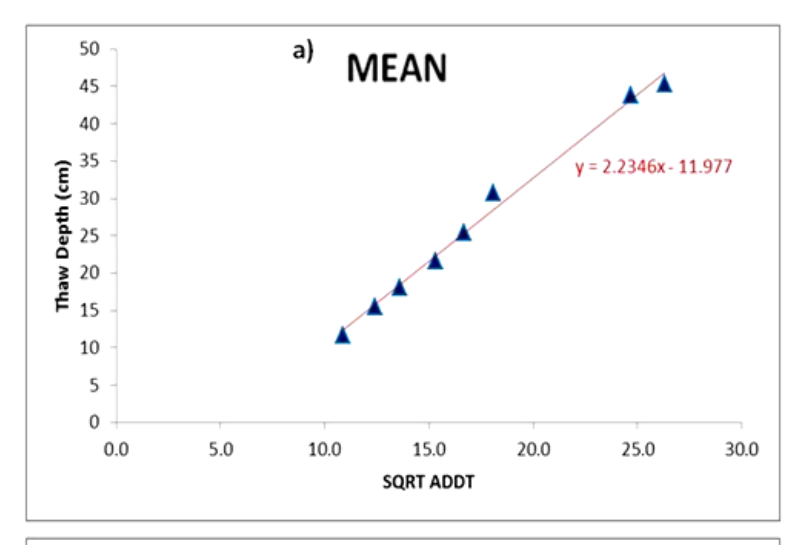


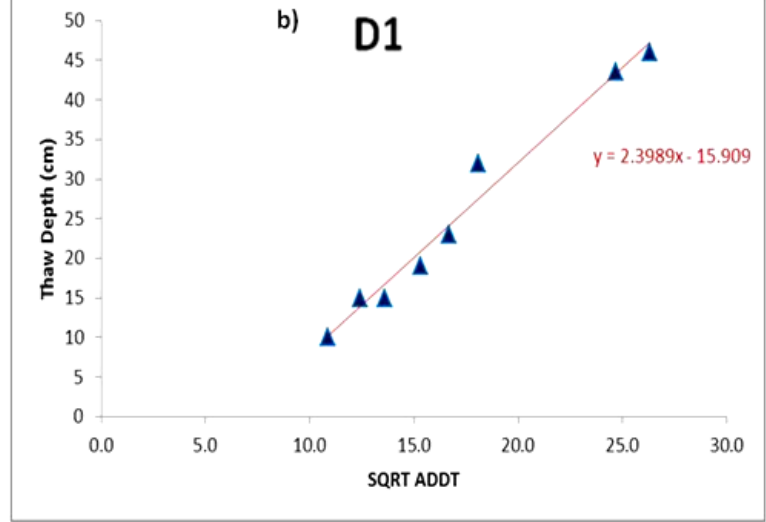
Fig. 4. 9. Active layer depth change between sites on June 24th, 2011 and August 24th, 2011.

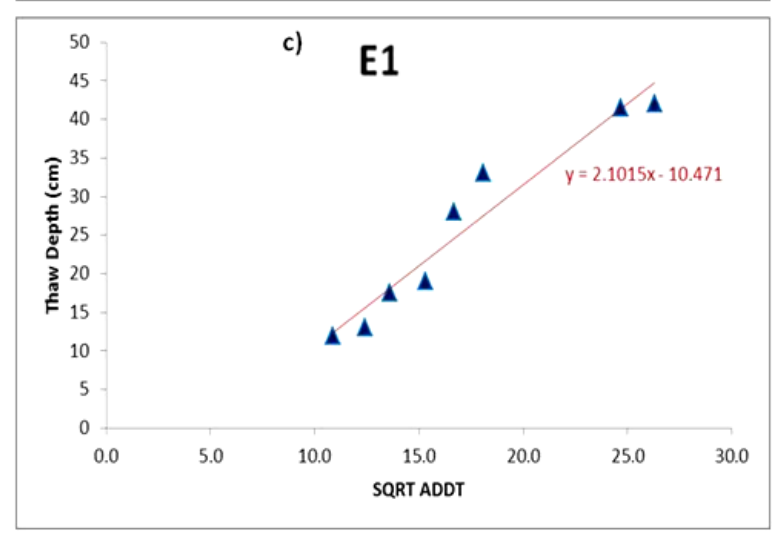
The shallower active layer depth below cotton grass tussocks can be explained by the fact that vegetation acts as a protective barrier between the atmosphere and the ground surface, lowering the amount of heat transferred to the underlying soil through evapotranspiration (Oke, 1987). Conversely, the significantly greater depth of the active layer in the tundra pond can be attributed to the high thermal conductivity of the surface water and the correspondingly greater amount of heat that can be transported to the underlying soil (Brown, 1979; Burn, 1988; Jorgenson et al., 2001; Hinkel et al., 2001; Zhang et al., 2008; Jorgenson et al. 2010). Significantly, a recent study by Jorgenson et al. (2010) on the resilience and vulnerability of permafrost in a warming climate, showed that the presence of standing water increased the near-surface temperature by ~10°C above the mean annual air temperature.

4.5.3. THERMAL CONSTANTS

As discussed in section 4.3.2, the thermal constant of a soil can be determined empirically by making regular measurements of the depth of the active layer at a given location over the duration of the thaw season and plotting this depth against the square root of the thawing degree days. If the relationship is linear, it is described by equation 3 and the thermal constant (**B**) is given by the slope of this line. This relationship was evaluated for all points on the ALM grid and in most cases proved to be linear (*Fig. 4.10. a-f*). The corresponding thermal constants ranged from 1.9 to 2.4 and averaged 2.23 (*Table 4.2.*). The two sites nearest the slump face, D1 and E1 yielded thermal constants of 2.4 and 2.10, respectively. The mean for the tussock locations was 2.12 and for the swamp locations was 2.22. These data show that the thermal properties and hence composition of the soils at all localities were remarkably similar.







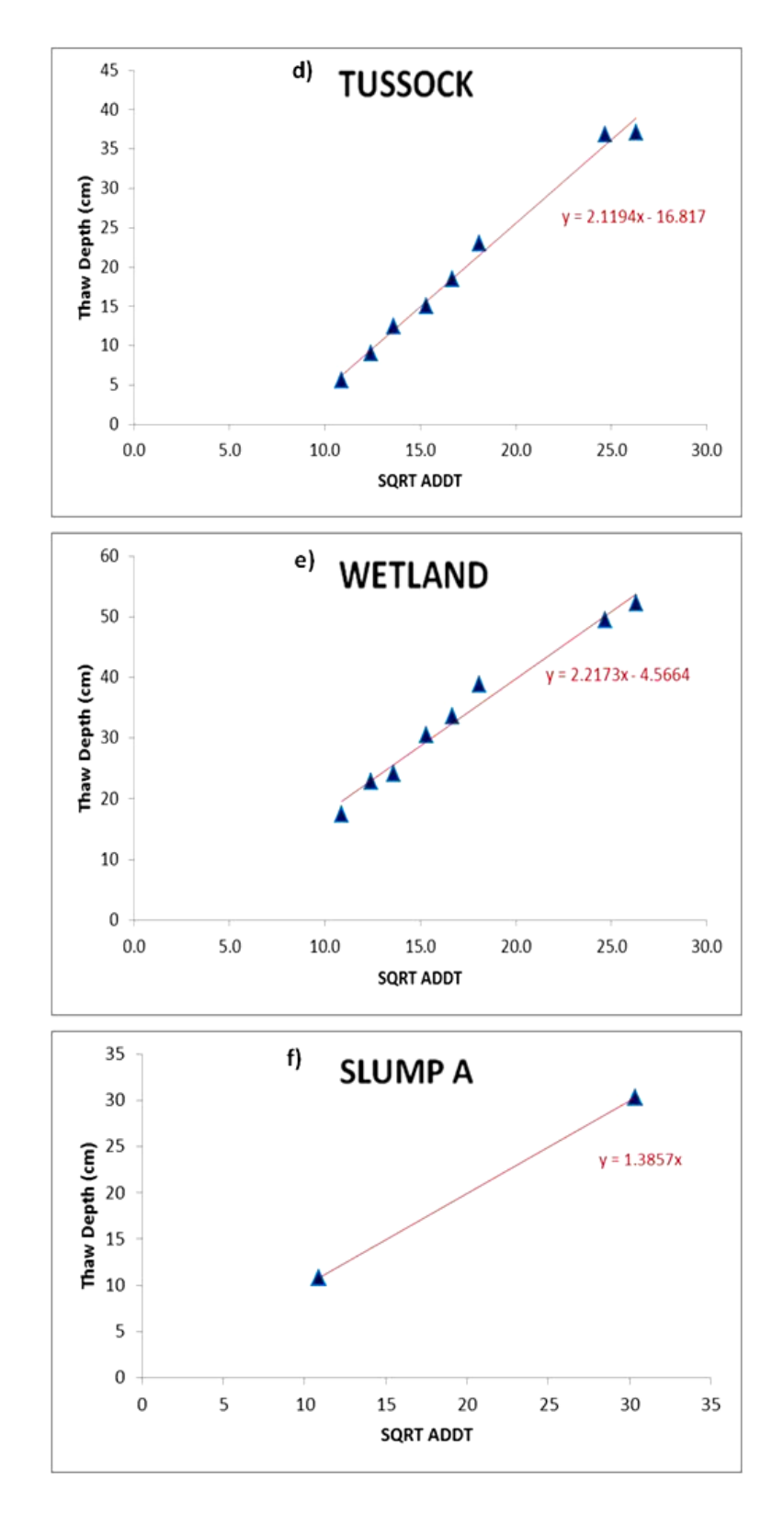


Fig. 4. 10. Relationships between thaw depth and accumulated thawing degree days for selected sites, for selected types of sites (tussock and wetland), Slump A and the entire ALM grid.

Table 4. 2.: Changes in mean thaw depth, cumulative temperature, thawing days, thawing degree days and thermal constants for the 2011 thaw season and end of 2010 thaw season.

Date	Mean Thaw Depth (cm)	Cum. Mean Temperature > 0°C (°C)	Thawing Days (days)	Thawing Degree Days (° <u>C:days</u>)	Thermal Constant
24/06/2011	11.4	3.3	36	118	1.0
29/06/2011	15.2	3.8	41	154	1.2
03/07/2011	17.8	4.1	45	185	1.3
08/07/2011	21.3	4.7	50	234	1.4
13/07/2011	25.2	5.1	55	278	1.5
18/07/2011	30.3	5.4	60	326	1.7
13/08/2011	43.5	7.1	86	609	1.8
24/08/2011	44.8	7.1	97	692	1.7
28/09/2011	Unknown	6.1	126	767	Unknown
23/09/2010	39.0	7.1	130	921	1.3

A thermal constant for the active face was also calculated using the thermal properties of the soils exposed on the face and equations 7 to 9. The thermal conductivity calculated using equations 7 and 8 (the De Vries method) was 0.79 and 0.71 W/m³ ·°C for the organic rich sections of the active layer (SOM >20%) and was 0.94 W/m³ ·°C for its mineral rich section (*Table 4.3.*). These values compare well with those reported for soils of similar composition (Farouki, 1981; Goodrich, 1986; Hinzman et al., 1991). The volumetric latent heat of fusion was 79.29 and 63.05 KJ/m³ in the organic-rich sections and 112.97 KJ/m³ in the mineral-rich sections. After being weighted for the relative thicknesses of the corresponding sections, these data yielded a thermal constant of 1.39 which is significantly lower than the values obtained for the ALM grid.

Table 4. 3.: Thermal constants calculated using the De Vries method.

Depth (cm)	Weighted Thermal Conductivity (W/m ³ ·°C)	Volumetric Latent heat of fusion (J/m³)	Bulk density (g/cm³)	Thermal Constant
0-12	0.79	79287.7	0.59	1.31
12-32	0.84	112974.2	0.85	1.20
32-39	0.77	63053.7	0.47	1.39

In part the reason for the higher thermal constants (empirical) estimated for the ALM grid is that the active layer thickness was estimated from the depth of penetration of a rigid metal rod (calibrated in cm) into the active layer to the point of resistance, interpreted to represent the limit of thawing. This method overestimates the thickness of the active layer by 6 to 8 % (Brown et al., 2000), because the rod typically penetrates below the frost table (0°C isotherm) into soil containing a mixture of ice and water. Moreover, the thickness of the mixed ice/water zone is likely to increase as the thaw season progresses, thereby increasing the slope of the thaw depth/ATTD function, or the value of the thermal constant. The other reason for the higher empirical thermal constants is their derivation from the relationship between the active layer thickness and the number of thawing degree days. They therefore represent not only the conductively transferred heat but also that transferred by advection.

4.6. GLOBAL WARMING AND THE STATE OF THE ACTIVE LAYER

According to the Arctic Climate Impact Assessment report (ACIA, 2005), increased greenhouse gas concentration is likely to have a greater impact on the Arctic climate than anywhere else on the planet. In order to permit prediction of the possible effects of future climate change, a variety of coupled atmosphere-land-ocean global models have been used to make projections about the

nature of the climate until the end of the 21^{st} century. For the purpose of this study, third generation Canadian Global Coupled Models (CGCM 3.1/T63) from the Canadian Centre for Climate Modelling and Analysis (CCCma) were used to predict the future temperature on Herschel Island. The two models used are based on simulations of the Intergovernmental Panel on Climate Change (IPCC), namely scenarios SRES A2 and SRES B1. In the SRES A2 scenario, CO₂, emissions are projected to reach over 800ppm, causing the surface temperature to rise between 2.0 to 5.4°C in the decade 2090-2099 relative to 1980 -1999. The SRES B1 scenario is more conservative, with CO₂ emissions projected to stabilize at 550 ppm, resulting in a projected temperature rise by 1.4 to 3.8°C in 2090-2099 relative to its level between 1980 and 1999 (Anisimov et al., 2001). The data obtained from the CGCM 3.1/T63 model are based on a surface grid with a spatial resolution of roughly 2.8° latitude by 2.8° longitude and 31 levels in the vertical dimension. The grid cell closest to Herschel Island is identified by $I_1 = 79$ and $J_1 = 57$, which corresponds to the coordinates, 140.62°W and 68.37°N.

Daily surface temperatures for the above cell were obtained for 2011, 2050 and 2100 for both the SRES A2 and SRES B1 scenarios. The projected cumulative mean temperatures for 2011 are compared in *Figures 4.11* and *4.12* with actual measurements of the cumulative mean temperature for dates on which active layer thickening on the ALM site was monitored during 2011 (24th June to 24th August).

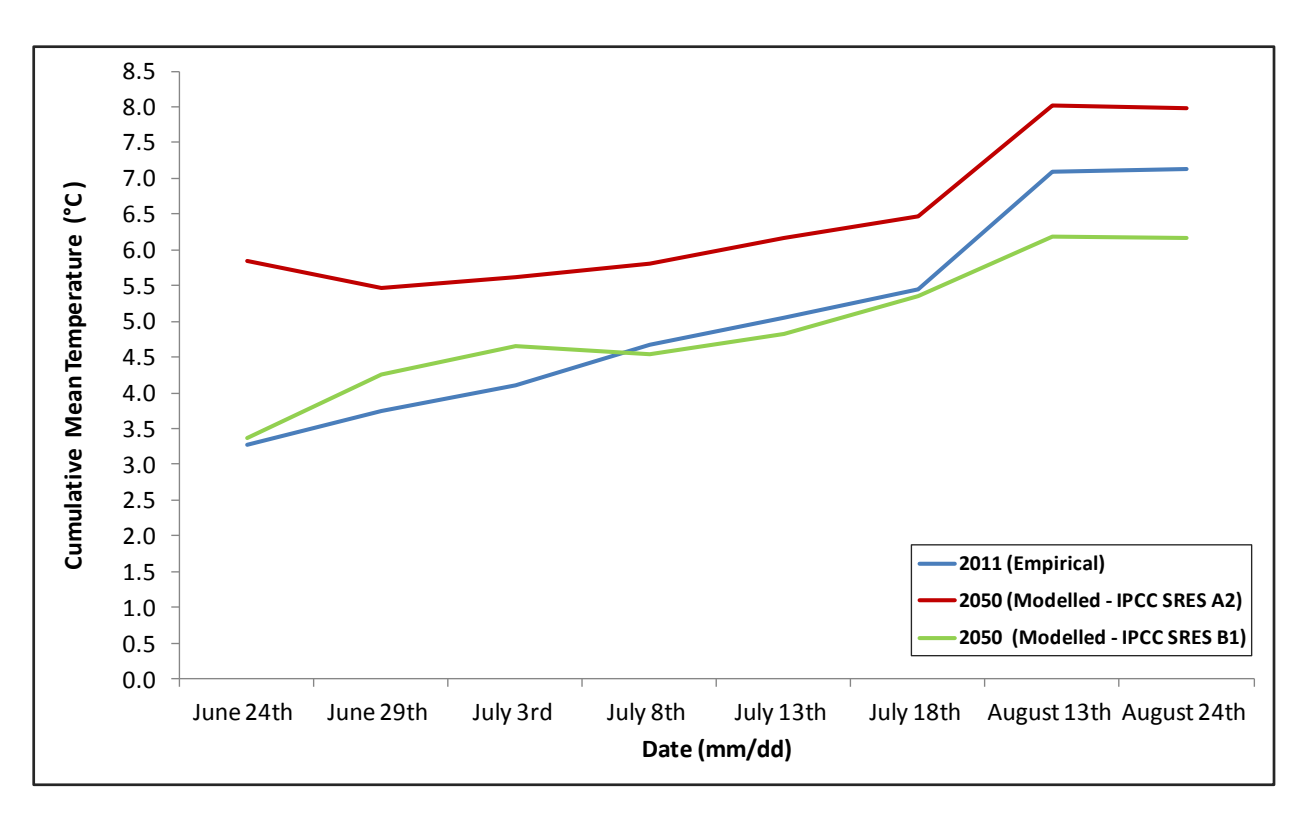


Fig. 4. 11. : Cumulative mean temperatures for measured (2011) and modelled (2050) data from June 24^{th} to August 24^{th} .

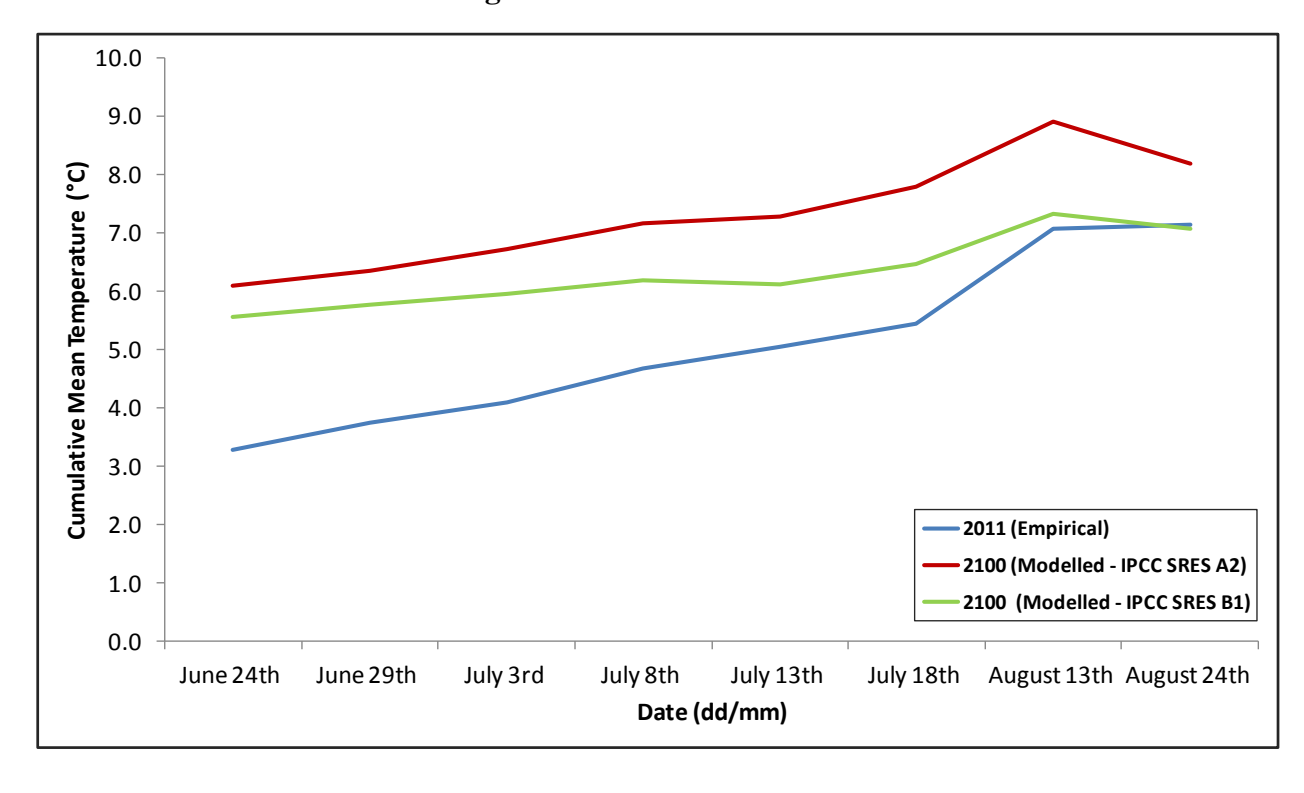


Fig. 4. 12. : Cumulative mean temperatures for measured (2011) and modelled (2100) data from June 24^{th} to August 24^{th} .

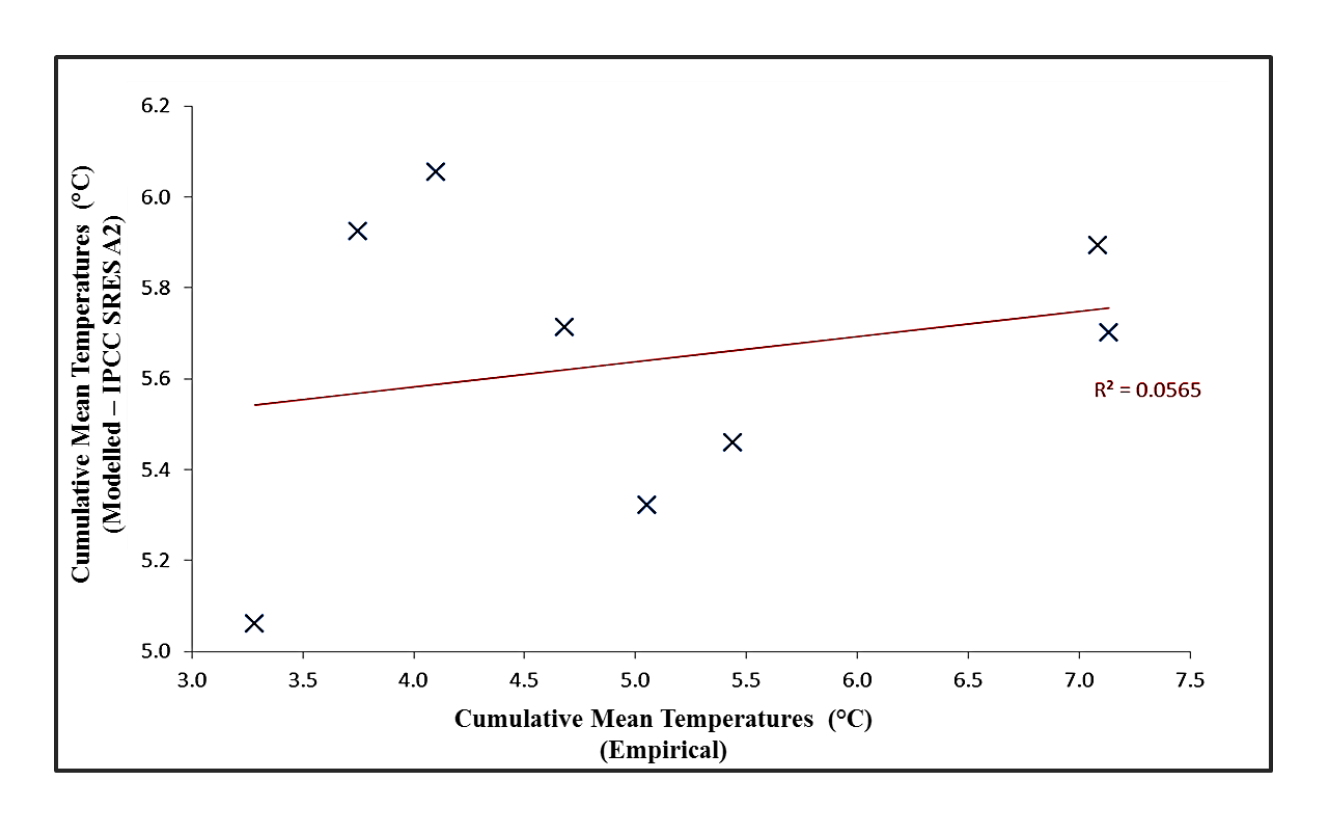


Fig. 4. 13.: Relationship between the cumulative mean temperatures generated from the IPCC SRES A2 scenario and those measured at Herschel Island, YK in 2011.

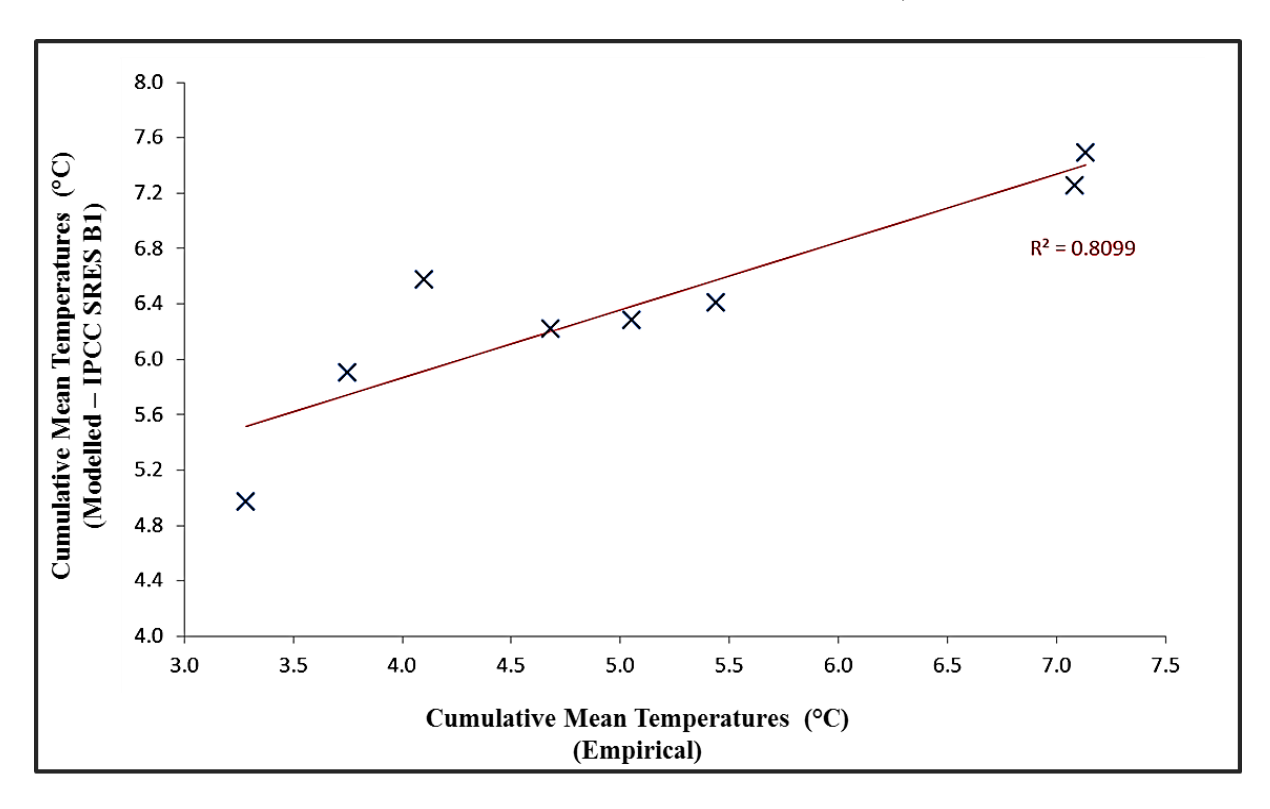


Fig. 4. 14.: Relationship between the cumulative mean temperatures generated from the IPCC SRES B1 scenario and those measured at Herschel Island, YK in 2011.

Although global climate models can be applied to specific areas of the Earth's surface, one of the limitations of these models is that they do not account for changes that can occur on a very small scale, producing micro-climates (Boer et al., 2000). Indeed, the cell encompassing the study area extends 149 km southwest of Herschel Island to an inland location approximately 130 km from the Yukon coastline, which is at an elevation of 419 m; the study area is at an elevation of 29-30 m and the maximum elevation on Herschel Island is 181 m. This large difference in elevation and the location of the study area adjacent to the ocean are highly likely to cause the temperature of the study area to be significantly different from the average of the cell and could easily account for the differences between the predicted and measured values. In view of this, the correlation between the measured temperatures and those projected by the B1 scenario are reasonably strong.

In Figures 4.15 and 4.16, we show the measured daily temperature for 2011 and projected daily temperatures for 2050 and 2100 for the A2 and B1 scenarios (May 1st to October 31st), and the corresponding thawing days (Tables 4.4.).

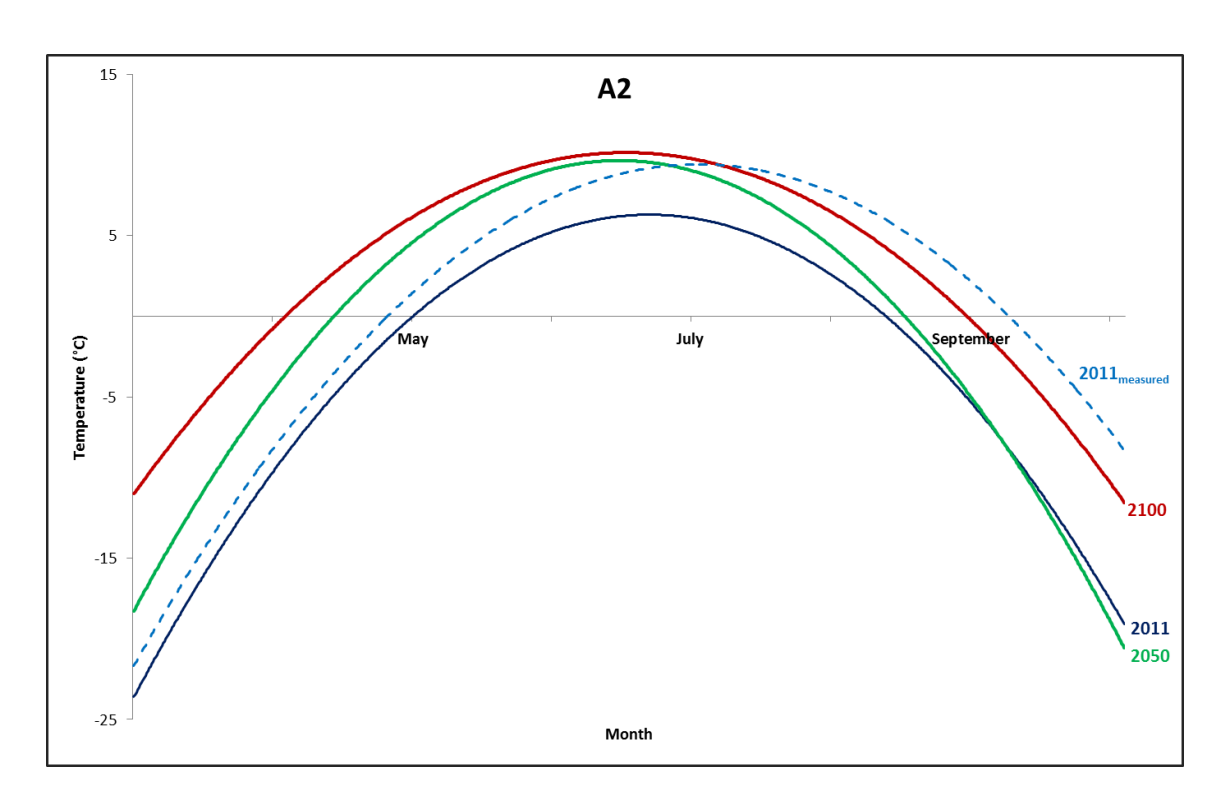


Fig. 4. 15. : Measured daily temperature for 2011 and projected daily temperatures for 2050 and 2100 for the A2 scenario from May 1st to October 31st.

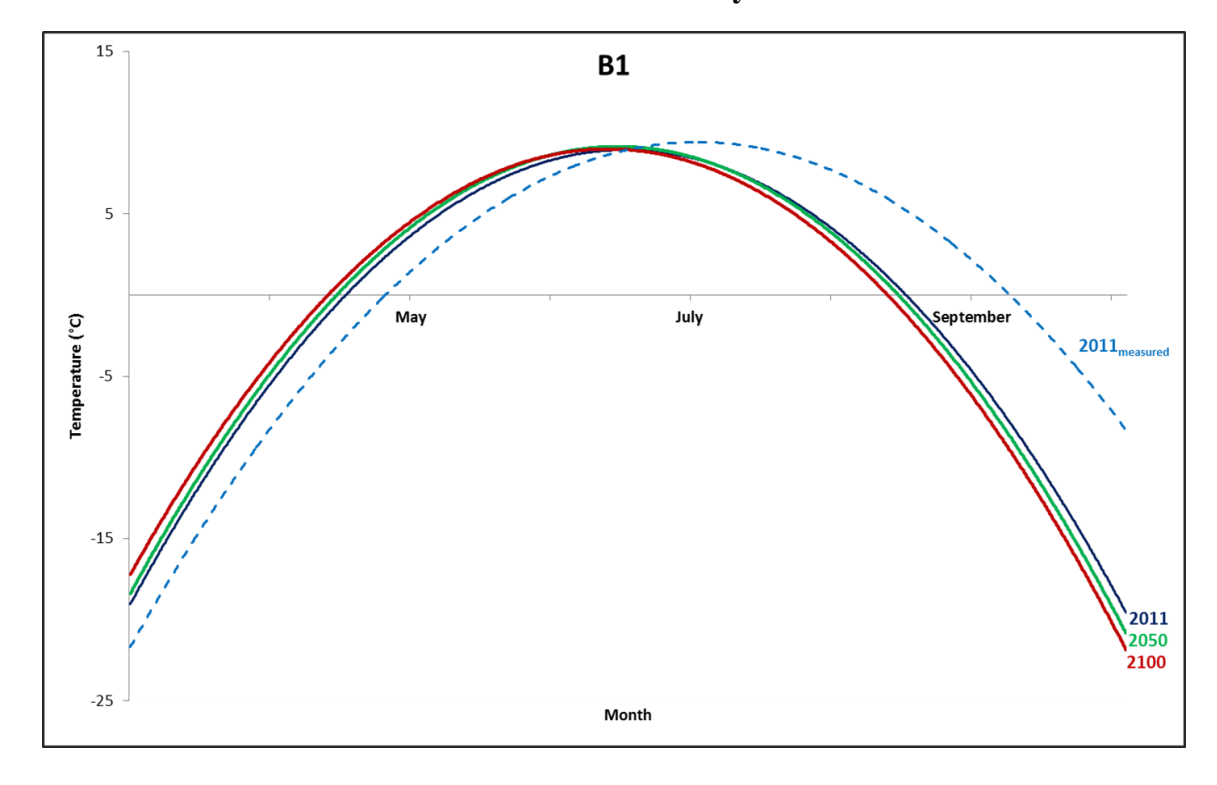


Fig. 4. 16. : Measured daily temperature for 2011 and projected daily temperatures for 2050 and 2100 for the B1 scenario from May 1st to October 31st.

Table 4. 4.: Thawing season changes based on IPCC SRES A2 and B1 scenarios using CGCM3.1/T63

	Thaw Start Date (dd/mm/yyyy)	Thaw End Date (dd/mm/yyyy)	Thawing Days (days)	Cumulative Thawing Degree Days (°C·days)
2011 (Empirical)	18/05/2011	28/09/2011	126	767
2011 (Modelled IPCC SRES A2)	17/05/2011	13/09/2011	123	527
2011 (Modelled IPCC SRES B1)	08/05/2011	04/09/2011	114	805
2050 (Modelled IPCC SRES A2)	14/05/2050	19/09/2050	114	830
2050 (Modelled IPCC SRES B1)	02/05/2050	17/09/2050	129	728
2100 (Modelled IPCC SRES A2)	02/05/2100	05/10/2100	137	1059
2100 (Modelled IPCC SRES B1)	12/05/2100	22/09/2100	113	759

From these figures and Table 4.4, it can be seen that the thaw season in 2011 started on the 18th of May and terminated on the 28th of September for a total of 126 days. The SRES A2 and B1 models (projected from the year, 2000) predicted thaw seasons of 123 and 114 days, respectively, i.e., both scenarios underestimated the actual length of the thaw season. However, the "accumulated thawing degree days" projected by the B1 model (the more conservative of the two scenarios) exceeds the measured "accumulated thawing degree days" (805 versus 767), whereas the A2 model, underestimates it considerably (527 days). For 2050, the order of "accumulated thawing degree days" projected by the A2 and B1 scenarios is reversed; the "accumulated thawing degree days" increases to 830 in A2 and decreases to 728 in B2. Finally, for 2100, both models project increases in the "accumulated thawing degrees" from 2050, although, as might be expected, the increase projected by the B1 model is relatively modest (31 days). The "accumulated thawing degree days" predicted by the A2 model is 1059. The average temperature during July (the middle of the thaw season) was projected by model A2 to increase from 5.8 °C in 2011 (the measured temperature was 9.9 °C) to 11.6 °C in 2050 and to 11.9 °C in 2100, representing temperature increases of 5.8 (or 1.7 °C based on the measured data for 2011)

and 0.3 °C, respectively. The corresponding temperature increases predicted by model B1 are 1.3 °C (or -0.8 °C based on the measured data for 2011) and 0.2 °C.

The maximum thaw depths for the study area were estimated for 2050 and 2100 using the Stefan equation, the total thawing degree days projected for the two IPCC SRES scenarios, and the thermal constants obtained theoretically (1.39) and empirically (2.23). For the year 2050, these depths are predicted to be 40 cm for the IPCC SRES A2 scenario and 37.5 cm for the IPCC SRES B1 scenario based on the theoretically determined thermal constant (Table 4.6.). By contrast, the corresponding maximum thaw depths predicted using the empirical thermal constant, are 64.2 cm and 60.2 cm respectively. The depths reported above correspond to a projected increase in the maximum thaw depth by 2050 of 4% for the IPCC SRES A2 scenario and a decrease of 2.58% for the IPCC SRES B1 scenario (Fig. 4.17.). For 2100, the maximum thaw depths, for the IPCC SRES A2 and B1 scenarios estimated using the theoretically determined thermal constant, were 45.2 cm and 38.3 cm, respectively, and using the empirically determined thermal constant were 72.6 cm and 61.4 cm, respectively. These depths correspond to an increase in the maximum thaw depth of 17.5% for the IPCC SRES A2 and a decrease of 0.52% for the IPCC SRES B1 scenario, relative to that measured in 2011. The variations in the percent increase of maximum thaw depth for the IPCC SRES A2 scenario and percent decrease for the IPCC SRES B1 scenario are significantly greater when based on the modelled 2011 temperatures rather than the measured 2011 temperatures. For 2050, the projected percent increase in maximum thaw depth estimated for the IPCC SRES A2 scenario using the modelled 2011 temperatures, is 25.5%, whereas for the IPCC SRES B1 scenario, a decrease of 4.9 % is projected for the same year. Similarly for 2100, the predicted increase in maximum thaw depth is

41.76 % for the IPCC SRES A2 scenario, whereas it decreases by 2.9 % for the IPCC SRES B1 scenario.

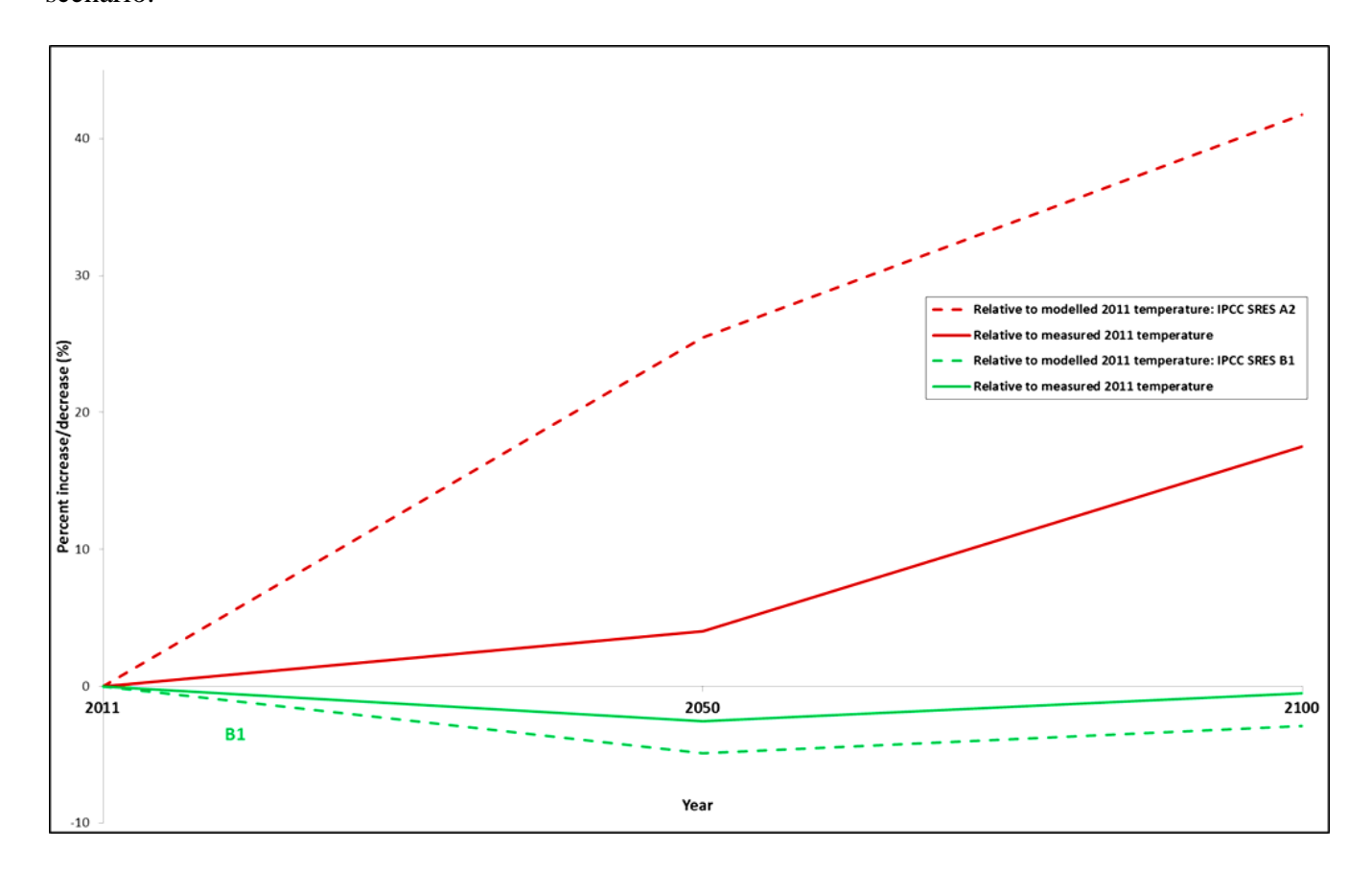


Fig. 4. 17. : Projected percent increase/decrease in maximum thaw depths for 2011, 2050 and 2100.

4.6.1. THERMOKARST AND GROUND SUBSIDENCE

According to French (2008), increases in surface temperature due to global warming and the resultant increase in the depth of the active layer can cause disruption of the thermal equilibrium of the permafrost. This leads to the development of thermokarst, which occurs when the ground ice volume that exceeds the saturated volume of the soil in water and results from the degradation of ice-rich permafrost and/or melting of massive ice (van Everdingen, 1998). However, it is important to note that during warming, heat exchanges within the soil may be diminished by increases in precipitation and cloud cover (French, 2008). This will reduce the rate

of downward advance of the active layer and, in turn, inhibit potential thermokarst development. In warming scenarios, such as those considered here, both snow fall and cloud cover are projected to increase, and therefore the intensity and frequency of thermokarst development are difficult to predict (French, 2007). Nevertheless, thermokarst development has been shown to be prevalent on regional scales across the Arctic, and to have occurred during extended periods of fluctuation between colder and warmer climates in the Quaternary and Holocene periods (Mackay, 1975; Burn et al., 1986; Burn, 1997; French, 1999; Romanovsky et al., 2000).

Ground subsidence is controlled primarily by the presence of excess ice, but also by the freezing and thawing cycle of the active layer (the act of thawing ice-rich sediments reduces their volume and, in turn, causes the ground surface to subside; Birkeland, 1999). If the water produced by this thawing process is in motion and is removed permanently from the soil, the subsidence will be permanent. Moreover, the subsidence may be amplified, because flowing water will promote thermal erosion (Mackay, 1970). The extent to which subsidence occurs depends on the rate of migration of water through the ground surface. If the sediments are fine-grained, the migration may be impeded and the extent of thaw subsidence will vary with the permeability and compressibility of the thawed ground. However, if migration is unimpeded, the extent of thaw subsidence is controlled entirely by the position of the thawing front (French, 2007).

In the case of Slump A, migration of water from the immediately adjacent soils can be assumed to be unimpeded as the water is expelled continuously from the thawing headwall. By contrast, migration of water at more distant sites within the ALM grid is likely to be quite variable, with some locations draining more rapidly than others. Evidence that some parts of the ALM site

drain much more poorly than others is provided by the formation and preservation of the ice wedge-produced pond in the northeast of the ALM grid in rows H, I and J. The tundra pond depth measurements taken during the sampling period ranged from 48 cm on July 3rd, 2011 to 87 cm on July 18th, 2011, indicating a much higher water input from melting and precipitation, than water loss through evaporation and drainage. Therefore, thaw subsidence in the ALM grid is not likely to be proportional to the volume of ice lost from the substrate, and any estimates made of ground subsidence would be unreliable, except close to the headwall of the slump. At the slump headwall, however, where migration of water is unimpeded, the subsidence related to future thickening of the active layer can be estimated from the volume proportion of water including excess ice (Crory, 1973; Pollard & French, 1980; Johnson et al., 1984; Pullman et al., 2007). This proportion was estimated from the ice content of the soil samples below the active layer (Table 4.5.) assuming that they have a porosity of 0.4, and was determined to be 139.7%. Based on this value and the empirical relationship of the volume proportion of water to the percentage subsidence established by Johnson et al. (1986) for thawed fine-grained soils, it is estimated that the percentage subsidence for well-drained soils in the study area was 66%. This corresponds to a subsidence of 6.6 cm for each 10 cm of permafrost thaw (active layer thickening), e.g., for the ALM sites immediately adjacent to the slump face (D1 and E1). This is a minimum estimate as it ignores any contribution from thermal erosion. Nonetheless, it is very similar to the average subsidence measured by Burn and Zhang (2009) from the protrusion of steel benchmarks at 9 sites at Collinson Head on Herschel Island, of 6.5 cm after 11 cm of active layer thickening between 2005 and 2007. Using the estimates of the thickness of the active layer, reported above, it can be predicted that the subsidence near Slump A will reach between 4 cm and 7 cm by 2100 for the different thermal constants and warming scenarios considered above.

Table 4. 5. : Excess ice contents with depth.

Depth	Volume of	Volume of	Porosity	Excess Ice	Weighted Excess
(cm)	water (%)	soil (%)	(%)	(%)	Ice (%)
45-50	67.4	32.6	40.0	27.4	(/0)
43-30	07.4	32.0	40.0	27.4	
50-122	80.6	19.4	40.0	40.6	39.7

4.6.2. IMPACT OF GLOBAL WARMING ON THE PALEO-ACTIVE LAYER

Botanical and cryostratigraphic records collected in northwest Canada provide evidence of a Holocene Thermal Maximum (HTM) beginning between 10.6 and 9.7 ka, in which the summer air temperature, was as much as 3°C higher than it is today (based on data for the Tuktoyuktuk Peninsula; Ritchie, 1984). This was followed by a cooling between 6.7 to 5.6 ka to temperatures similar to those prevailing at present (Ritchie and Hare, 1971; Cwynar and Spear, 1995). The Holocene thermal maximum (also referred to as the Hypsithermal) was marked by active layer thickening and a distinct thaw unconformity across the Arctic (Mackay, 1975; Burn, 1997). Based on cryostratigraphic and chemical observations at Slump A (see Williams-Jones et al., 2012a), the thaw unconformity marking the base of the paleo-active layer in this area fluctuated between an uncorrected depth of 107 cm and 192 cm (includes excess ice).

Assuming that the active layer at Slump A reaches the maximum values projected for the IPCC SRES A2 scenario for 2100, it follows that the annual increase in active layer thickening will be 0.08 cm to 0.12 cm and the corresponding ground subsidence will be 0.05 cm to 0.08 cm (66% subsidence). By integrating these steps and correcting for the subsidence, we predict that the active layer will reach a depth equivalent to 18 cm below the current thaw unconformity. This depth is 2-3 cm above an inferred thermal maximum indicated by peak in weathering indices

(Williams-Jones et al., 2012a) suggesting that the temperatures influencing the formation of this accumulation layer were greater than those predicted by the CGCM 3.1/T63 climate model for 2100. However, it should be noted that the predicted active layer depths, even under the most extreme climate scenario (i.e. IPCC SRES A2), may be underestimated, as was observed for the modelled 2011 temperatures. If this is the case, then there is a possibility that the active layer will extend into the Hypisthermal layer, making this the first breach of this layer in the past 6,000 years. It should, however, also be noted that the subsidence estimates determined above are for a condition of unimpeded water migration, i.e., near the slump face. Elsewhere in the ALM grid, e.g., in the northeast where there is evidence of thermokarst, subsidence will be considerably lower and in these parts the active layer probably will not reach the hypsithermal layer.

4.7. CONCLUSIONS

A fundamental challenge in assessing how the active layer will respond to future climate warming, is to understand how soil properties affect heat transfer from the ground surface to the underlying permafrost. Stefan's equation provides an important means for gaining such understanding by allowing measurements of thaw depth to be used in conjunction with thawing degree days to derive empirical thermal constants, and the soil properties (de Vries equations) to predict these constants. The results of the current study show that the theoretical and empirical values of these constants for the soils on Herschel Island differ significantly. The empirical values are consistently higher, an observation that is attributed in part to the method used (mechanical probing) to determine the thickness of the active layer. The method overestimates the depth of this layer because the probe passes through a zone of partially thawed soil and, thus

below the zero isotherm, before reaching the permafrost; this zone increases with increasing active layer thickness. In large part, however, the discrepancy is likely due to the fact that the theoretical estimate of the thermal constant considers only conductive heat transfer, whereas the empirical constant considers heat of all types, including that advectively transferred.

An equally demanding challenge is to translate understanding of the transfer of heat from the ground surface to the permafrost into a reliable evaluation of the relationship of climate warming to active layer thickening and permafrost degradation, and, in turn, landscape disturbance. Based on third generation Canadian Global Coupled Models (CGCM 3.1/T63) from the Canadian Centre for Climate Modelling and Analysis (CCCma), namely the IPCC SRES A2 and B1 scenarios, and the thermal constants referred to above, the active layer is predicted to thicken by as much as 17.5% before the end of this century. This will lead to thermokarst-related ground subsidence on the order of 4 to 7 cm in well-drained areas where flow of water from excess icemelting is unimpeded, and somewhat less subsidence in more poorly drained areas where flow is impeded. If, however, IPCC modelled temperatures instead of measured temperatures are used for 2011, these estimates will increase significantly.

Irrespective of the role that the hydrological regime plays in enhancing or mitigating ground subsidence and further active layer thickening, knowledge of the potential magnitude of ground subsidence is important in assessing the likely extent of landscape disturbance. It must be emphasized, however, that the variability of periglacial climates makes it challenging to generalize about the scale on which climate-induced changes in the ground thermal equilibrium will produce terrain modification. Moreover, it is important to bear in mind that land

disturbances, such as thermokarst, are naturally occurring geomorphic processes in periglacial environments, and are fundamental to Arctic terrain diversity (Britton, 1957). Although climate change will undoubtedly affect the thermal equilibrium within frozen environments, potentially enhancing erosional activity, whether this rate of change will be greater or less than in the past will depend largely on the ability of the landscape's hydrology, soils, and vegetation to minimize potential disturbances.

Knowledge of the thermal properties of the soil and the range of changes resulting from any disruption in the equilibrium maintained by these properties is important in predicting long-term disturbance. This study demonstrates that the Stefan's equation can be used in conjunction with theoretically calculated thermal constants to make first order predictions of future active layer depth changes. However, in lower Arctic environments, these predictions will be improved if a correction for advective heat transfer can be made to the equation as has been recommended by other researchers, e.g. Kersten (1949), Zhang et al. (2000), Woo et al. (2004), Carey and Woo (2005), Yi et al. (2006) and Hayashi et al. (2007). Finally, although this study provides new insight into how ongoing climate warming will affect active-layer development, further research is needed to better quantify the extent to which permafrost degradation will disturb the landscape.

CHAPTER 5

CONCLUSIONS

5.1. CONCLUSIONS

The main findings of this study are:

- Contrary to the widely held view that weathering in lower Arctic soils is almost entirely a
 physical phenomenon, chemical weathering played an important role in the development of
 soils on Herschel Island, Yukon.
- 2. Soil chemical processes are important drivers for weathering on Herschel Island, Yukon. This is supported by observations that soluble cations have been release from soil particles and have accumulated at specific horizons, notably within thaw unconformities. Further support for this, is provided by high weathering indices.
- 3. Breaks in the permafrost record on Herschel Island, e.g. thaw unconformities, are readily detected as sharp changes in the chemical composition of soils and soil pore waters.
- 4. The paleo-active layer on Herschel Island, corresponding to the Holocene climatic optimum, was subjected to less chemical weathering than the modern active layer, but is associated with significantly higher weathering indices than the underlying perennially frozen permafrost. The modern active layer has been experiencing thaw since before the Hypsithermal.
- 5. Among the weathering indices tested, the most effective for reliably evaluating chemical weathering in periglacial environments such as that at Herschel Island, were those relating mobile to immobile element concentrations in the bulk soil.

- 6. The chemical composition of pore waters in the permafrost provides strong evidence supporting the marine origin of the sediments that make up Herschel Island. This marine signature and the lack of evidence of chemical weathering also shows that the perennially frozen permafrost has not previously experienced prolonged periods of thawing, as has been the case for the modern active layer, which shows no such signature.
- 7. Theoretical determinations of active-layer thickness made using the Stefan and De Vries (for estimating thermal conductivity) equations, significantly under-estimated the observed thickness of the active-layer at the study site on Herschel Island.
- 8. Empirical estimates of the thermal constant of soils in the study area made using the Stefan equation in conjunction with measurements of active-layer thickness and accumulated thawing degree days, were significantly higher than evaluated theoretically from soil thermal properties (2.23 versus 1.39). The discrepancy between the theoretically determined and empirically estimated thermal constants is attributed to the failure of the Stefan formula to consider advective heat flux and an overestimate of active layer thickness using a mechanical probe.
- 9. Although previous studies have suggested that a Stefan equation based entirely on conductive heat transfer, the results obtained in this research demonstrate that, at least in lower Arctic environments, it should be modified to account for some advective heat transfer.

10. Global coupled climate models used in conjunction with the Stefan equation and empirical and theoretical estimates of thermal constant, predict that the thickness of the active layer on Herschel Island will increase by between 4.03 and 17.5% by 2100. As the temperature in the study area in 2011 had already reached levels close to those predicted for 2050, the actual increase in active layer thickness is likely to be significantly higher.

CHAPTER 6

REFERENCES

6.1. REFERENCES

- Agriculture Canada Expert Committee on Soil Survey (ACECSS). 1987. The Canadian System of Soil Classification. 2nd ed., Research Branch, Agriculture Canada: Ottawa, 164.
- Arctic Climate Impact Assessment (ACIA), 2005. Scientific Report. New York: Cambridge University Press.
- Andersland, O.B., and Ladanyi, B., 2004. An introduction to frozen ground engineering.

 Chapman and Hall: New York.
- Anisimov, O., Fitzharris B., Hagen J. O., Jeffries R., Marchant H., Nelson F. E., Prowse T., and Vaughan D. G., 2001. Polar Regions (Arctic and Antarctic). In: Climate Change: Impacts, Adaptation, and Vulnerability, the Contribution of Working Group II of the Intergovernmental Panel on Climate Change, Third Assessment Review. Cambridge, UK: Cambridge University Press, 801-841.
- Anisimov, O., Reneva, S., 2006. Permafrost and changing climate: the Russian perspective. Ambio, 35, 169–175.
- Are, A.L, Demchenko, R., 1972. Some results of long-term monitoring of the active layer in the Yakutsk vicinity. In Experimental Studies of Heat Exchange in Frozen Soils. Akademiia Nauk SSSR: Moscow; 91–96
- Arocena, J.M., Hall, K., Zhu, L.P., 2012. Soil formation in high elevation and permafrost areas in the Qinghai Plateau, China. Spanish Journal of Soil Science, 2, 34-49.
- Benson, C.S., and Sturm, M., 1993. Structure and wind transport of seasonal snow on the Arctic Slope of Alaska. Annals of Glaciolology, 18, 261–267.
- Berger, A.R., Iams, W.J. (Eds.), 1996. Geoindicators: tools for assessing rapid changes in earth systems. Balkema: Rotterdam.

- Berner, R. A. and Berner, E. K., 1997. Silicate weathering and climate. In Tectonic Uplift and Climate Change, Ruddiman W. F. (Ed.). Plenum Press: 353–364.
- Birkeland, P.W., 1999. Soils and Geomorphology. Oxford University Press: Oxford.
- Bjorgo, E., Johannessen, O. M., and Miles, M. W., 1997. Analysis of merged SSMR-SSMI time series of Arctic and Antarctic sea ice parameters 1978–1995, Geophysical Research Letters, 24, 413–416.
- Bland, W. and Rolls, D., 1998. Weathering: An Introduction to the Scientific Principles. Arnold: London.
- Blume, HP, Schwertmann, U., 1969. Genetic evaluation of profile distribution of aluminum, iron and manganese oxides. Soil Science Society of America Proceedings 33: 438–444.
- Bockheim, J.G., 1982. Properties of a chronosequence of ultraxerous soils in the TransAntarctic Mountains. Geoderma 28, 239–255.
- Bockheim, J.G., Tarnocai, C., Kimble, J.M., Smith, C.A.S., 1997. The concept of gelic materials in the new Gelisol order for permafrost-affected soils. Soil Science: 927–939.
- Bockheim, J., and Tarnocai, C., 1998. Recognition of cryoturbation for classifying permafrost-affected soils. Geoderma, 81(3-4): 281–293.
- Bockheim, J.G., Hinkel, K.M., and Nelson, F.E., 2003. Predicting carbon storage in tundra soils of arctic Alaska. Soil Science Society of America Journal 67:648–650.
- Boer, G.J., Flato, G.M., Reader, M.C., Ramsden, D., 2000. A transient climate change simulation with greenhouse gas and aerosol forcing: experimental design and comparison with the instrumental record for the twentieth century. Climate Dynamics 16: 405–425.
- Boer, J. and Yu, B., 2003. Climate sensitivity and response. Climate Dynamics 20: 415-429.
- Boyd, D.W., 1976. Normal freezing and thawing degree days from normal monthly

- temperatures. Canadian Geotechnical Engineering Journal, National Research Council of Canada 13: 176–180.
- Britton, M.E., 1957. Vegetation of the arctic tundra. In Hansen H.P. (Ed.). Arctic biology. 2nd ed. Oregon State University: Corvallis; 26–72.
- Brown, J. and Grave, N.A., 1979. Physical and thermal disturbance and protection of permafrost.

 Special Report, 79-5, U.S. Army CRREL.
- Brown, J., Hinkel, K.M. and Nelson, F.E., 2000. The Circumpolar Active Layer Monitoring (CALM) program: Research designs and initial results. Polar Geography 24:165–258.
- Buggle, B., Glaser, B., Hambach, U., Gerasimenko, N., Markovic S., 2010. An evaluation of geochemical weathering indices in loess paleosol studies. Quaternary International 240: 12-21.
- Burn, C.R., 1986. On the origin of aggradational ice in permafrost. Ph.D. Thesis, Carleton University, Ottawa: Ontario.
- Burn, C.R., and Smith, C.A.S., 1988. Observations of the "thermal offset" in near-surface mean annual ground temperatures at several sites near Mayo, Yukon Territory, Canada. Arctic 41(2): 99–104.
- Burn, C. R., 1997. Cryostratigraphy, paleogeography, and climate change during the early Holocene warm interval, western Arctic coast Canada. NRC Research Press. Canadian Journal of Earth Sciences 925: 912–925.
- Burn, C. R., 2000. The thermal regime of a retrogressive thaw slump near Mayo, Yukon Territory. Canadian Journal of Earth Sciences 37(7): 967–981.
- Burn, C. R., and Zhang, Y., 2009. Permafrost and climate change at Herschel Island (Qikiqtaruq), Yukon Territory, Canada. Journal of Geophysical Research 114(F2): 1-16.

- Calmels, F., Delisle G. and Allard, M., 2008. Internal structure and the thermal and hydrological regime of a typical lithalsa: significance for permafrost growth and decay. Canadian Journal of Earth Sciences 45: 31-43.
- Campbell, I.B., Claridge, G.G.C., 1982. Influence of moisture on the development of soils of the cold deserts of Antarctica. Geoderma 28: 221-238.
- Campbell, I.B., Claridge, G.G.C., 1987. Antarctica: Soils, Weathering Processes and Environment. Elsevier: NY.
- Carey, S. K., and Woo M.-K., 2005. Freezing of subarctic hillslopes, Wolf Creek Basin, Yukon, Canada. Arctic, Antarctic and Alpine Research 37: 1–10.
- Chapin, F.S. III, Sturm, M., Serreze, M.C., McFadden, J.P., Key, J.R., Lloyd, A.H., McGuire,
 A.D., Rupp, T.S., Lynch, A.H., Schimel, J.P., Beringer, J., Chapman, W.L., Epstein, H.E.,
 Euskirchen, E.S., Hinzman, L.D., Jia, G., Ping, C.-L., Tape, K.D., Thompson, C.D.C.,
 Walker, D.A., and Welker, J.M., 2005. Role of land-surface changes in Arctic summer
 warming. Science 310: 657–660.
- Childs, C.W., 1985. Towards understanding soil mineralogy, II. Notes on ferrihydrite. New Zealand Soil Bureau Laboratory Report CM7, DSIR: New Zealand.
- Chittleborough, D.J., 1991. Indices of weathering for soils and paleosols formed on silicate rocks. Australian Journal of Earth Sciences 38: 115–120.
- Cleaves, E. T., 1974. Petrologic and chemical investigation of chemical weathering in mafic rocks, eastern Piedmont of Maryland. Report of Investigations. Maryland Geological Survey 25: 28.
- Couture, N. J., and Pollard, W. H., 2007. Modelling geomorphic response to climatic change. Climatic Change 85(3-4): 407-431.

- Coffin, D.E., 1963. A method for the determination of free iron in soils and clays. Canadian Journal Soil Science 43: 7–17.
- Comiso, J. C., 2002. A rapidly declining Arctic Perennial Ice Cover. Geophysical Research Letters 29: 1956.
- Crory, F. E., 1973. Settlement associated with the thawing of permafrost. In Proceedings of the 2nd International Conference on Permafrost. North American Contribution. National Academy of Sciences Press: Washington D.C.; 599–609.
- Darmody, R.G., Thorn, C.E., Allen, C.E., 2005. Chemical weather and boulder mantles, Kärkevagge, Swedish Lapland. Geomorphology 67: 159–170.
- Davidson, E.A, and Janssens, I.A., 2006. Temperature sensitivity of soil carbon decomposition and feedbacks to climate change. Nature 440: 165–173.
- Day, J. H., and Rice, H. M., 1964. The characteristics of some permafrost soils in the Mackenzie Valley, N.W.T. Arctic 17: 222-236.
- Day, P.R., 1965. Particle fractionation and particle-size analysis. In Black, C.A., Evans, D.D., and Dinauer, R.C. (Eds.). Methods of soil analysis, Part 1.Agronomy 9:545-567.
- de Vries, D.A., 1963. Thermal properties of soil. In van Wijk W.R. (Ed.). Physics of Plant Environment. North-Holland: Amsterdam; 210-235.
- de Vries, D.A., 1987. The theory of heat and moisture transfer in porous media revisited.

 International Journal of Heat Mass Transfer 30 (7): 1343–1350.
- Duzgoren-Aydin, N.S., Aydin, A., Malpas, J., 2002. Re-assessment of chemical weathering indices: case study on pyroclastic rocks of Hong Kong. Engineering Geology 63: 99–119.
- Everett, K. R. and Brown, J., 1982. Some recent trends in the physical and chemical

- characterization and mapping of tundra soils. arctic slope of Alaska. Soil Science 133: 264-280.
- Farouki, O. 1981. Thermal Properties of Soils. CRREL Monograph 81-1, U.S. Army Corps of Engineers Cold Regions Research and Engineering Laboratory: Hanover, NH.
- Feustel, I. C., Dutilly A., and Anderson M. S., 1939. Properties of soils from North American Arctic regions. Soil Sciences 48: 183-199.
- French, H.M. and Guglielmin, M., 1999. Observations on the ice-marginal, periglacial geomorphology of Terra Nova Bay, northern Victoria Land, Antarctica. Permafrost and Periglacial Processes 10: 331–347.
- French, H. M., 2007. The Periglacial Environment (3rd ed.), Addison Wesley, Longman Limited, Harlow: United Kingdom.
- French, H.M, Demitroff, M., Forman, S.L., 2003. Evidence for Late-Pleistocene permafrost in the NewJersey Pine Barrens (latitude 39-N), Eastern USA. Permafrost and Periglacial Processes 14: 259–274.
- Forman, S., Ingolfsson, O., Gataullin, V., Manley, W., and Lokrantz, H., 2002. Late Quaternary stratigraphy, glacial limits and paleoenvironments of the Marresale Area, Western Yamal Peninsula, Russia. Quaternary Research 57: 355–370.
- Fritz, M., Wetterich, S., Meyer, H., Schirrmeister, L., Lantuit, H., and Pollard, W. H., 2011.

 Origin and characteristics of massive ground ice on Herschel Island (western Canadian Arctic) as revealed by stable water isotope and Hydrochemical signatures. Permafrost and Periglacial Processes, 22(1): 26–38.
- Froese, D.G., Westgate, J.A., Reyes, A.V., Enkin, R.J., and Preece, S.J., 2008. Ancient permafrost and a future, warmer Arctic. Science 321(5896): 1648.

- Gardener, L.R., Kheoruenromne, I., and Chen, H.S., 1978. Isovolumetric geochemical investigation of buried granite saprolite near Columbia, SC, USA. Geochimica et Cosmochimica Acta 42: 417-424.
- Gardener, L.R., 1980. Mobilization of Al and Ti during rock weathering isovolumetric geochemical evidence. Chemical Geology 30: 151-165.
- Gardener, L.R., Kheoruenromne, I., and Chen, H.S., 1981. Geochemistry and mineralogy of an unusual diabase saprolite near Columbia, South Carolina. Clays and Clay Minerals 29: 184-190.
- Gold, L.W., and Lachenbruch, A.H., 1973. Thermal conditions in permafrost—a review of North American literature. Proceedings Second International Conference on Permafrost, Yakutsk, U.S.S.R., North American Contribution. National Academy of Sciences Press: Washington D.C.; 3–25.
- Goodrich, L. E., 1982. The influence of snow cover on the ground thermal regime. Canadian Geotechnical Journal 19: 421–432.
- Goodrich, L. E., 1986. Field measurements of soil thermal conductivity. Canadian Geotechnical Journal 23: 51 -59.
- Goulden, M. L., Wofsy, S. C., Harden, J. W., Trumbore, S. E., Crill, P. M., Gower, S. T., Fries,T., Daube, B.C., Fan, S.-M., Sutton, D.J., Bazzaz, A., and Munger, J.W., 1998.Sensitivity of Boreal Forest Carbon Balance to Soil Thaw. Science 279: 214-217.
- Grom, J.D., and Pollard, W.H., 2008. A study of high Arctic retrogressive thaw slump dynamics, Eureka Sound Lowlands, Ellesmere Island. In Proceedings of the Ninth International Conference on Permafrost, 29 June 3 July 2008, Fairbanks, Alaska. Edited by D.L. Kane and K.M. Hinkel. Institute of Northern Engineering, University of Alaska:

- Fairbanks; 545–550.
- Hall, K., Thorn, C. E., Matsuoka, N., and Prick, A., 2002. Weathering in cold regions: some thoughts and perspectives. Progress in Physical Geography 26(4): 577-603.
- Harnois, L., 1988. The CIW Index: a new chemical index for weathering. Sedimentary Geology 55: 319–322.
- Hayashi, M., Goeller, N., Quinton, W., and Wright, N., 2007. A simple heat-conduction method for simulating the frost-table depth n hydrological model. Hydrological Processes 21: 2610-2622.
- Hendershot, W. H., Lalande, L. and Duquette, M., 1993. Soil reaction and method of exchangeable acidity. In Carter, M. R. (Ed). Sampling and method of analysis. Canadian Society of Soil Science. Lewis Publisher: London; 141 145.
- Hinkel, K.M., and Nicholas, R.J., 1995. Active layer thaw rate at a boreal forest site in central Alaska, U.S.A. Arctic and Alpine Research 27(1): 72-80.
- Hinkel, K., Paetzold, F., Nelson, F., and Bockheim, J., 2001. Patterns of soil temperature and moisture in the active layer and upper permafrost at Barrow, Alaska: 1993–1999. Global and Planetary Change 29: 293–309
- Hinzman, L.D., Kane, D.L., Gieck, R.E., and Everett, K.R., 1991. Hydrologic and thermal properties of the active layer in the Alaskan Arctic. Cold Regions Science and Technology 19 (2): 95-110.
- Houghton, J.T., Jenkins, G.J., and Ephraums, J.J. (Eds.), 1990. Climate Change. The IPCC Scientific Assessment. Cambridge University Press: Cambridge.
- Houghton, J.T., Callander, B.A., and Varney, S.K., 1992. Climate Change 1992 -The Supplementary Report to the IPCC Scientific Assessment. WMO/UNEP

- Intergovernmental Panel on Climate Change. Cambridge University Press: Cambridge.
- Intergovernmental Panel on Climate Change (IPCC), 2007. Summary for Policymakers. In Solomon, S., Qin, D., Manning, M., Chen, Z., Marquis, M., Averyt, K.B., Tignor, M., and Miller, H.L. (Eds). Climate Change 2007. The Physical Science Basis. Contribution of Working Group I to the Fourth Assessment Report of the Intergovernmental Panel on Climate Change. Cambridge University Press: Cambridge.
- Jenkins, D.G., 1985. Southern mid-latitude Paleocene to Holocene planktic foraminifera. In Bolli, H.M., Saunders, J.B., and Perch-Nielsen, K., Plankton Stratigraphy. Cambridge: United Kingdom; 263-282.
- Johnson, N.M., Likens, G.E., Bormann, F.H., and Pierce, R.S., 1968. Rate of chemical weathering of silicate minerals in New Hampshire. Geochimica et Cosmochimica Acta, 32(5): 531-545.
- Johnson, G.A.L., 1984. Subsidence and sedimentation in the Northumberland Trough.

 Proceedings of the Yorkshire Geological Society 45: 71–83.
- Johnson, D.L., and Watson-Stegner, D., 1987. Evolution model of pedogenesis. Soil Science 143: 349-366.
- Jorgenson, M.T., Racine, C.H., Walters, J.C., and Osterkamp, T.E., 2001. Permafrost degradation and ecological changes associated with a warming climate in central Alaska. Climate Change 48(4): 551–579.
- Jorgenson, M.T., Romanovsky, V., Harden, J., Shur, Y., Donnell, J.O., Schuur, E.A.G., and Kanevskiy, M., 2010. Resilience and vulnerability of permafrost to climate change. Canadian Journal of Forest Research 40: 1219-1236.
- Jumikis, A.R., 1977. Thermal Geotechnics. Rutgers University Press: New Brunswick.

- Kabata-Pendias, A., 2011. Trace Elements in Soil and Plants. 4th Ed., CRC Press, Florida: USA.
- Kalinenko, V.V., 2001. Clay Minerals in Sediments of the Arctic Seas. Lithology and Mineral Resources 36: 362–72.
- Kane, D.L., Hinzman, L.D., and Zarling, J.P., 1991. Thermal Response of the Active Layer in a Permafrost Environment to Climatic Warming. Cold Regions Science and Technology 19(2):111-122.
- Kaverin, D., 2008. Study of the transient layer developed in permafrost-affected soils of southern tundra (European North-East of Russia). A position paper presented for the 5th NRF Open Meeting. Anchorage: Alaska;

 http://www.nrf.is/Open%20Meetings/Anchorage/Position%20Papers/Kaverin_5thNRF_p osition_paper_session2.pdf
- Keller, K., Blum, J.D., and Kling, G.W., 2007. Geochemistry of Soils and Streams on Surfaces of Varying Ages in Arctic Alaska. Arctic, Antarctic, and Alpine Research 39(1): 84–98.
- Kersten, M.S., 1949. Thermal properties of soils. University of Minnesota, Institute of Technology, Engineering Experiments Station, Bulletin No. 28, University of Minnesota: Minneapolis; 226.
- Kokelj, S.V., Smith, C.A.S., and Burn, C.R., 2002. Physical and chemical characteristics of the active layer and permafrost, Herschel Island, western Arctic Coast, Canada. Permafrost and Periglacial Processes 13(2): 171–185.
- Kudriavtsev, V.A., 1954. The Temperature of Upper Horizons of Permafrost in the USSR. USSR Academy of Sciences: Moscow.
- Lachenbruch, A.H., 1959. Contraction theory of ice-wedge polygons. Bulletin of the Geological Society of America 70(12): 1796.

- Lachenbruch, A.H., Sass, J.H., Marshall, B.V., and Moses Jr., T. H., 1982. Permafrost, heat flow and geothermal regime at Prudhoe Bay, Alaska. Journal of Geophysical Research 87(B11): 9301–9316.
- Lantuit, H., and Pollard, W.H., 2005. Temporal stereophotogrammetric analysis of retrogressive thaw slumps on Herschel Island, Yukon Territory. Natural Hazards and Earth System Sciences, 5: 413–423.
- Lantuit, H., and Pollard, W. H., 2008. Fifty years of coastal erosion and retrogressive thaw slump activity on Herschel Island, southern Beaufort Sea, Yukon Territory, Canada. Geomorphology 95: 84–102.
- Lawrence, D.M., and Slater, A.G., 2005. A projection of severe near surface permafrost degradation during the 21st century. Geophysical Research Letters: 32.
- Lewkowicz, A.G., 1987. Nature and importance of thermokarst processes, Sand Hills moraine, Banks Island, Canada. Geografiska Annaler 69A: 321–327.
- Linell, K.A., and Tedrow, J.C.F., 1981. Soil and permafrost surveys in the Arctic. Oxford University Press: New York.
- Lipson, D.A, Jha, M., Raab, T. K., and Oechel, W. C., 2010. Reduction of iron (III) and humic substances plays a major role in anaerobic respiration in an Arctic peat soil. Journal of Geophysical Research 115(June): 1-13.
- Liston, G.E., and Hall, D. K., 1995. An energy balance model of lake ice evolution. Journal of Glaciology 41: 373–382.
- Luo, L.F., Robock, A., Vinnikov, K.Y., Schlosser, C.A., Slater, A.G., Boone, A., Braden, H., Cox, P., de Rosnay, P., Dickinson, R.E., Dai, Y.J., Duan, Q.Y., Etchevers, P., Henderson-Sellers, A., Gedney, N., Gusev, Y.M., Habets, F., Kim, J.W., Kowalczyk, E., Mitchell,

- K., Nasonova, O.N., Noilhan, J., Pitman, A.J., Schaake, J., Shmakin, A.B., Smirnova, T.G., Wetzel, P., Xue, Y.K., Yang, Z.L., and Zeng, Q.C., 2003. Effects of frozen soil on soil temperature, spring infiltration, and runoff: Results from the PILPS 2 (d) experiment at Valdai, Russia. Journal of Hydrometeorology 4: 334–351.
- Mackay, J.R., 1959. Glacier ice-thrust features of the Yukon Coast. Geographical Bulletin 13: 5–21.
- Mackay, J.R., 1970. Geomorphic processes, Mackenzie valley, Arctic coast, District of Mackenzie. Report of Activities, Part A, Geological Survey of Canada, Paper 71A: 189-190.
- Mackay, J.R., 1971. Ground ice in the active layer and the top portion of permafrost. Permafrost Seminar on the Active Layer Processes. NRCC, Technical Memo 103: 26-30.
- Mackay, J.R., 1972. Geomorphic processes, Mackenzie valley, Arctic coast, District of Mackenzie. Report of Activities, Part A, Geological Survey of Canada, Paper 71A: 192-184.
- Mackay, J.R., 1974. Reticulate ice veins in permafrost, Northern Canada. Canadian Geotechnical Journal 11: 230-237
- Mackay, J.R., 1975. The stability of permafrost and recent climatic change in the Mackenzie valley, N.W.T. Geological Survey of Canada, Paper 75-1B: 173-176
- Mackay, J.R., 1977. Probing for the bottom of the active layer. Geological Survey of Canada Paper 77-1A: 327-328.
- Mackay, J.R., 1978. Quaternary and permafrost features, Mackenzie delta area. In Young, F.G. (Ed.), Geological and geographical guide to the Mackenzie delta area. Canadian Society of Petroleum Geologists: 42-50.

- Mahaney, W. C., Kalm, V., Hancock, R. G. V., Michel, F., and Kapran, B., 2010. Geochemistry and extractable Fe and Al in cold-temperature soils of northwestern Siberia. Journal of Quaternary Science 25(July 2009): 178-189.
- Marchenko, S., Romanovsky, V., and Range, B., 2006. Numerical Modeling of Spatial Permafrost Dynamics in Alaska. In Proceedings of the Ninth International Conference on Permafrost, 29 June–3 July 2008, Fairbanks, Alaska. Institute of Northern Engineering, University of Alaska, Fairbanks.
- Masiello, C.A., Chadwick, O.A., Southon, J., Torn, M.S., and Harden, J.W., 2004. Mechanisms of carbon storage in grassland soils. Global Biogeochemical Cycles 18: 1-9.
- McKeague, J.A. and Day, J. H., 1966. Dithionite and oxalate- extractable Fe and Al as aids in differentiating various classes of soils. Canadian Journal of Soil Science 46: 13-22.
- McKeague, J. A., 1967. An evaluation of 0.1 M pyrophosphate and pyrophosphatedithionite in comparison with oxalate as extractants of the accumulation products in podzols and some other soils. Canadian Journal of Soil Science 46: 61-81.
- McKeague, J. A., Brydon, J. E., and Miles, N. M., 1971. Differentiation of forms of extractable iron and aluminum in soils. Soil Science Society of America Proceedings 35: 33-38.
- Meunier, A., 2005. Clays. Springer, Berlin.
- Michaelson, G.J., Ping, C.L., and Kimble, J.M., 1996. Carbon storage and distribution in tundra soils of arctic Alaska, U.S.A. Arctic, Antarctic and Alpine Research 28: 414–424.
- Moeys, J., 2012. The soil texture wizard: R functions for plotting, classifying, transforming and exploring soil texture. Website accessed 12/07/2012.
 - http://cran.r-project.org/web/packages/soiltexture/vignettes/soiltexture_vignette.pdf
- Myneni, R.B., Keeling, C.D., Tucker, C.J., Asrar, G., and Nemani, R.R., 1997. Increased plant

- growth in the northern high latitudes from 1981 to 1991. Nature 386: 698–702.
- Nicolsky, D.J., Romanovsky, V.E., and Panteleev, G.G., 2009. Cold Regions Science and Technology Estimation of soil thermal properties using in-situ temperature measurements in the active layer and permafrost. Cold Regions Science and Technology 55(1): 120-129.
- Nixon, J., and McRoberts, E., 1973. A study of factors affecting the thawing of frozen soils.

 Canadian Geotechnical Journal 20: 439-452.
- Oechel, W.C., Hastings, S.J., Vourlitis, G., Jenkins, M., Riechers, G. and Grulke, N., 1993.

 Recent change of Arctic tundra ecosystems from a net carbon dioxide sink to a source.

 Nature 361: 520-523.
- Oke, T.R., 1987. Boundary Layer Climates. 2nd ed., Methuen & Co. Ltd.: New York.
- Ortiz, J. D., 2011. Application of Visible/near Infrared derivative spectroscopy to Arctic paleoceanography. IOP Conference Series: Earth and Environmental Science 14: 012011.
- Osterkamp, T.E., 1983. Response of Alaskan permafrost to climate. 4th International Conference on Permafrost. National Academy Press: Washington D.C.
- Osterkamp, T.E., and Romanovsky, V.E., 1999. Evidence for warming and thawing of discontinuous permafrost in Alaska. Permafrost and Periglacial Processes 10: 17–37.
- Osterkamp, T. E., 2007. Characteristics of the recent warming of permafrost in Alaska. Journal Geophysical Research 112: F02S02.
- Outcalt, S. I., Goodwin, C., Weller, G., and Brown, J., 1975. Computer simulation of snowmelt and soil thermal regime at Barrow, Alaska. Water Resources Research 11(5): 709–715.
- Pavlov, A.V., 1997 .Patterns of frozen ground formation accompanying recent climate changes.

 Polar Geography 21: 137-153.
- Parfitt, R. L. and Childs, C. W., 1988. Estimation of forms of Fe and Al; a review, and analysis of

- contrasting soils by dissolution and Moessbauer methods. Australian Journal of Soil Research 26: 121-144.
- Parker A., 1970. An Index of weathering for silicate rocks. Geological Magazine 107: 501–504.
- Péwé, T.L., 1975.Quaternary Geology of Alaska. U.S. Geological Survey Professional Paper 835: 145.
- Ping, C.L., Bockheim, J.G., Kimble, J.M., Michaelson, G.J., Walker, D.A., and Fliet-Lanoe, F., 1998. Characteristics of cryogenic soils along a latitudinal transect in Arctic Alaska.

 Journal of Geophysical Research 103 (D22): 28917-28928.
- Pollard, W.H. and French, H.M., 1980. A first approximation of the volume of ground ice, Richard Island, Pleistocene Mackenzie delta, NWT.; Canadian Geotechnical Journal, 17, 509-516.
- Pollard, W.H., 1990. The nature and origin of ground ice in the Herschel Island area, Yukon Territory. Proceedings of the Fifth Canadian Permafrost Conference, Quebec City, Quebec. National Research Council Canada, Collection Nordicana 54: 23–30.
- Pollard, W.H., 2005. Thermokarst. In: Nuttall, M. (Ed.), Encyclopedia of the Arctic. Routledge: New York; 2021–2023.
- Price, R.C., Gray, C.M., Wilson, R.E., Frey, F.A., and Taylor, S.R., 1991. The effects of weathering on rare-earth element, Y and Ba abundances in Tertiary basalts from southeastern Australia. Chemical Geology 93: 245–265.
- Price, D.G., 1995. Weathering and weathering processes. Quarterly Journal of Engineering Geology 28 (3): 243–252.
- Price, J.R., and Velbel, M.A., 2003. Chemical weathering indices applied to weathering profiles developed on heterogeneous felsic metamorphic parent rocks. Chemical Geology 202:

- 397–416.
- Pullman, E. R., Jorgenson, M. T., and Shur, Y., 2007. Thaw settlement in soils of the Arctic Coastal Plain, Alaska. Arctic, Antarctic and Alpine Research 39: 468–476.
- Rains, M.C., 2002. The effects of periglacial processes on landforms, soils and vegetation in terrestrial ecosystems. In Mount, J., Moyle, P., and Yarnell, S. (Eds.). Glacial and Periglacial Processes and Hydrogeomorphic and Ecological Drivers in High-Latitude Watersheds. Davis: California.
- Rampton, V.N., 1982. Quaternary geology of the Yukon Coastal Plain. Bulletin 317. Ottawa: Geological Survey of Canada.
- Rampton, V.N., 1988. Quaternary geology of the Tuktoyaktuk coastlands, Northwest Territories.

 Geological Survey of Canada Memoir 423: 98.
- Rieger, S., 1974. Arctic soils. In Ives, J.D., and Barry, R.G. (Eds.), Arctic and Alpine Environments. Methuen: London; 749–769.
- Riseborough, D., Shiklomanov, N., Etzelmuller, B., Gruber, S., and Marchenko, S., 2008. Recent advances in permafrost modelling. Permafrost and Periglacial Processes 19: 137–231.
- Ritchie, J.C., 1984. Past and Present Vegetation of the Far Northwest of Canada. University of Toronto Press: Toronto.
- Romanovsky, V. E., and Osterkamp, T. E., 1997. Thawing of the Active Layer on the Coastal Plain of the Alaskan Arctic. Permafrost and Periglacial Processes, 8(1): 1-22.
- Romanovsky, V.E., and Osterkamp, T.E., 2000. Effects of unfrozen water on heat and mass transport processes in the active layer and permafrost. Permafrost Periglacial Processes 11(3): 219–239.
- Romanovsky, V.E., Smith, S.L., and Christiansen, H.H., 2010. Permafrost thermal state in the

- polar Northern Hemisphere during the international polar year 2007-2009: a synthesis. Permafrost and Periglacial Processes, 21(2): 106-116.
- Rothrock, D. A., Yu, Y., and Maykut, G., 1999. Thinning of the Arctic sea-ice cover. Geophysical Research Letters 26: 3469–3472.
- Ruxton, B.P., 1968. Measures of the degree of chemical weathering of rocks. Journal of Geology 76: 518-527
- Schaetzl, R.J., and Anderson, S., 2005. Soils; genesis and geomorphology. Cambridge University Press: New York; 817.
- Schulte, E.E., Kaufmann, C., and Peter, J.B., 1991. The influence of Boca Raton, FL. sample size and heating time on soil weight loss-on-ignition. Communications in Soil Science and Plant Analysis 22:159–168.
- Schwertmann, U., 1966. Inhibitory effect of soil organic matter on the crystallization of amorphous ferric hydroxide. Nature 212: 645-646.
- Schwertmann, U., Schulze, D. G., and Murad, E., 1982. Identification of ferrihydrite in soils by dissolution kinetics, differential X-ray diffraction and Mossbauer spectroscopy. Soil Science Society of America Journal 46: 869-875.
- Shur, Y.L., Hinkel, K.M., and Nelson, F.E., 2005. The transient layer: implications for geocryology and global-change science. Permafrost and Periglacial Processes 16(1): 5-11.
- Shur, Y.L., and Jorgenson, M.T., 2007. Patterns of permafrost formation and degradation in relation to climate and ecosystems. Permafrost and Periglacial Processes 18: 7–19.

- Schuur, E.A.G., Bockheim, J., Canadell, J.G., Euskirchen, E., Christopher, B., Goryachkin, S.V., Hagemann, S., Kuhry, P., Lafleur, P.M., Lee, H., Mazhitova, G., Nelson, F.E., Rinke, A., Romanovsky, V.E., Shiklomanov, N.Y., Tarnocai, C., Venevsky, S., Vogel, J.G., and Zimov, S.A., (2008). Vulnerability of Permafrost Carbon to Climate Change: Implications for the Global Carbon Cycle. BioScience 58(8): 701-714.
- Sheldrick, B.H., and Wang, C., (1993). Particle size distribution. In: Carter, M.R. (Ed.), Soil Sampling and Methods of Analysis. Lewis Publications/CRC Press, Boca Raton: Florida; 499–511.
- Skjemstad, J.O., Bushby, H.V.A., and Hansen, R.W., 1989. Extractable Fe in the surface horizons of a range of soils from Queensland. Australian Journal of Soil Resources. 28: 259-66.
- Sloan, H., and Pollard, W.H., 2012. Disturbance responses, resiliency, and climate change: a characterization of revegetation patterns related to retrogressive thaw slumps on Herschel Island, Yukon Territory, Canada. MSc. Thesis. McGill University. In prep.
- Smith, V.R., 1988. Production and Nutrient Dynamics of Plant Communities on a Sub-Antarctic Island. 5. Nutrient Budgets and Turnover Times for Mire-Grasslands, Fjaeldmark and Fernbrakes'. Polar Biolology 8: 255–269.
- Smith, C.A.S., Kennedy, C.E., Hargrave, A.E., McKenna, K.M., 1989. Soil and vegetation of Herschel Island, Yukon Territory. Yukon Soil Survey Report No. 1. Land Resource Research Centre, Agriculture Canada: Ottawa.
- Smith, L.C., MacDonald, G.M., Velichko, A.A., Beilman, D.W., Borisova, O.K., Frey, K.E., Kremenetski, K.V., Sheng, Y., 2004. Siberian peatlands a net carbon sink and global methane source since the early Holocene. Science 303: 353–356.

- Soil Classification Working Group., 1998. The Canadian system of soil classification. 3rd ed. Published 1646. Agriculture and Agri-Food Canada: Ottawa.
- Sparks, D.L., 2003. Environmental Soil Chemistry. Academic Press, London: United Kingdom.
- Sposito, G., 2008. The Chemistry of Soils. Oxford University Press: New York.
- Stendel, M., Romanovsky, V.E., Christensen, J.H., and Sazonova, T., 2007. Using dynamical downscaling to close the gap between global change scenarios and local permafrost dynamics. Global and Planetary Change 56: 203-214.
- Stumm, W., 1992. Chemistry of the solid-water interface. Wiley: New York.
- Sturm, M. and Johnson, J. B., 1991. Thermal conductivity measurement of depth hoar. Journal of Geophysical Research 97(B2): 2129–2139.
- Sturm, M., Racine, C., and Tape, K., 2001. Increasing shrub abundance in the Arctic. Nature 411: 546–547.
- Tarnocai, C., Canadell, J.G., Schuur, E.A.G., Kuhry, P., Mazhitova, G., and Zimov, S., 2009. Soil organic carbon pools in the north- ern circumpolar permafrostregion. Global Biogeochemical Cycles 23(2): GB2023.
- Tedrow J.C.F., 1977. Soils of the Polar Landscapes. Rutgers University Press: New Jersey.
- Usai, M.R., 1996. Paleosol Interpretation. Micromorphological and Pedological Studies. William Sessions: York.
- van Everdigen, R.O., 1998. Multi-language glossary of permafrost and related ground- ice terms.

 Definitions 78.
- van Wijk, W.R., and de Vries, D.A., 1963. Periodic temperature variations. In van Wijk, W.R., (Ed.), Physics of plant environment (2nd ed.), North-Holland Publishing Co.: Amsterdam.

- Vinnikov, K. Y., Robock, A., Stouffer, R. J., Wals, J. E., Parkinson, C. L., Cavalieri, D. J., Mitchell, J. F. B., Garrett, D. and Zakharov, V. F., 1999. Global warming and northern hemisphere sea ice extent. Science 286:1934–1937.
- Walker, J. C. G., Hays, P. B., and Kasting, J. F., 1981. A negative feedback mechanism for the long-term stabilization of earth's temperature. Journal of Geophysical Research 86: 9776–9782.
- Washburn, A.L., 1980. Geocryology—A Survey of Periglacial Processes and Environments.

 John Wiley and Sons: New York.
- White, K.P., Rifkin, S.A., Hurban, P. and Hogness, D.S., 1999. Microarray analysis of Drosophila development during metamorphosis. Science 286: 2179–2184.
- Williams-Jones, L-A., Pollard, W.H. and Hendershot, W.H., 2012a. Soil Weathering Processes on Herschel Island, Yukon. MSc. Thesis. McGill University. In prep.
- Williams-Jones, L-A., Pollard, W.H. and Hendershot, W.H., 2012b. Active Layer Thickening on Herschel Island, Yukon. MSc. Thesis. McGill University. In prep.
- Woo, M.K., Arain, M.A., Mollinga, M., and Yi, S., 2004. A two-directional freeze and thaw algorithm for hydrologic and land surface modelling, Geophysical Research Letters, 31.
- Woo M.K., Mollinga M., Smith S.L., 2006. Simulating active layer thaw in a boreal environment. Geographic Physique et Quaternaire 60: 9–17.
- Woo, M.K., Kane, D.L., Carey, S.K., and Yang, D.Q., 2008. Progress in permafrost hydrology in the new millennium, Permafrost and Periglacial Processes, 19: 237-254.
- Yang, S. Y., Jung, H.S., and Li, C.X., 2004. Two unique weathering regimes in the Changjiang and Huanghe drainage basins: geochemical evidence from river sediments. Sedimentary Geology 164:19–34.

- Yi, S., Arain, A. M., and Woo, M.-K., 2006. Modifications of a land surface scheme for improved simulation of ground freeze-thaw in northern environments. Geophysical Research Letters 33: L13501.
- Zazula, G. D., Hare, P. G., and Storer, J., 2009. New Radiocarbon-Dated Vertebrate Fossils from Herschel Island: Implications for the Paleoenvironments and Glacial Chronology of the Beaufort Sea Coastlands. Arctic 62(3): 273-280.
- Zhang, Z., Kane, D. L., and Hinzman, L. D., 2000. Development and application of a spatial-distributed Arctic hydrological and thermal process model. Hydrological Processes 14: 1591–1611.
- Zhang, Y. Chen, W. and Cihlar, J., 2003. A process- based model for quantifying the impact of climate change on permafrost thermal regimes. Journal of Geophysical Research 108(D22): 4695.
- Zhang, Y., Chen, W., Smith, S.L., Riseborough, D.W. and Cihlar, J., 2005. Soil temperature in Canada during the twentieth century: complex responses to atmospheric climate change.

 Journal of Geophysical Research. 110: D03112.
- Zhang, Y. Chen, W. and Riseborough, D.W., 2006. Temporal and spatial changes of permafrost in Canada since the end of the Little Ice Age. Journal of Geophysical Research 111: D22103.
- Zhang, T., Osterkamp, T. E., and Stamnes, K., 2007. Effects of climate on the active layer and permafrost on the North Slope of Alaska, U.S.A. Permafrost and Periglacial Processes 8 (1): 45-67.
- Zhang, Y., Carey, S., and Quinton, W., 2008. Evaluation of the algorithms and parameterizations for ground thawing and freezing simulation in permafrost regions. Journal of Geophysical

Research 113: D17116.

CHAPTER 7

APPENDICES

7.1. APPENDIX

Table 7. 1.: Active layer depth measurements within the ALM grid from June 24th, 2011 to August 24th, 2011.

	24-Jun	29-Jun	3-Jul	8-Jul	13-Jul	18-Jul	13-Aug	24-Aug	
Site #				Depth	(cm)				Comments:
A1	17.5	20	23	28.5	30	36	50.5	51	
A2	12.5	15	17.5	20	25	30	44	46	
A3	14.5	15	18	20	21.5	29	43	44	
A4	13	15	17.5	26	30	41	44	45	
A5	15	20	20.5	25.5	30	35	45	45	
A6	9	10	10	10.5	15	26	38.5	39.5	
A7	11	15	21.5	28	30.5	34	45	46	
A8	10	10	13.5	22	19.5	29	39	40	
A9	8	10	11.5	14.5	20.5	28	40.5	39	
A10	12	12.5	12.5	13	20	28	41	41.5	
B1	15	20	24.5	28	30	37	50	50.5	
B2	5.5	8	11.5	12	13.5	19	35	33.5	Tussock (7cm)
В3	16.5	20	20.5	27	28	32	46	46	
B4	15	15	15.5	21	23.5	32	46	44	
B5	8	17.5	20.5	21	21	32	39	40	
В6	10.5	12.5	16.5	19.5	24.5	27	42	42	
В7	9	8.5	16	19	22	24	35	33.5	Tussock (9 cm)
B8	16	15	19	20	30	32	45	45	
В9	18	20	27.5	30	29	33	46	46	
B10	13.5	15	16.5	18.5	23	30	43	45	
C1	6	9	9.5	15.5	21	30	42	46.5	
C2	8	15	18	22	24.5	31	42.5	47	
C3	10	11	14.5	19.5	15.5	23	40	41	
C4	8	10.5	14	15.5	18.5	25.5	37	36	Tussock (14.5 cm)
C5	14.5	25	27	28	28	32.5	42	43.5	
C 6	13	15	17	22	25	27	40	39.5	
C7	11	12.5	13	16	24	31	43	45	
C8	16	20	26.5	28	30	37	50	50	
C 9	14	17	18.5	20	26	30	42.5	42.5	
C10	23	30	30	32.5	35	38	47.5	49.5	
D1	10	15	15	19	23	32	43.5	46	
D2	9	10	13	14	20	26	44	48	
D3	9	12.5	21	23	24	30	40.5	43	
D4	8	15.5	15.5	20	27	32	45.5	47.5	

D5 9 10 10.5 20 22 30 44 4	6
D6 12 13.5 15.5 18.5 29 34 46 46	8
D7 15 17.5 19.5 25 26 30 46 4.	3
D8 12.5 13 15 16.5 27.5 34.5 46.5 47	.5
D9 19.5 20 20 22.5 30.5 40 49 55	
D10 19 20 26.5 30 32.5 37 52 5.	
E1 12 13 17.5 19 28 33 41.5 43	
E2 6 13.5 13.5 20.5 23.5 29.5 39 4.6	' '
E3 8 12 15.5 27 28 28 40 40	.5
E4 14 15 17.5 20.5 23.5 30 41.5 43	
E5 7 10 10 13 15.5 20 39 40	
E6 10 10 11.5 14 17 20 41 4	
E7 7.5 12.5 20.5 24 31 35 50 5	
E8 9.5 10 10.5 18 20.5 21.5 42 41	
E9 10.5 22.5 25.5 27 29.5 30.5 45 48	
E10 14 20 21 24.5 30 34.5 44.5 50	
F1 8 15 15 19 22.5 30 44 43	
F2 9.5 10 22.5 29.5 30.5 33 46 4	
F3 10 15 20 24.5 30 36.5 50.5 5.5	
F4 10.5 11.5 12 19 25 29 39.5 40	.5
F5 19 20 26 30.5 32.5 38 47 50	
F6 9.5 10 12 13 15 22 40 40	6
F7 18 21 22.5 29.5 31 36.5 51 55	2
F8 10 20 12.5 21 25.5 31 39.5 4.	
F9 7.5 8 12 19 22 27 36.5 37	.5 Tussock (13cm)
F10 17 25 25 30 32.5 35 41.5 4	5 Swamp
G1 6.5 10 13 15 20 27 41.5 43	.5
G2 9 17.5 19 19.5 23 28 41 41	5
G3 13.5 15 18.5 19 25 28 44.5 4	5
G4 9 12.5 25 25.5 27 30.5 42.5 46	.5
G5 14 20 23.5 22 25 34 41 41	5
G6 9 20 20 24 30 40 50 44	8
G7 8 10 10.5 16 20.5 30 42 4	4
G8 11.5 15 17 19 22 25 37.5 4	0
G9 11 14.5 19.5 22 22.5 24 41 4	4
G10 8 15 20 21 25 32 46.5 46	8
H1 9.5 20 23 24.5 29 32 48 49	9
H2 15 20 20.5 21 25.5 30.5 43 4	5
H3 13 20 21.5 29.5 32 35 48.5 50	.5
H4 6.5 10 10.5 11.5 20 25 39 40	0
H5 12 15 21.5 27 30 35 48 50	.5
H6 7 10 10 18 29 39 49 48	.5
H7 14 17.5 17 26 23.5 32 43.5 4	7
H8 11 12.5 14.5 17 23 29 44 44	8
H9 16 20 23.5 25 32 39 58.5 6	0 Swamp
H10 3.5 11.5 14.5 16.5 21.5 26.5 42 41	.5 Tussock (18.5 cm)
11 9.5 17.5 20.5 24 25 32 45.5 46	6
12 14 20 21.5 25 30 33.5 44.5 4	3

13	17.5	22.5	26.5	31	34	35	49	50.5	
14	10	12.5	13	18	20	25	45	45.5	Depression (6.5cm)
15	8	12.5	25.5	15	22	30	43	44	
16	2.5	3	8	9	15	20	39	39	Tussock (12 cm)
17	8.5	10	12.5	14	26	23	45	46	
18	6	15	16.5	18	24.5	28	41.5	47	
19	15	20	20	24	30	29	41	40.5	Depression (5cm)
I10	10.5	20	21	30	30	37	44	48	Swamp
J1	5	9.5	13	13.5	14	15.5	28.5	29.5	Tussock (15.5cm)
J2	15	15.5	16	22	28	30	42.5	44	
J3	10.5	15	15.5	17	20	22	37.5	40	
J4	14	21.5	22	29.5	31.5	38	48.5	50	
J5	9	15	24.5	27	28	32	42	42	
J6	3	9	10	10	16.5	20	40	41.5	Tussock (10 cm)
J7	8.5	15	16.5	16.5	18	18.5	35.5	41	
J8	26.5	26.5	27	37	40	44	54	56	Swamp
J9	11	12	15	20	28	28	51	52	Edge of small pond
J10	15	17.5	19	22	24.5	28	39.5	40.5	

Table 7. 2.: Empirical thermal constant change across ALM Grid from June 24th, 2011 to August 24th, 2011 using the Stefan formula.

	24-Jun	29-Jun	3-Jul	8-Jul	13-Jul	18-Jul	13-Aug	24-Aug	
Site #				Depth	(cm)				Comments:
A1	1.61	1.61	1.69	1.86	1.80	1.99	2.05	1.94	
A2	1.15	1.21	1.29	1.31	1.50	1.66	1.78	1.75	
A3	1.33	1.21	1.32	1.31	1.29	1.61	1.74	1.67	
A4	1.20	1.21	1.29	1.70	1.80	2.27	1.78	1.71	
A5	1.38	1.61	1.51	1.67	1.80	1.94	1.82	1.71	
A6	0.83	0.81	0.74	0.69	0.90	1.44	1.56	1.50	
A7	1.01	1.21	1.58	1.83	1.83	1.88	1.82	1.75	
A8	0.92	0.81	0.99	1.44	1.17	1.61	1.58	1.52	
A9	0.74	0.81	0.85	0.95	1.23	1.55	1.64	1.48	
A10	1.10	1.01	0.92	0.85	1.20	1.55	1.66	1.58	
B1	1.38	1.61	1.80	1.83	1.80	2.05	2.03	1.92	
B2	0.51	0.64	0.85	0.78	0.81	1.05	1.42	1.27	Tussock (7cm)
В3	1.52	1.61	1.51	1.77	1.68	1.77	1.86	1.75	
B4	1.38	1.21	1.14	1.37	1.41	1.77	1.86	1.67	
B5	0.74	1.41	1.51	1.37	1.26	1.77	1.58	1.52	
В6	0.97	1.01	1.21	1.27	1.47	1.50	1.70	1.60	
B7	0.83	0.68	1.18	1.24	1.32	1.33	1.42	1.27	Tussock (9 cm)
B8	1.47	1.21	1.40	1.31	1.80	1.77	1.82	1.71	
B9	1.66	1.61	2.02	1.96	1.74	1.83	1.86	1.75	
B10	1.24	1.21	1.21	1.21	1.38	1.66	1.74	1.71	
C1	0.55	0.73	0.70	1.01	1.26	1.66	1.70	1.77	
C2	0.74	1.21	1.32	1.44	1.47	1.72	1.72	1.79	
C3	0.92	0.89	1.07	1.27	0.93	1.27	1.62	1.56	
C4	0.74	0.85	1.03	1.01	1.11	1.41	1.50	1.37	Tussock (14.5 cm)
C5	1.33	2.01	1.99	1.83	1.68	1.80	1.70	1.65	
C6	1.20	1.21	1.25	1.44	1.50	1.50	1.62	1.50	
C7	1.01	1.01	0.96	1.05	1.44	1.72	1.74	1.71	
C8	1.47	1.61	1.95	1.83	1.80	2.05	2.03	1.90	
C9	1.29	1.37	1.36	1.31	1.56	1.66	1.72	1.62	
C10	2.12	2.42	2.21	2.12	2.10	2.10	1.92	1.88	
D1	0.92	1.21	1.10	1.24	1.38	1.77	1.76	1.75	
D2	0.83	0.81	0.96	0.92	1.20	1.44	1.78	1.82	
D3	0.83	1.01	1.54	1.50	1.44	1.66	1.64	1.63	
D4	0.74	1.25	1.14	1.31	1.62	1.77	1.84	1.81	
D5	0.83	0.81	0.77	1.31	1.32	1.66	1.78	1.75	
D6	1.10	1.09	1.14	1.21	1.74	1.88	1.86	1.82	
D7	1.38	1.41	1.43	1.63	1.56	1.66	1.86	1.63	
D8	1.15	1.05	1.10	1.08	1.65	1.91	1.88	1.81	
D9	1.80	1.61	1.47	1.47	1.83	2.22	1.99	1.94	

								ī	
D10	1.75	1.61	1.95	1.96	1.95	2.05	2.11	1.98	
E1	1.10	1.05	1.29	1.24	1.68	1.83	1.68	1.60	
E2	0.55	1.09	0.99	1.34	1.41	1.63	1.58	1.60	Tussock (16.5cm)
E3	0.74	0.97	1.14	1.77	1.68	1.55	1.62	1.54	
E4	1.29	1.21	1.29	1.34	1.41	1.66	1.68	1.65	
E5	0.64	0.81	0.74	0.85	0.93	1.11	1.58	1.54	
E6	0.92	0.81	0.85	0.92	1.02	1.11	1.66	1.79	
E7	0.69	1.01	1.51	1.57	1.86	1.94	2.03	1.94	
E8	0.87	0.81	0.77	1.18	1.23	1.19	1.70	1.58	
E9	0.97	1.81	1.87	1.77	1.77	1.69	1.82	1.82	
E10	1.29	1.61	1.54	1.60	1.80	1.91	1.80	1.90	
F1	0.74	1.21	1.10	1.24	1.35	1.66	1.78	1.60	
F2	0.87	0.81	1.65	1.93	1.83	1.83	1.86	1.75	
F3	0.92	1.21	1.47	1.60	1.80	2.02	2.05	1.98	
F4	0.97	0.93	0.88	1.24	1.50	1.61	1.60	1.54	
F5	1.75	1.61	1.91	1.99	1.95	2.10	1.90	1.92	
F6	0.87	0.81	0.88	0.85	0.90	1.22	1.62	1.75	
F7	1.66	1.69	1.65	1.93	1.86	2.02	2.07	1.98	
F8	0.92	1.61	0.92	1.37	1.53	1.72	1.60	1.60	
F9	0.69	0.64	0.88	1.24	1.32	1.50	1.48	1.43	Tussock (13cm)
F10	1.56	2.01	1.84	1.96	1.95	1.94	1.68	1.71	Swamp
G1	0.60	0.81	0.96	0.98	1.20	1.50	1.68	1.65	•
G2	0.83	1.41	1.40	1.27	1.38	1.55	1.66	1.58	
G3	1.24	1.21	1.36	1.24	1.50	1.55	1.80	1.71	
G4	0.83	1.01	1.84	1.67	1.62	1.69	1.72	1.77	
G5	1.29	1.61	1.73	1.44	1.50	1.88	1.66	1.58	
G6	0.83	1.61	1.47	1.57	1.80	2.22	2.03	1.82	
G7	0.74	0.81	0.77	1.05	1.23	1.66	1.70	1.67	
G8	1.06	1.21	1.25	1.24	1.32	1.38	1.52	1.52	
G9	1.01	1.17	1.43	1.44	1.35	1.33	1.66	1.67	
G10	0.74	1.21	1.47	1.37	1.50	1.77	1.88	1.82	
H1	0.87	1.61	1.69	1.60	1.74	1.77	1.95	1.86	
H2	1.38	1.61	1.51	1.37	1.53	1.69	1.74	1.71	
Н3	1.20	1.61	1.58	1.93	1.92	1.94	1.97	1.92	
H4	0.60	0.81	0.77	0.75	1.20	1.38	1.58	1.52	
Н5	1.10	1.21	1.58	1.77	1.80	1.94	1.95	1.92	
Н6	0.64	0.81	0.74	1.18	1.74	2.16	1.99	1.84	
H7	1.29	1.41	1.25	1.70	1.41	1.77	1.76	1.79	
Н8	1.01	1.01	1.07	1.11	1.38	1.61	1.78	1.82	
H9	1.47	1.61	1.73	1.63	1.92	2.16	2.37	2.28	Swamp
H10	0.32	0.93	1.07	1.08	1.29	1.47	1.70	1.58	Tussock (18.5 cm)
I1	0.87	1.41	1.51	1.57	1.50	1.77	1.84	1.75	1 0.000011 (10.00 0.11.)
12	1.29	1.61	1.58	1.63	1.80	1.86	1.80	1.63	
13	1.61	1.81	1.95	2.03	2.04	1.94	1.99	1.92	
14	0.92	1.01	0.96	1.18	1.20	1.38	1.82	1.73	Depression (6.5cm)
15	0.74	1.01	1.87	0.98	1.32	1.66	1.74	1.67	2001000011 (0.00111)
16	0.23	0.24	0.59	0.59	0.90	1.11	1.58	1.48	Tussock (12 cm)
17	0.23	0.24	0.92	0.92	1.56	1.27	1.82	1.75	1 4 5 5 5 6 1 1 1 1 1 1 1 1 1 1 1 1 1 1 1 1
17	0.70	0.01	0.52	0.52	1.50	1.21	1.02	1.75	1

18	0.55	1.21	1.21	1.18	1.47	1.55	1.68	1.79	
19	1.38	1.61	1.47	1.57	1.80	1.61	1.66	1.54	Depression (5cm)
I10	0.97	1.61	1.54	1.96	1.80	2.05	1.78	1.82	Swamp
J1	0.46	0.77	0.96	0.88	0.84	0.86	1.15	1.12	Tussock (15.5cm)
J2	1.38	1.25	1.18	1.44	1.68	1.66	1.72	1.67	
J3	0.97	1.21	1.14	1.11	1.20	1.22	1.52	1.52	
J4	1.29	1.73	1.62	1.93	1.89	2.10	1.97	1.90	
J5	0.83	1.21	1.80	1.77	1.68	1.77	1.70	1.60	
J6	0.28	0.73	0.74	0.65	0.99	1.11	1.62	1.58	Tussock (10 cm)
J7	0.78	1.21	1.21	1.08	1.08	1.02	1.44	1.56	
J8	2.44	2.14	1.99	2.42	2.40	2.44	2.19	2.13	Swamp
J9	1.01	0.97	1.10	1.31	1.68	1.55	2.07	1.98	Edge of small pond
J10	1.38	1.41	1.40	1.44	1.47	1.55	1.60	1.54	

Table 7. 3.: Changes in extractable ion concentrations with depth for the undisturbed sites 2 and 3.

SITE 2

Depth	Extracta	ble Ions - O	xalate	Depth	Extracta	ble Ions - C	xalate
	Fe	Al	Mn		Fe	Al	Mn
(cm)		(%)		(cm)		(%)	
2-0	0.43	0.11	0.03	2-0	0.50	0.13	0.03
7-2	0.70	0.16	0.04	12-2	0.79	0.16	0.04
12-7	0.72	0.17	0.03	22-12	0.86	0.18	0.04
17-12	0.84	0.16	0.04	32-22	0.74	0.15	0.03
24-17	0.83	0.16	0.04	39-32	0.85	0.19	0.01
31-24	0.81	0.16	0.03	47-39	1.01	0.11	0.03
39-31	0.78	0.15	0.03	82-47	0.59	0.09	0.02
47-39	0.74	0.16	0.03	107-82	0.52	0.08	0.02
52-47	0.81	0.16	0.02	157-107	0.54	0.09	0.02
102-52	1.08	0.26	0.01	192-157	1.47	0.12	0.03
122-102	0.57	0.07	0.02	282-192	1.49	0.12	0.02

Depth	Extractab	le Ions - Ph	yrophosphate	Depth	-	ractable Ioi rophospha	_
	Fe	Al	Mn		Fe	Al	Mn
(cm)		(%)		(cm)		(%)	
2-0	0.15	0.08	0.02	2-0	0.20	0.08	0.02
7-2	0.35	0.10	0.02	12-2	0.37	0.14	0.02
12-7	0.35	0.15	0.01	22-12	0.33	0.11	0.01
17-12	0.28	0.10	0.01	32-22	0.25	0.06	0.01
24-17	0.30	0.11	0.01	39-32	0.53	0.21	0.01
31-24	0.28	0.08	0.01	47-39	0.16	0.03	0.02
39-31	0.27	0.07	0.01	82-47	0.14	0.03	0.02
47-39	0.28	0.09	0.01	107-82	0.12	0.03	0.02
52-47	0.34	0.14	0.01	157-107	0.15	0.02	0.02
102-52	0.66	0.33	0.01	192-157	0.11	0.04	0.01
122-102	0.14	0.04	0.01	282-192	0.14	0.03	0.01

 $Table \ 7. \ 4.: Bulk \ soil \ chemical \ composition \ with \ depth \ for \ site \ 3 \ using \ XRF \ analysis.$

Analyte		SiO ₂	Al_2O_3	Fe ₂ O ₃	CaO	MgO	Na₂O	K ₂ O	MnO	TiO ₂	P_2O_5	Cr ₂ O ₃
Unit		%	%	%	%	%	%	%	%	%	%	%
Detection Limit		0.1	0.01	0.01	0.01	0.01	0.01	0.01	0.01	0.01	0.01	0.001
Sample	Depth	0.1	0.01	0.01	0.01	0.01	0.01	0.01	0.01	0.01	0.01	0.001
Туре	(cm)											
Soil												
Pulp	2-0	38.2	7.6	3.55	1.96	1.06	0.42	1.41	0.06	0.41	0.23	0.008
Soil												
Pulp	12-2	57.3	12.27	5.07	0.96	1.34	0.61	2.2	0.07	0.62	0.15	0.015
Soil												
Pulp	22-12	57.2	12.15	5.58	1.25	1.32	0.61	2.18	0.08	0.63	0.18	0.015
Soil												
Pulp	32-22	55.9	12.47	5.37	1.81	1.58	0.61	2.26	0.07	0.61	0.2	0.017
Soil												
Pulp	39-32	36.3	9.29	3.43	2.77	1.14	0.38	1.65	0.03	0.4	0.17	0.013
Soil												
Pulp	47-39	60.7	12.86	5.22	3.29	2.03	0.66	2.43	0.07	0.68	0.19	0.017
Soil	02.47	500	42.57		2.65	2.20	0.64	2.55	0.07	0.7	0.22	0.03
Pulp	82-47	59.8	13.57	5.75	3.65	2.29	0.64	2.55	0.07	0.7	0.22	0.02
Soil Pulp	107-82	62	13.19	5.4	3.03	2 21	0.69	2.48	0.09	0.69	0.22	0.01
Soil	107-82	02	13.19	5.4	3.03	2.21	0.69	2.48	0.09	0.69	0.22	0.01
Pulp	157-107	59.8	13.32	5.82	3.52	2.34	0.72	2.52	0.07	0.67	0.22	0.02
Soil	137-107	33.6	13.32	3.02	3.32	2.34	0.72	2.52	0.07	0.07	0.22	0.02
Pulp	192-157	58.3	13.91	5.51	3.7	2.29	0.73	2.64	0.07	0.67	0.21	0.01
Soil	132 137	50.5	13.51	5.51	5.,	2.23	0.75	2.04	0.07	0.07	0.21	0.01
Pulp	282-192	58.9	13.37	5.78	3.99	2.34	0.91	2.56	0.07	0.65	0.21	0.01
Soil	_0_ 102	30.3	13.37	3.70	3.33	2.5	0.51	2.55	0.07	0.03	0.21	0.01
REP Pulp	282-192	58.9	13.37	5.78	3.99	2.34	0.91	2.56	0.07	0.65	0.21	0.01

Table 7. 5.: Bulk soil chemical composition with depth for site 3 using XRF analysis (cont...)

Analyte		LOI	Ва	Cu	Ni	Pb	SO ₃	Sr	V_2O_5	Zn	Zr
Unit		%	%	%	%	%	%	%	%	%	%
Detection											
Limit		-5.11	0.01	0.001	0.001	0.001	0.002	0.002	0.002	0.001	0.002
Sample Type	Depth (cm)										
Soil	(0,										
Pulp Soil	2-0	44.48	0.06	<0.001	0.002	<0.001	0.01	0.007	0.016	0.013	0.01
Pulp Soil	12-2	18.74	0.09	0.001	0.004	0.001	<0.002	0.007	0.029	0.01	0.014
Pulp Soil	22-12	18.2	0.08	<0.001	0.004	<0.001	<0.002	0.006	0.029	0.01	0.013
Pulp Soil	32-22	19.27	0.09	0.002	0.006	0.001	0.029	0.007	0.032	0.012	0.014
Pulp Soil	39-32	43.99	0.08	<0.001	0.005	<0.001	0.008	0.011	0.022	0.01	0.009
Pulp Soil	47-39	11.53	0.09	<0.001	0.006	<0.001	0.092	0.013	0.031	0.011	0.015
Pulp Soil	82-47	10.65	0.09	<0.001	0.005	<0.001	0.077	0.013	0.031	0.012	0.013
Pulp Soil	107-82	10.01	0.09	<0.001	0.004	<0.001	0.111	0.016	0.031	0.012	0.015
Pulp Soil	157-107	10.43	0.08	<0.001	0.015	<0.001	0.115	0.013	0.032	0.013	0.013
Pulp Soil	192-157	11.09	0.09	0.001	0.004	<0.001	0.194	0.012	0.032	0.013	0.012
Pulp Soil	282-192	10.9	0.08	<0.001	0.006	<0.001	0.159	0.014	0.032	0.013	0.014
REP Pulp	282-192	10.9	0.08	< 0.001	0.006	<0.001	0.159	0.014	0.032	0.013	0.014